Schweizerische Eidgenossenschaft
Confédération suisse
Confederazione Svizzera
Confederaziun svizra

Federal Department of the Environment, Transport, Energy and Communications DETEC

Swiss Federal Office of Energy SFOE
Energy Research and Cleantech

Final report dated 12.07.2024

H2-DI Hydrogen Direct Injection Combustion Process

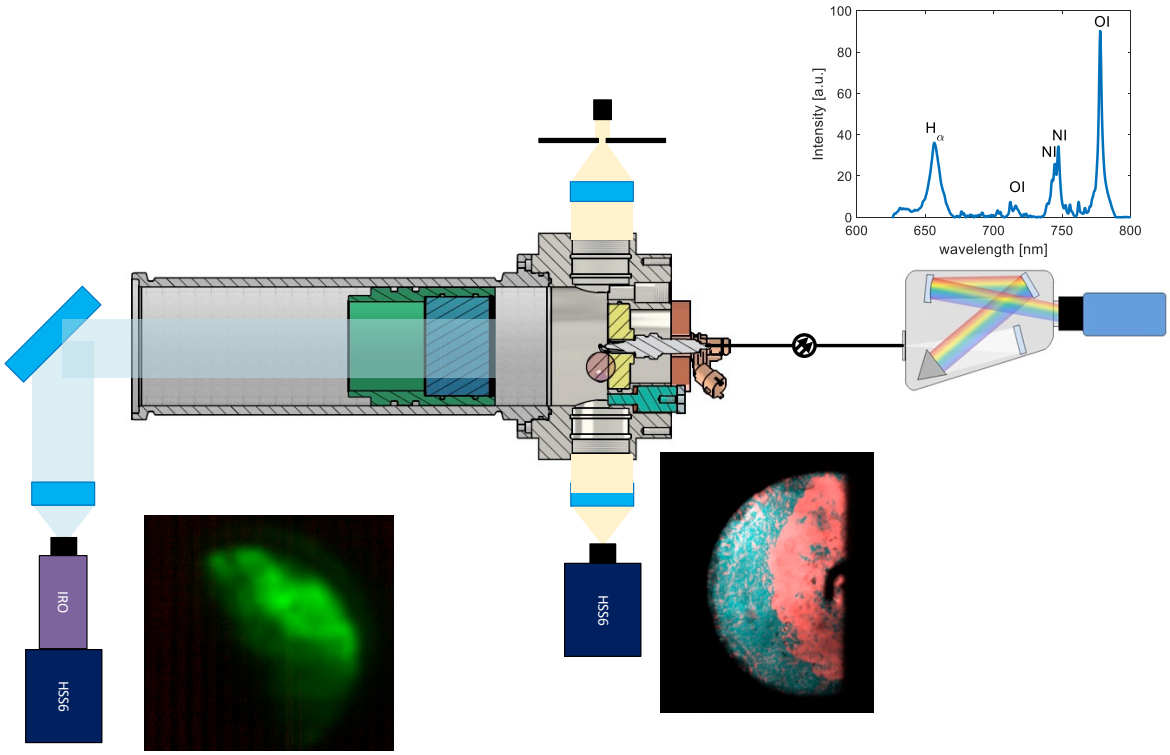

Source: Empa 2023

Empa
Materials Science and Technology

Date: 12.07.2024

Location: Bern

Publisher:

Swiss Federal Office of Energy SFOE
Energy Research and Cleantech
CH-3003 Bern
www.bfe.admin.ch

Co-financing:

FVV e.V. (Forschungsvereinigung Verbrennungskraftmaschinen e.V.)
Lyoner Str. 18, 60528 Frankfurt am Main, Germany
www.fvv-net.de

Subsidy recipients:

Empa - Eidgenössische Materialprüfungs- und Forschungsanstalt
Überlandstrasse 129 8600 Dübendorf Schweiz
www.empa.ch

Authors:

Dr. Patrik Soltic, patrik.soltic@empa.ch
Dr. Laura Merotto, laura.merotto@empa.ch
Dr. Yuri M. Wright, yuri.wright@empa.ch
Michelangelo Balmelli, michelangelo.balmelli@empa.ch
Christian Bach, christian.bach@empa.ch

SFOE project coordinators:

Stephan Renz, renz@renzconsulting.ch
Dr. Carina Alles, carina.alles@bfe.admin.ch

SFOE contract number: SI/502205-01

Zusammenfassung

Wasserstoff-Verbrennungsmotoren sind eine attraktive Lösung für gewisse schwierig zu elektrifizierende Anwendugen. Sie bauen auf robuster, kostengünstiger und langlebiger Technik auf. Zudem sind sie, im Gegensatz zu Brennstoffzellen, sehr tolerant in Bezug auf die Treibstoffreinheit und sie ertragen problemlos Anwendungen mit hohen Vibrationen, wie sie beispielsweise bei Baumschinen vorkommen. Um NO_x Emissionen zu minimieren sowie um Klopfen und Vorentflammungen zu vermeiden, werden die Motoren sehr mager betrieben, typischerweise bei λ Werten über 2. Dies bringt Herausforderungen bezüglich der Aufladung, der Verbrennungsspitzendrücke sowie der Leistungsdichte mit sich. Um dies zu umgehen wäre also ein Brennverfahren vorteilhaft, welche sehr magere Verbrennung umgeht, allerdings ohne zu Klopf- oder Vorentflammungsproblemen zu führen.

Dieses Projekt befasst sich mit einem solchen Ansatz für effiziente H_2-Verbrennungsmotoren hoher Leistungsdichte. H_2 soll dazu direkt in den Brennraum eingeblasen und an der Strahlperipherie fremdgezündet werden, wobei die anschliessende Kraftstoffumwandlung überwiegend im geschichteten, strahlgeführten Modus erfolgt. Dabei soll das Potenzial für eine Verbrennung gegen λ=1, ohne die üblichen Klopfbegrenzungen, eröffnet werden. Dies, weil die Gemischbildung so gestaltet ist, dass eine Vormischung weitgehend vermieden wird. Das Hauptaugenmerk des Projekts liegt auf einem vertieften Verständnis der physikalisch-chemischen Prozesse, welche die Verbrennungsmodi von Wasserstoff bestimmet, basierend auf einem kombinierten experimentellen und numerischen Ansatz. Die aus dem Projekt gewonnenen Erkenntnisse und Werkzeuge dienen der späteren Umsetzung solcher Verbrennungskonzepte, was v.a. im Bereich der Stationärmotoren (z.B. Wärme-Kraft-Kopplung) sowie der schweren Nutzfahrzeuganwendungen relevant ist.

Das Projekt kann als Erfolg bezeichnet werden: es ist gelungen, das Gemischbildungs- und Brennverfahren wie gewünscht umzusetzten. Die Arbeiten am sogenanten Einhubtriebwerk, ein Versuchsträger mit optischen Zugang, haben gezeigt, dass eine hauptsächlich diffusionsgesteuerte Verbrennung von Wasserstoff möglich ist. Dies eröffnet Wasserstoffmotoren das Potenzial, Wirkungsgradmässig auf Diesel-Niveau zu kommen. Dass das Brennverfahren funktioniert, konnte an einem Einzylinder-Versuchsmotor der Universität Stuttgart demonstriert werden. Mit Hilfe der begleitenden numerischen Forschung wurde zudem gezeigt, welche Prozesse dabei eine Rolle spielen. So wurde im Rahmen dieses Projekes die Grundlage für ein komplett neues Brennverfahren für Wasserstoff gelegt. Zukünftige Forschungsarbeiten können nun das Ziel verfolgen, dieses grundlegende Verständnis in Richtung echtem motorischem Betrieb zu entwickeln. Dies umfasst beispielsweise das Verständnis bzw. die Optimierung von Injektorgeometrie, die Wahl der Ladungsbewegung, die Auslegung von Distanzen zwischen Injekttor und Zündquelle sowie die Gestaltung des Zündvorganges.

Für die Schweizer Situation wurde identifiziert, dass die Schweiz Waserstoff-Versorgungspfade aus Gebieten, welche reicht an erneuerbaren Ressourcen sind, entwickeln sollte. Technologien dafür sind recht weit entwickelt, es fehlt aber an grossen Umsetzungsprojekten aufgrund fehlender Investitionssicherheit, bzw. aufgrund eines zu tiefen "Policy-Radyness-Levels".

Résumé

Les moteurs à combustion interne à hydrogène sont une solution intéressante pour certaines applications difficiles à électrifier. Ils reposent sur une technologie robuste, peu coûteuse et durable. De plus, contrairement aux piles à combustible, ils sont très tolérants en ce qui concerne la pureté du carburant et supportent sans problème les applications à fortes vibrations, comme c'est le cas par exemple pour les arboriculteurs. Afin de minimiser les émissions de NO_x et d'éviter le cliquetis et le pré-inflammation, les moteurs fonctionnent de manière très pauvre, typiquement avec des valeurs λ supérieures à 2. Cela pose des défis en termes de suralimentation, de pressions de pointe de combustion ainsi que de densité de puissance. Pour y remédier, il serait donc avantageux d'utiliser un procédé de combustion qui contourne la combustion très pauvre, mais sans entraîner de problèmes de cognement ou de pré-inflammation.

Ce projet porte sur une telle approche pour des moteurs à combustion H_2 efficaces et à haute densité de puissance. Pour ce faire, H_2 doit être injecté directement dans la chambre de combustion et allumé de manière externe à la périphérie du jet, la conversion du carburant qui s'ensuit s'effectuant principalement en mode stratifié et guidé par le jet. Ce faisant, il s'agit d'ouvrir le potentiel d'une combustion vers λ=1, sans les limitations de cliquetis habituelles. Ceci parce que la formation du mélange est conçue de manière à éviter en grande partie un prémélange. L'objectif principal du projet est d'approfondir la compréhension des processus physico-chimiques qui déterminent les modes de combustion de l'hydrogène, en se basant sur une approche expérimentale et numérique combinée. Les connaissances et les outils acquis dans le cadre du projet serviront à la mise en œuvre ultérieure de tels concepts de combustion, ce qui est particulièrement important dans le domaine des moteurs stationnaires (par ex. couplage chaleur-force) et des applications pour véhicules utilitaires lourds.

Le projet peut être qualifié de succès : il a été possible de mettre en œuvre le procédé de formation du mélange et de combustion comme souhaité. Les travaux sur le "rapid-compression-expansion-machine", un véhicule expérimental avec accès optique, ont montré qu'il est possible de réaliser une combustion de l'hydrogène principalement contrôlée par diffusion. Cela ouvre aux moteurs à hydrogène le potentiel d'atteindre le niveau de rendement du diesel. Le fonctionnement de ce procédé de combustion a pu être démontré sur un moteur d'essai monocylindre de l'université de Stuttgart. La recherche numérique qui l'accompagne a en outre permis de montrer quels processus jouent un rôle dans ce processus. Ainsi, ce projet a jeté les bases d'un tout nouveau procédé de combustion de l'hydrogène. Les travaux de recherche futurs peuvent maintenant avoir pour objectif de développer cette compréhension fondamentale en vue d'un véritable fonctionnement du moteur. Cela comprend par exemple la compréhension ou l'optimisation de la géométrie de l'injecteur, le choix du mouvement de la charge, la conception des distances entre l'injecteur et la source d'allumage ainsi que la conception du processus d'allumage.

Pour la situation suisse, il a été identifié que la Suisse devrait développer des filières d'approvisionnement en hydrogène à partir de régions riches en ressources renouvelables. Les technologies sont bien développées, mais les projets de mise en œuvre à grande échelle font défaut en raison du manque de sécurité des investissements ou d'un niveau de "policy-radyness" trop bas.

Summary

Hydrogen combustion engines are an attractive solution for certain applications that are difficult to electrify. They are based on robust, cost-effective and durable technology. In addition, unlike fuel cells, they are very tolerant in terms of fuel purity and can easily withstand applications with high vibrations, such as those found in construction machinery. To minimize NO_x emissions and to avoid knocking and pre-ignition, the engines are operated at very lean conditions, typically at λ values above 2. This poses challenges in terms of turbocharging, peak combustion pressures and power density. To avoid this, a combustion process that avoids very lean combustion, but without leading to knocking or pre-ignition problems, would therefore be advantageous.

This project deals with such an approach for efficient H_2 combustion engines with high power density. H_2 is to be injected directly into the combustion chamber and externally ignited at the jet periphery, with the subsequent fuel conversion taking place predominantly in stratified, jet-guided mode. The aim is to open up the potential for combustion towards λ=1, without the usual knock limitations. This is because the mixture formation is designed in such a way that premixing is largely avoided. The main focus of the project is on a deeper understanding of the physico-chemical processes that determine the combustion modes of hydrogen, based on a combined experimental and numerical approach. The knowledge and tools gained from the project will be used for the subsequent implementation of such combustion concepts, which is particularly relevant in the field of stationary engines (e.g. combined heat and power) and heavy commercial vehicle applications.

The project can be described as a success: the mixture formation and combustion process has been implemented as desired. The work on the so-called rapid-compression-expansion-machine, a test setup with optical access, has shown that a mainly diffusion-controlled combustion of hydrogen is possible. This opens up the potential for hydrogen engines to reach diesel levels of efficiency. The fact that the combustion process works was demonstrated on a single-cylinder test engine at the University of Stuttgart. With the help of the accompanying numerical research, it was also shown which processes play a role. This project thus laid the foundation for a completely new combustion process for hydrogen. Future research work can now pursue the goal of developing this fundamental understanding in the direction of real engine operation. This includes, for example, the understanding and optimization of injector geometry, the choice of charge movement, the design of distances between the injector and ignition source and the design of the ignition process.

For the Swiss situation, it was identified that Switzerland should develop hydrogen supply paths from areas that are rich in renewable resources. Technologies for this are quite well developed, but there is a lack of large-scale implementation projects due to a lack of investment security or because the "policy readiness level" is too low.

Main findings

- It is possible to realize a combustion concept for internal combustion engines where hydrogen is direct-injected late in the compression stroke, ignited shortly after injection start and combusted in a predominantly diffusion-controlled manner.
- The resulting combustion consists of a premixed part (i.e. mainly the amount of H_2 which is already injected before combustion starts) and a diffusion-contolled part which lasts as long, as injection is active.
- This combustion concept was experimentally verified in a Rapid Compression Expansion Machine as well as on a single cylinder research engine.
- Numerical simulation (CRFD) is able to explain / predict the behaviour.
- Open points are the optimal injection configuration (e.g. type of injector, spray pattern), the optimal distance between injector and ignition source, the ignition itself as well as the optimal charge motion.

Contents

Abbreviations

CFD - Computational Fluid Dynamics

CVC - Constant Volume Cell

DI - Direct Injection

EGR – Exhaust Gas Recirculation

EOI – End of injection

HPDI- High Pressure Direct Injecton

LIF – Laser Induced Fluorescence

LOHC – Liquid Organic Hydrocarbons

NRPD - Nanosecond Repetitively Pulsed Discharge

PFI - Port Fuel Injection

PIV – Particle Imaging Velocimetry

RCEM - Rapid Compression Expansion Machine

SI – Spark Ignition

SIBS - Spark Induced Breakdown Spectroscopy

SOI – Start of injection

TDC – Top Dead Center

UHC – Unburned Hydrocarbons

1 Introduction

1.1 Background information and current situation

The majority of heavy-duty engines in use today employ compression-ignition concepts, using Diesel as the high-reactivity fuel to enable self-ignition and diffusion-controlled combustion. In contrast, most alternative heavy-duty engines made for the low-reactivity fuels methane or hydrogen as a fuel, employ a comparably simple approach: port-fuel injection of the fuel and spark ignition ("Otto engines"). This concept has a knock limitation, power densities are low, component temperature can be high and efficiency leverls are considerably lower that for Diesel engines. Direct Injection (DI) of methane (CH_4) into the chamber and conversion in “Diesel” mode is a topic recently receiving considerable attention[1,2,3,4,5], while a recent project in the context of FVV hereto is reported in[6]. Most investigations cited looked into engine operation, starting out from a Diesel baseline.

However, carbon-free fuels such as hydrogen, ammonia as well as e-fuels (such as synthetic CH_4, methanol or DME) are among the candidates for future powertrains, offering similar CO_2 benefits from a “cradle-to-grave” life-cycle analysis perspective compared to purely battery-electric vehicles as discussed in[7]. These fuels may become very important in the future for applications, which cannot be directly electrified (e.g. heavy-duty on- and non-road vehicles) as well as in industrial applications, e.g. for high-temperature heat processes. Hydrogen has attracted the attention of researchers at least since the 1930’s with a huge body of literature present reviewed repeatedly every few decades[8,9,10,11,12]. Among the challenges when using hydrogen in internal combustion engines, aside storage and distribution infrastructure topics, is the very low volumetric efficiency (and hence power density) when using Port Fuel Injection (PFI) owed to the very low density of hydrogen and a stoichiometric air/fuel ratio twice the value for CH_4 – which is typically needed to eleininate NO_x emissions. Further drawbacks with PFI include abnormal combustion phenomenon such as pre-ignition and also backfire, cf. e.g.[10,13]. This was realized at an early stage and DI is viewed as the most promising solution to overcome these problems, cf.[12,14]. Comparisons between direct vs. port injection was the topic of a number of former

[1] Banholzer, M., et al., *Numerical investigation of the flow characteristics of underexpanded methane jets.* Physics of Fluids, 2019. 31(5): p. 056105.
[2] Banholzer, M., et al., *Numerical Investigation of Nozzle-Geometry Variations and Back-Pressure Changes on High Pressure Gas Injections under Application-Relevant Conditions.* SAE Technical Paper No. 2018-01-1138 2018.
[3] Vera-Tudela, W., et al., *An experimental study on the effects of needle dynamics on the penetration of a high-pressure methane jet.* Fuel, 2019. 253: p. 79-89.
[4] Rochussen, J. and P. Kirchen, *Characterization of reaction zone growth in an optically accessible heavy-duty diesel/methane dual-fuel engine.* International Journal of Engine Research, 2018: p. In press, 2019.
[5] Rochussen, J., J. Yeo, and P. Kirchen, *Effect of Fueling Control Parameters on Combustion and Emissions Characteristics of Diesel-Ignited Methane Dual-Fuel Combustion.* SAE Technical Paper no. 2016-01-0792, 2016.
[6] Vera-Tudela, W., et al., *Final report FVV project 1236 "Gas Diesel Combustion"*. 2020: FVV e.V.
[7] Bothe, D. and T. Steinfort, *Cradle-to-Grave Life-Cycle Assessment in the Mobility Sector – A Meta-Analysis of LCA Studies on Alternative Powertrain Technologies*, in *Frontier Economics Ltd.* 2020.
[8] Das, L.M., *Hydrogen engines: A view of the past and a look into the future.* International Journal of Hydrogen Energy, 1990. 15(6): p. 425-443.
[9] Escher, W.J.D. and E.E. Ecklund, *Recent Progress in the Hydrogen Engine.* SAE Technical Paper No. 760571, 1976.
[10] Verhelst, S., R. Sierens, and S. Verstraeten, *A Critical Review of Experimental Research on Hydrogen Fueled SI Engines.* SAE Technical Paper No. 2006-01-0430, 2006.
[11] White, C.M., R.R. Steeper, and A.E. Lutz, *The hydrogen-fueled internal combustion engine: a technical review.* International Journal of Hydrogen Energy, 2006. 31(10): p. 1292-1305.
[12] Yip, H.L., et al., *A Review of Hydrogen Direct Injection for Internal Combustion Engines: Towards Carbon-Free Combustion.* Applied Sciences, 2019. 9(22): p. 4842.
[13] Lee , J.T., et al., *An Investigation of a Cause of Backfire and Its Control Due to Crevice Volumes in a Hydrogen Fueled Engine.* Journal of Engineering for Gas Turbines and Power, 2000. 123(1): p. 204-210.
[14] Wimmer, A., et al., *H2-Direct Injection – A Highly Promising Combustion Concept.* SAE Technical Paper No. 2005-01-0108, 2005.

studies, see e.g.[14,15,16] and references therein. Most studies employed premixed (either lean or stoichiometric) Spark Ignition (SI) engine concepts. With premixed operation, striving for a good power density and efficient exhaust gas aftertreatment by implementing λ=1 operation normally implied severe knock problems, as hydrogen is very prone to knock. DI strategies with late injection during compression[17,18] or multiple injections leading to substantial stratification have therefore also been followed[19].

From a more fundamental perspective, fuel/air-mixing has been the focus of a number of studies in optical engines and vessels with a variety of diagnostics (LIF, PIV, SIBS), see e.g.[20,21]; numerical studies hereto include e.g.[22,23]. Compression-Ignition concepts have also been attempted, requiring high compression ratios in combination with preheating of the intake air[24] or an ignition assist mechanism such as a glow plug[25], due to the high auto-ignition temperature of hydrogen despite its low minimum ignition energy.

This project seeks to revisit hydrogen combustion in SI engines using HPDI, ignited at the jet periphery with subsequent fuel conversion occurring predominantly in stratified, jet-guided, diffusion-controlled mode. With the development of a jet-guided combustion process for the use of hydrogen in combustion engines, an innovative approach is being pursued, aimed at achieving high power density and high thermal efficiency. For this reason, a operation with high-pressure H_2 injection in the compression stroke near top dead centre is to be investigated. At ignition phasing shortly after the start of injection, this allows an almost free shaping of the combustion process as a function of the hydrogen injection rate, which of course would need a targeted development of injection equipment. At the same time, the heat release controlled by the fuel injection rate should ensure the suppression of knocking phenomena and thus allow for combustion phasing for maximal thermodynamic efficiency. This is accompanied by lowered exhaust gas temperatures, which are necessary for component protection and thus the longevity of components, which is particularly important in the heavy-duty sector.

In the framework of the present project, full metal engine investigations are being carried out in a single cylinder engine at the University of Stuttgart, and knowledge is being gained from Rapid Compression Expansion Machine (RCEM) experiments as well as from numerical simulations at Empa. Due to the complexity of the physical processes, this project is tackled by applying fundamental diagnostics using optical test rigs as well as Computational Fluid Dynamic (CFD) simulations to characterize under-expanded hydrogen jets at engine relevant conditions. The combination of high-speed imaging data and flow field information from the validated CFD sheds light into evolutions of spray morphology, mixing

[15] Eichlseder, H., et al., *The Potential of Hydrogen Internal Combustion Engines in a Future Mobility Scenario.* SAE Technical Paper No. 2003-01-2267, 2003.
[16] Rottengruber, H., et al., *Direct-Injection Hydrogen SI-Engine - Operation Strategy and Power Density Potentials.* SAE Technical Paper No. 2004-01-2927, 2004.
[17] Mohammadi, A., et al., *Performance and combustion characteristics of a direct injection SI hydrogen engine.* International Journal of Hydrogen Energy, 2007. 32(2): p. 296-304.
[18] Welch, A., et al., *Hydrogen Direct Injection Technology - Challenges and Opportunities*, in *NHA Sacramento*. 2008
[19] Wallner, T., et al., *Assessment of Multiple Injection Strategies in a Direct-Injection Hydrogen Research Engine.* SAE Technical Paper No. 2009-01-1920, 2009.
[20] bin Abdul Rahman, M.T., N. Kawahara, and E. Tomita, *Mixing Process of Direct Injection Hydrogen Jet in a Constant Volume Vessel by Using Spark-Induced Breakdown Spectroscopy.* SAE Technical Paper No. 2013-01-2526, 2013.
[21] Kaiser, S. and C.M. White, *PIV and PLIF to Evaluate Mixture Formation in a Direct-Injection Hydrogen-Fuelled Engine.* SAE Technical Paper No. 2008-01-1034, 2008.
[22] Messner, D., et al., *Application and Validation of the 3D CFD Method for a Hydrogen Fueled IC Engine with Internal Mixture Formation.* SAE Technical Paper No. 2006-01-0448, 2006.
[23] Scarcelli, R., et al., *Numerical and Optical Evolution of Gaseous Jets in Direct Injection Hydrogen Engines.* SAE Technical Paper No. 2011-01-0675, 2011.
[24] Gomes Antunes, J.M., R. Mikalsen, and A.P. Roskilly, *An experimental study of a direct injection compression ignition hydrogen engine.* International Journal of Hydrogen Energy, 2009. **34**(15): p. 6516-6522.
[25] Welch, A.B. and J.S. Wallace, *Performance Characteristics of a Hydrogen-Fueled Diesel Engine with Ignition Assist.* SAE Technical Paper No. 902070, 1990.

and turbulence fields as well as improves the understanding of the ignition and combustion processes under the specific conditions. Full-metal engine measurements provide large quantities of thermodynamic data under real-life conditions. Measurements performed at similar conditions as in the optical rigs support and complement the fundamental studies. The engine further allows for the extension to higher loads, providing additional thermodynamic data for these operating conditions. The experimental as well as the numerical part of the project are characterized by the use of highly specific experimental test rigs and simulation methods.

1.2 Purpose of the project

The scope of this project is the understanding and the numerical characterization of High-Pressure Direct Injection combustion of gaseous fuels in a spark ignited context. To this end, the specific expertise of two research institutes (Empa and IFS of the University of Stuttgart) is combined to address the challenges in this research. Empa's task is to develop fundamental numerical and experimental data and IFS is transferring the findings to a running single-cylinder engine. With the results of this more fundamental project, it will later be possible to design a proper setup (injection system, ignition system, charge motion) for a heavy-duty engine in the highly relevant 300-400 kW class.

An optically accessible Rapid Compression Expansion Machine (RCEM) is used to perform fundamental investigations of the jet evolution under highly under-expanded conditions. An optically accessible ignition chamber at Empa as well as a fibre-optic spark plug installed in the RCEM is used to apply Spark Induced Breakdown Spectroscopy (SIBS), enabling characterization of the state of mixing at spark timing and at spark plug location. At the IFS of Stuttgart University, a full-metal single-cylinder research engine is employed to provide additional insights for a wide range of operation under engine conditions. These synergistic experimental investigations are supported by numerical simulations also performed at Empa to complement and support the fundamental findings and model developments.

1.3 Structure of the project

The project is structured in five work packages which consist of the following activities:

WP1: Encompasses measurements in the optically accessible ignition cell to characterize fuel/air mixtures at ignition location, as well as measurements in the RCEM to characterize jet evolutions, ignition and combustion behaviour. The outcome of WP1 is a detailed knowledge of the jet evolutions, ignition and mixing dynamics under engine relevant conditions.

WP2: Beside the experiments, 3D-CFD models are developed for highly under-expanded jets. The availability of numerical results at high resolution in space and time over the entire domain is exploited to complement the experimental findings, providing additional insights to the non-reactive and reactive processes of under-expanded jets.

WP3: The experimental campaign is carried out at a reinforced single-cylinder passenger car engine at IFS of the University of Stuttgart. This investigation covers the H_2-DI-Injection for homogenous and stratified part load operation as well as jet guided, spark ignited operation at higher loads. Outcomes of WP4 are integral measurements of H_2 DI processes in the single cylinder research engine.

WP4: Deals with the joint analysis of experimental data from all test rigs at the two research institutes in conjunction with numerical results providing additional insights. The combination of all techniques allows for synergies in data interpretation and provides insights with respect to the processes taking place.

WP5: presents an assessment of the potential of the proposed strategy. Additionally, the potential role of hydrogen in the future Swiss energy system is assessed qualitatively.

1.4 **Objectives**

The objectives of the present project are:

- Understanding / modelling of the injection and mixing process for hydrogen direct injection at high cylinder pressure levels, shortly before ignition
- Understanding / modelling of the injection and mixing process for hydrogen direct injection at combustion modes with early injection at diluted conditions
- Development, application and validation of appropriate CFD-based simulation tools for future use to design best concepts for this combustion mode in H_2-engines
- Development of a fibre-optic SIBS measurement technique suitable to detect the air-fuel equivalence ratio between the spark plug electrodes at time of ignition, transfer of the method to the RCEM
- Simultaneous high-speed imaging data of under-expanded jets and combustion (Schlieren, OH* chemiluminescence) from the RCEM in combination with thermodynamic data providing deep understanding of H_2-HPDI combustion process at engine relevant conditions
- Development of optimal injection strategies for high pressure injection of H_2
- Assessment of limits of knock-free operation with jet-guided mixture formation
- Assessment of efficiency potentials and power density (BMEP levels) for the different combustion modes
- Proposal of a concept for efficient H_2 engines, with a special focus on heavy-duty applications, which has to be addressed at a next stage

The research questions include gaining insights w.r.t. the combustion process for H_2-HPDI and optimal engine operation, as well as how to use the experimental data for the development and validation of numerical models, useful for optimization of future H_2-HPDI combustion systems.

The developed measurement techniques together with the experience gained from the experimental characterization can guide the development and commercialization of new equipment for H_2-HPDI combustion. These measures ensure an efficient transfer of the project results into industrial application.

This project focuses on the work performed at Empa (Work Packages 1, 2, 4 and 5). Work package 3 was performed at the University of Stuttgart, funded by AiF (Germany). A detailed description including WP3 is published by FVV (final report of the project "High-efficiency combustion process for hydrogen-based fuels", project number 1446).

2 Facilities, procedures and methodology

This chapter describes the facilities, procedures and methodologies for the hardware-centered work packages 1, 2 and 3.

WP1 deals with the fundamental investigations of under-expanded jet flow field evolutions, the state of mixing (the air-fuel-equivalence ratio) at ignition timing and the characterization of the ignition and combustion process. This work package is divided into two tasks, one to be performed at a constant volume cell setup, and the other at a Rapid Compression Expansion Machine (RCEM).

Spark Induced Breakdown Spectroscopy Method

Task 1.1 is dedicated to characterize air/fuel mixtures at spark timing and at spark location by applying Spark Induced Breakdown Spectroscopy (SIBS) in an optically accessible ignition chamber. Figure 1 shows a schematic of Empa's constant volume ignition cell used for SIBS development[26,27,28]. This test rig allows direct optical access with intensified high-speed diagnostics and further enables calibration of a fibre-optic spark plug employed concurrently. Figure 2 shows the spark plug equipped with fibre optics and the simultaneous application of the standard optical access. A validation of the fibre-optic spark plug technique was performed for methane combustion[28]. Results confirm that the same trends are obtained for both setups, in all the tested conditions.

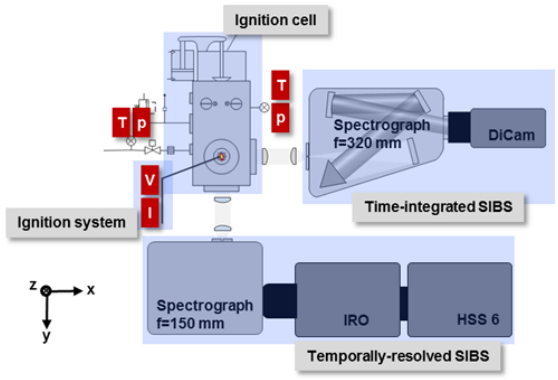

Figure 1: schematic of the ignition cell installed at Empa for SIBS investigations

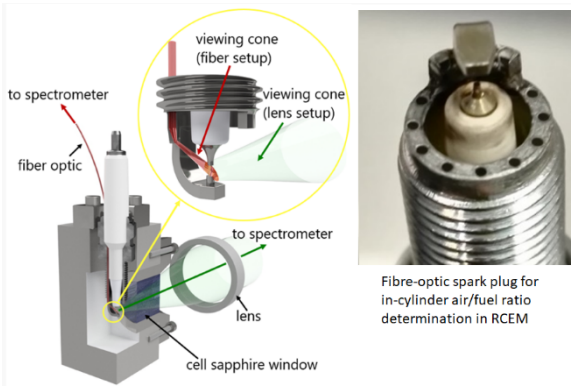

Figure 2: schematic of simultaneous application of full optical access and fibre-optic spark plug

A typical inductive ignition system's discharge process is divided into three phases: breakdown, arc discharge, and glow discharge. During the breakdown phase, a highly conductive plasma channel is formed between the spark electrodes. The plasma temperature is high enough to dissociate and ionize the molecules in the spark channel. This temperature decreases with time down to values in the order of the adiabatic flame temperature, due to plasma expansion and recombination phenomena, while ionization and dissociation energy are transformed into thermal energy (arc phase). After the arc phase, a glow discharge can be formed and maintained for several milliseconds due to the secondary coil in a conventional spark-ignition system. Due to the transient nature of spark-induced plasmas, the atomic

[26] T. Kammermann, W. Kreutner, M. Trottmann, L. Merotto, P. Soltic, D. Bleiner, Spark-induced breakdown spectroscopy of methane/air and hydrogen-enriched methane/air mixtures at engine relevant conditions, Spectrochimica Acta Part B: Atomic Spectroscopy. 148 (2018) 152–164.

[27] T. Kammermann, L. Merotto, D. Bleiner, P. Soltic, Spark-induced breakdown spectroscopy for fuel-air equivalence ratio measurements at internal combustion engine-relevant conditions, Spectrochimica Acta Part B: Atomic Spectroscopy. 155 (2019) 79–89.

[28] L. Merotto, T. Kammermann, P. Soltic, Ignition Diagnostics in EGR- and Air-diluted Methane/Air Mixtures Using Spark Induced Breakdown Spectroscopy, Combustion Science and Technology. (2019) 1–16.

and ionic populations rapidly evolve with time and location. As a consequence, the spectra emitted by the plasmas vary significantly, depending upon the observation time after the breakdown. At early times (up to a few microseconds after ignition), the plasma emission consists of an intense continuum, characteristic of the emission of hot free electrons in the presence of positive ions, that decreases with time. At later times, emission lines due to the radiative decay of excited species dominate the radiation process as the plasma cools and expands, thus the broad ionized lines gradually disappear and are replaced by emissions from excited neutral atoms[29]. Plasma-cooling eventually results in recombination to form lower energy species, emitting at own characteristic wavelengths. Consequently, a proper selection of the gating strategy allows gaining different information from the same event (atomic emissions at earlier times, molecular emissions some microseconds after breakdown).

From the SIBS spectral response, the local fuel/air ratio of different fuels such as methane[30], hydrogen[31,32], propane and isooctane[33] can be derived. Therefore, spectral emissions from the plasma formed between the spark plug electrodes due to electrical discharge are a fingerprint of the local gas composition and their features (relative peaks intensity and peaks width) can be correlated with the local A/F ratio in the ignition location[34],[26]. Since fuel concentration at ignition timing is one of the most critical parameters in determining not only successful ignition, but also flame stability, and ultimately engine performance, efficiency, and emissions, a pointwise measurement of fuel concentration at ignition location is highly interesting.

Task 1.1 focuses on the testing of air/hydrogen mixtures having different air-to-fuel ratios at density conditions relevant to engine applications. Atomic emissions from hydrogen (656 nm), oxygen (777 nm) and nitrogen (746 nm) are measured, and their spectral features are correlated to the mixture A/F ratio. Subsequently, a validation is carried out with the fibre-optic spark plug by comparing the simultaneous measurement obtained by the standard optical path measurement and by the fibre optic setup. Finally, the fibre-optic spark plug SIBS is transferred to the RCEM rig, allowing the measurement of local mixture composition at the ignition location under engine relevant conditions. The possibility to quickly detect the A/F ratio at the ignition location offered by the SIBS technique is of major interest to obtain valuable information on the conditions at the spark location.

Rapid Compression Expansion Machine Test Rig

Task 1.2 focuses on the morphology evolutions of under-expanded jet, which will be characterized experimentally in an optically accessible Rapid Compression Expansion Machine (RCEM) under non-reactive and reactive conditions for various pressure levels and pressure ratios.

Figure 3 provides a schematic of the RCEM, which has a pneumatic/hydraulic driven free moving piston. Excellent optical access to the combustion chamber is possible through the piston as well as the cylinder head via lateral windows. The test rig is perfectly suited for the characterization jet morphology evolution

[29] M. Sabsabi, P. Cielo, Quantitative Analysis of Aluminum Alloys by Laser-Induced Breakdown Spectroscopy and Plasma Characterization, Applied Spectroscopy. 49 (1995) 499–507.
[30] N. Kawahara, E. Tomita, S. Takemoto, Y. Ikeda, Fuel concentration measurement of premixed mixture using spark-induced breakdown spectroscopy, Spectrochimica Acta Part B: Atomic Spectroscopy. 64 (2009) 1085–1092.
[31] K.M. Rahman, N. Kawahara, D. Matsunaga, E. Tomita, Y. Takagi, Y. Mihara, Local fuel concentration measurement through spark-induced breakdown spectroscopy in a direct-injection hydrogen spark-ignition engine, International Journal of Hydrogen Energy. 41 (2016) 14283–14292.
[32] M.K. Roy, N. Kawahara, E. Tomita, T. Fujitani, Jet-guided combustion characteristics and local fuel concentration measurements in a hydrogen direct-injection spark-ignition engine, Proceedings of the Combustion Institute. 34 (2013) 2977–2984.
[33] T.D. Fansler, B. Stojkovic, M.C. Drake, M.E. Rosalik, Local fuel concentration measurements in internal combustion engines using spark-emission spectroscopy, Applied Physics B: Lasers and Optics. 75 (2002) 577–590.
[34] Abdul Rahman, M.T., et al., *Visualization and concentration measurement of a direct-injection hydrogen jet in a constant-volume vessel using spark-induced breakdown spectroscopy.* International Journal of Hydrogen Energy, 2014. **39**(31): p. 17896-17905.

by means of Schlieren imaging, as well as ignition and combustion by means of high-speed chemiluminescence (OH*) imaging. The variable initial and final position of the free-floating piston in conjunction with variable driving pressures enable wide ranges of engine relevant pressure/temperature evolutions during the compression stroke. A schematic of the simultaneous application of Schlieren imaging along the line of sight and OH* chemiluminescence is shown in Figure 4.

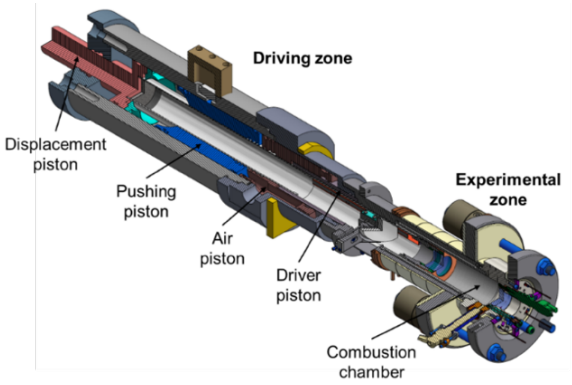

Figure 3: Schematic of the Rapid Compression Expansion Machine (RCEM)

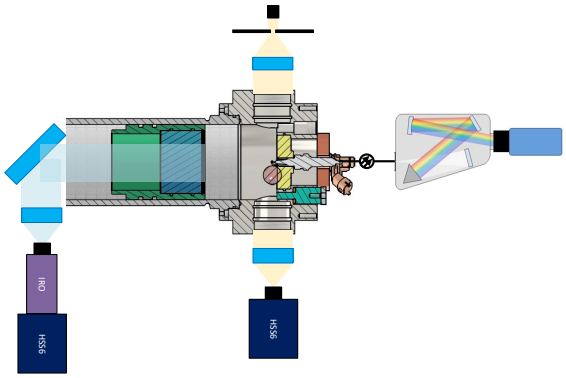

Figure 4: Schematic of simultaneous Schlieren, OH* chemiluminescence and SIBS imaging in RCEM

The processes after ignition, namely combustion of the jet for the jet-guided conditions or flame propagation for the low-load partially premixed conditions, is also investigated in Task 1.2. In addition to the optical high-speed imaging techniques, pressure indication is carried out to obtain pressure traces and heat release rates.

The fibre-optic spark plug employed in Task 1.1 is used as an ignition source. It is important to note, that the high-pressure jet carries significant momentum and exhibits high velocities. Significant turbulence is produced in the shear layer which is likely to contribute to increased ignition delay, cycle to cycle variations and might even result in failure of the ignition attempt. Therefore, under such challenging conditions, the risk of flame extinction due to the hydrogen jet needs to be taken into account. If quenching problems arise, the robustness of ignition will be improved by replacing the standard (inductive) ignition system with a Nanosecond Repetitively Pulsed Discharge (NRPD) system able to "chase" the flame and prevent quenching. In such a system, a pulse generator delivers to the spark plug short duration pulses (pulse rise time < 4 ns, maximum pulse energy 30 mJ, repetition rate up to 100 kHz), leading to the formation of a non-equilibrium plasma between the electrodes. The sharp increase of voltage in such a nanosecond-ignition system (rise times in the order of nanoseconds) results in efficient deposition of the discharge energy in highly non-equilibrium states of molecules, leading to radicals formation, which is further promoted through collisions with excited species. These processes induce very favourable conditions for ignition and combustion[35,36] . The promising potential of NRPD ignition in IC engines at high pressure conditions has been investigated by several researchers, showing its effectiveness in improving ignitability, flame stabilization, and engine

[35] Starikovskaia, S.M., *Plasma assisted ignition and combustion.* Journal of Physics D: Applied Physics, 2006. 39(16): p. R265-R299.
[36] Tropina, A.A., et al., *Comparative Analysis of Engine Ignition Systems.* Ieee Transactions on Plasma Science, 2009. 37(12): p. 2286-2292.

performance, as well as in extending engine operation to leaner mixtures[36,37,38,39,40] , and thus offering a promising solution for challenging ignition conditions. In the framework of the present project, the NRPD ignition system could be integrated in the RCEM test rig to provide insight on the possibility of promoting stable ignition of the hydrogen jet.

Computational Fluid Dynamics

Three-dimensional Computational Fluid Dynamics activities were carried out in **WP2** for non-reacting underexpanded hydrogen jets and for reactive conditions in the RCEM, thereby complementing activities in WP1. STAR-CCM+, licensed by SIEMENS has been used, a highly versatile, finite volume Computational Continuum Mechanics solver, capable of handling time-varying complex geometries. STAR-CCM+ further features a comprehensive real gas framework. As discussed in [41], due to the high-pressure injection, real-gas properties must be accounted for. These include not only a real gas variant for the equation of state (governing largely the momentum flux and hence the injected mass and jet penetration), but also a correction term in the enthalpy transport equation to account for real gas caloric properties. The modified Soave-Redlich-Kwong real gas equation of state has been adopted as in a previous FVV project[42].

A RANS framework is followed using the RNG variant of the two-equation k-epsilon turbulence model. Combustion is modeled using the Turbulent Flame Speed Closure approach, which can treat premixed, non-premixed and auto-ignition phenomena, which can all be expected in dependence of the specific operating condition.

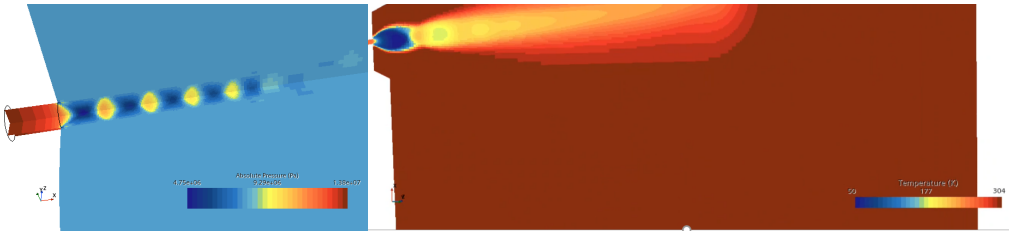

Figure 5: Pressure distribution at pressure ratios of ca. 2 on the left and temperature distribution at pressure ratios of ca. 8.

From the preliminary simulations shown in Figure 5, STAR CCM+ is capable of resolving the physics of highly under expanded jets. Several experimental and numerical works have shown that the Pressure Ratio (PR) effects the near-nozzle jet behavior the most. At low PR, the jet is moderately under expanded and it is characterized by a series of diamond-shaped shocks (left in Figure 5) while at PR above ca. 4 the jet becomes highly under-expanded and is characterized by a barrel shaped structure as shown in the right in Figure 5 [43]

[37] Cathey, C.D., et al., *Nanosecond plasma ignition for improved performance of an internal combustion engine.* Ieee Transactions on Plasma Science, 2007. 35(6): p. 1664-1668.
[38] Pancheshnyi, S.V., et al., *Ignition of propane-air mixtures by a repetitively pulsed nanosecond discharge.* Ieee Transactions on Plasma Science, 2006. 34(6): p. 2478-2487.
[39] Shiraishi, T., T. Urushihara, and M. Gundersen, *A trial of ignition innovation of gasoline engine by nanosecond pulsed low temperature plasma ignition.* Journal of Physics D: Applied Physics, 2009. 42(13): p. 135208.
[40] Starikovskiy, A. and N. Aleksandrov, *Plasma-assisted ignition and combustion.* Progress in Energy and Combustion Science, 2013. 39(1): p. 61-110.
[41] V.D. Sakellarakis, Mixing and Autoignition of Underexpanded Methane Jets at High Pressure Conditions, ETH Zurich, 2020. https://doi.org/10.3929/ETHZ-B-000474652.
[42] W. Vera-Tudela, et. al., Final report FVV project 1236 “Gas Diesel Combustion,” (2020)
[43] H.L. Yip, A. Srna, X. Liu, S. Kook, E.R. Hawkes, Q.N. Chan, Visualization of hydrogen jet evolution and combustion under simulated direct-injection compression-ignition engine conditions, International Journal of Hydrogen Energy 45 (2020) 32562–32578. https://doi.org/10.1016/j.ijhydene.2020.08.220.

Single Cylinder Engine Experiments

In **WP3**, experimental investigations on a single-cylinder unit are carried out at IFS of the University of Stuttgart. For this purpose, a single cylinder unit provided by Daimler AG is reinforced and upgraded for operation at combustion chamber peak pressures of up to 160 bar. The fuel supply and measuring system (Coriolis) are selected and modified for hydrogen operation. The used HPDI injector is the Bosch HDEV 4 outward opening piezo injector. A crankcase ventilation using an electrically driven disk separator is used to prevent the formation of explosive mixtures in the crankcase.

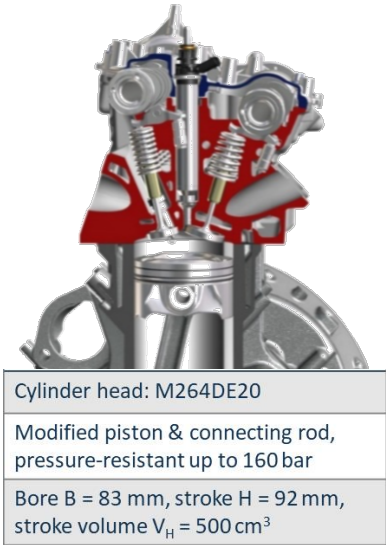

Figure 6: Single cylinder engine, M2654DE20

Figure 6 shows a sectional view of the engine and the main data of the aggregate. A predecessor of this engine was already used in FVV projects 1126 and 1213 (methane-fuels I + II) and papers therefrom[44,45,46,47,48,49,50,51,52] . The specifications of the test bench as well as the most important measurement technology are shown in Table 1.

[44] Urban, L., et al., *Ansatz für die Klopfmodellierung methanbasierter Kraftstoffe auf Basis reaktionskinetischer Untersuchungen*, in *16. Tagung "Der Arbeitsprozess des Verbrennungsmotors"*. 2017: Graz - Austria.
[45] Bargende, M., M. Eberbach, and S. Hann, *Final report FVV project 1213 "Methane Fuels II : Combustion Modelling"*. 2019: FVV e.V.
[46] Bargende, M., S. Scharlipp, and L. Urban, *Final report FVV project 1126 "Methane Fuels: Potentials and Characteristic Numbers"*. 2015: Würzburg.
[47] Eberbach, M., H.-J. Berner, and M. Bargende, *Methanbasierte Kraftstoffe und hochoktanige Flüssigkraftstoffe bei klopfender Verbrennung*, in *13. Tagung Gasfahrzeuge*. 2019: Stuttgart, Germany.
[48] Hann, S., et al., *Influence of Binary CNG Substitute Composition on the Prediction of Burn Rate, Engine Knock and Cycle-to-Cycle Variations.* SAE Int. J. Engines, 2017. **10**(2): p. 501-511.
[49] Bargende, M., S. Scharlipp, and L. Urban, *Knocking Characteristics of Methane Based Fuels 2016*, in *JSAE Annual Congress (Spring)*. 2016: Yokohama - Japan.
[50] Scharlipp, S., et al., *Klopfeigenschaften methanhaltiger Kraftstoffe*, in *10. Tagung Gasfahrzeuge; Stuttgart, .* 2015.
[51] Scharlipp, S., L. Urban, and M. Bargende, *Methane Based Fuels: Potential Study and Key Figures*, in *JSAE Annual Congress (Spring)*. 2016: Pacifico Yokohama, Japan.
[52] Urban, L., et al., *Simulation of Autoignition, Knock and Combustion for Methane-Based Fuels.* SAE Technical Paper No. 2017-01-2186, 2017.

Table 1: Specification of test bench

Dynamometer	
type	Horiba Dyna LI 145
max power	145 kW
max speed	10000 min^{-1}
max torque	308 Nm
automatisation	D2T Morphee 2
Pressure Transducer	
type HP	Kistler 6061B
type LP (inlet)	Kistler 4045A
Type LP (outlet)	Kistler 4075A
ECU	
type	IAV FI2RE
Exhaust gas measurement	
Typ	Horiba Mexa 7100

External charging System	
type	screw compressor
boost pressure	3 bar abs.
Indicating System	
type	AVL 631 / Indicom
resolution	0,1°KW
Gas Supply H2	
max pressure	200 bar
max flow	30Nm^3/h
conditioning units	
coolant	temperature
charge air	pressure, temp.
EGR	temperature

This engine represents a passenger car engine geometry. However, the goal of this project is to derive a proof of concept and the understanding of a predominantly diffusion-controlled combustion of hydrogen and it is therefore not important, on which engine geometry this proof is performed.

3 Activities and results

The activities performed in the present project are summarized in the following paragraphs of this Section. A detailed discussion of the results is provided in Section 4.

3.1 WP1 (Optical Research) Activities and results

In WP1, tests were performed to investigate the fuel/air mixtures at the ignition location and to characterize the jet evolutions, ignition and combustion behaviors.

The main focus of the present project is on jet-guided ignition and combustion of pure hydrogen, but methane and a mixture of methane (80% vol.) and hydrogen (20% vol.) were also tested for comparison.

After re-commissioning and adapting the RCEM setup with Schlieren and OH chemiluminescence visualization techniques, and after selection and calibration of the injector type to be used for the test campaign, a spectroscopy (SIBS) method was transferred to the RCEM setup.

The ignition and combustion of hydrogen jets was characterized in a test campaign, in which different combustion modes were investigated (premixed, partially premixed and jet-guided or diffusion-controlled), showing that injection at the periphery of hydrogen jets is successfully obtained also in very lean overall conditions. Heat release rate analysis allowed gaining interesting insights on the premixed and diffusive phases of the jets combustion. Indications were derived as to how to optimize hydrogen jet-guided combustion in a future work, and the results were compared to WP3 results. Additionally, NRPD ignition was tested and discussed in comparison to standard coil ignition.

3.2 WP2 Numerical Research Activities and results

Various computational setups of the RCEM have been constructed with fixed and moving geometries and varying levels of detail.

In Task 2.1 first non-reactive HPDI simulations at different injection pressures were carried out and compared to the experimental results. It was seen, that mesh resolutions around 10 µm and time-steps of the order of 10^{-8} seconds are necessary to correctly capture the physics of the fully under-expanded jet structure and run-times amount to weeks on hundreds of CPUs for several milliseconds of physical time. The simulations overpredict the mass flow rate considerably for the prescribed (nominal) injection and back pressures and estimated nozzle orifice diameter (no geometric details of the injector interior are available). Since the injector was originally designed for liquid fuels, it is probable that the pressure at the orifice outlet differs considerably from the upstream nominal pressure due to nozzle-internal pressure drops. The mass flow rates were hence estimated from the experimental heat release rate during the mixing-controlled phase of the combustion and different combinations of injection pressure and discharge coefficient were compared showing good agreement with the measured value.

Reactive simulations have further been carried out for two premixed cases with hydrogen at different equivalence ratios. The Turbulent Flame Closure (TFC) combustion model was used "out of the box" in conjunction with detailed hydrogen chemical kinetics (Warnatz). While the trends are well captured for both equivalence ratios, discrepancies in the pressure evolutions are nonethelessstill apparent. A model was developed for jet-guided combustion, also using the TFC combustion model in conjunction with a table for the laminar flame speed and adaptive mesh refinement based on combustion quantities. .

3.3 WP3 (Single Cylinder Engine Experiments) Activities and results

WP3 deals with the experimental investigation of the single-cylinder unit at IFS. Three direct injection operating modes are investigated. First, homogenous operations are present when the fuel is injected during the intake stroke or during the early compression stroke. Second, stratified operations are

achieved with injections later during the compression stroke but still with EOI before ignition. Third, jet-guided operations are defined for experiments where the ignition is during (or before) the injection.

At high lambda, stratified combustion results in a faster HRR when compared to premixed ones. The HRR for jet-guided operations is highly non-symmetrical. The hydrogen slip increases in jet-guided operations. The HRR in jet-guided operations presents a premixed peak affected by the delay between SOI and ignition (the longer, the higher). After the premixed peak, a rather constant HRR is present, lasting till EOC. After EOC, a tail of HRR is present, lasting longer the lower the lambda. At stoichiometric conditions, the tail of the HRR lasts till EVO, and the hydrogen slip emissions are the highest. The high-pressure gradients present in jet-guided operations result in pressure oscillations that can be reduced (or suppressed) with proper injection and ignition timings.

Due to temperature limitations of the experimental setup, only low-medium loads are tested. The knock limit in premixed operations is, therefore, not reached. The suppression of the knock phenomenon in jet-guided combustion is thus not seen.

3.4 **WP4 (Joint Data Anaysis) Activities and results**

A detailed joint data analysis was performed of the experimental results obtained in WP1 and WP3.

It was concluded that similar findings are achieved in WP1 and WP3 despite the different test rigs and injectors used. The RCEM experiments have highlighted fundamental insights into hydrogen jet-guided combustion, while the experiments performed in the single-cylinder engine have shown the practical feasibility of this combustion concept while highlighting some limitations, such as high temperatures and incomplete combustion due to stoichiometric operations being impossible to investigate in the RCEM. The cooperation between Empa and the University of Stuttgart has outlined procedures to control the heat release rate shape and cope with the pressure oscillations that can rise due to the high-pressure gradient present when a high HRR is present at the beginning of the jet-guided combustion. Some results are presented in Section 4.1.12. A detailed discussion is published by FVV (final report of the project "High-efficiency combustion process for hydrogen-based fuels", project number 1446).

3.5 **WP5 (Assessment) Activities and results**

WP5 is a work package, which tries to put the project results and hydrogen as a potential important future fuel into a bigger picture. The results can be found in the next chapter.

4 Detailed results and discussion

4.1 **Work Package 1: Optical Experiments**

4.1.1 Selection of gas mixtures

One side question of the project is, if such a jet-guided combustion concept, which is described later, can be directly transferred also to methane combustion, or to hydrogen/methane mixtures. Therefore, some experiments were performed with gas mixtures. The selection of the CH_4/H_2 gas mixtures was performed in cooperation with IFS, taking into account the characteristics of the gases, their energy content and the energy share in the mixture.

The Wobbe index of the mixture was taken into account in order to estimate the fesibility of injection equiplent to work gases of changing compositions. The Wobbe index is an indicator of fuel gases interchangeability:

$$I_W = \frac{LHV}{\sqrt{\rho_{std}/\rho_{air,std}}}$$

The Wobbe index of a methane/hydrogen mixture is shown in Figure 7. It can be seen that a CH_4/H_2 mixture containing at least 80 vol% of hydrogen has a Wobbe index similar to that of pure hydrogen. If the mixture energy share is taken into account (Figure 8), it can be seen that pure methane has a LHV of 50 MJ/kg, which is similar to that of a CH_4/H_2 mixture having 91% hydrogen in volume (55.76% in mass).

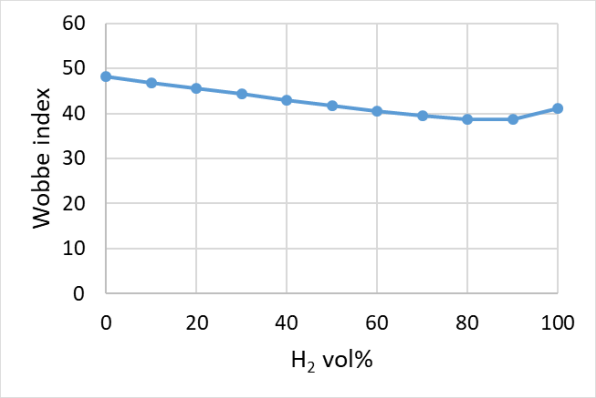

Figure 7: Wobbe index of a CH_4/H_2 mixture vs. its hydrogen volume content

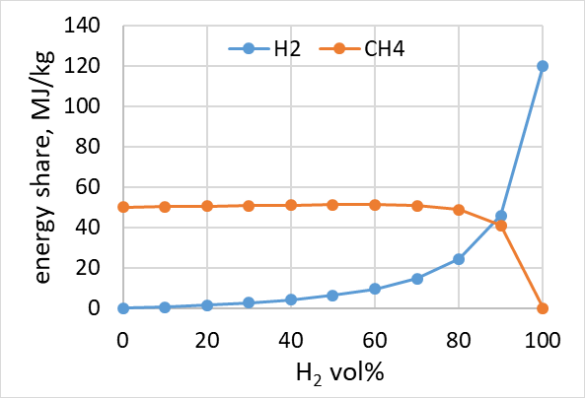

Figure 8: energy share of a CH_4/H_2 mixture vs. its hydrogen volume content

Also the air needed for burning the fuel mixture must be taken into account. The stoichiometric air demand per fuel mass is shown in Figure 9, together with the mixture lower heating value, vs. the mixture methane content.

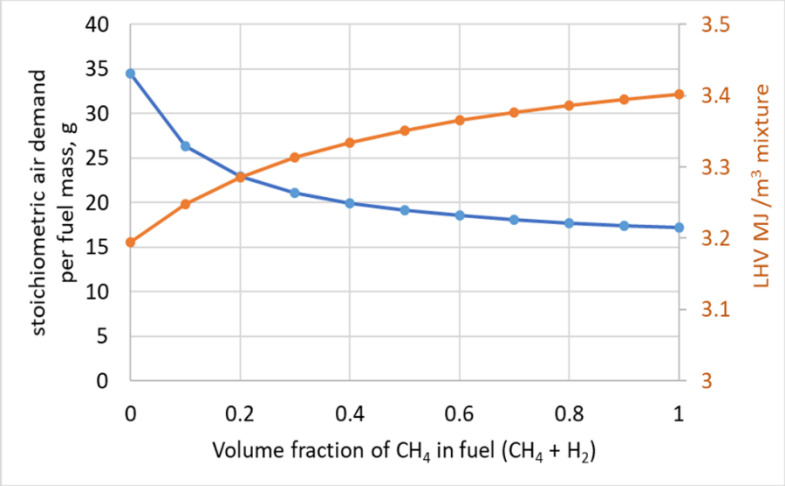

Figure 9: Stoichiometric air demand per fuel mass and mixture LHV vs. mixture methane content

Compared to pure methane, the stoichiometric intake mixture heating value of pure hydrogen is reduced by almost 6%, while this reduction is only 0.6% for 20% vol. H_2 in fuel. The stoichiometric air demand is increased by + 53% when 90% vol. fuel is H_2, by +3% for 20% vol. H_2 in fuel.

Taking into account the aforementioned results, the mixtures selected for the experimental tests in the framework of the present project are pure hydrogen, pure methane and 20% H_2 in CH_4. Depending on the intermediate results, an additional mixture (5% CH_4 in H_2) can also be tested.

4.1.2 Injectors selection and calibration

The injectors used for the RCEM experiments was a Bosch HDEV1 gasoline injector. This is a single-hole injector with a non-axial orifice of 0.60 mm diameter. Single-hole is chosen in order to enable an unambiguous jet pattern interpretation for the line-of-sight optical measurement techniques. A non-axial orifice was chosen in order to be able to vary the jet orientation by turning the injector. A schematic of HDEV1 is shown in Figure 10.

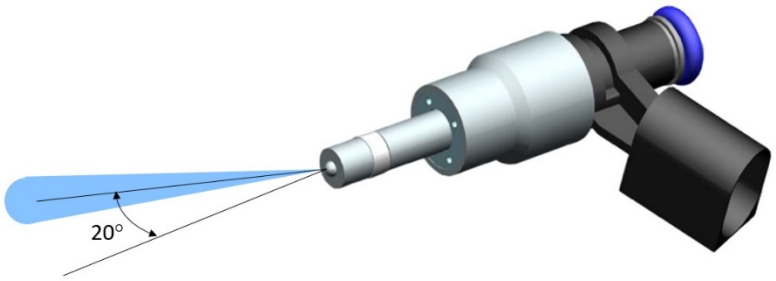

Figure 10: schematic of HDEV1 injector

The injector's jet cone was measured by videorecording the exiting jet when a colored liquid is injected and then analyzing the frames to estimate the cone angles. An example is shown in Figure 11. Results showed that the apparent inclination angle of the injector hole with respect to the injector symmetry axis (γ) is 20°.

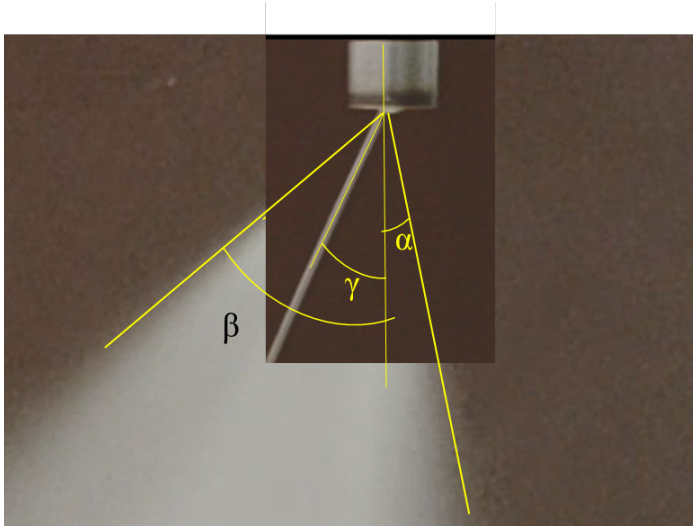

Figure 11: Determination of injection cone (HDEV1 type A injector). Since the injection cone is not symmetric with respect to the injector axis (α+β), images were recorded from different angles in order to determine the orientation γ of the injector hole with respect to the injector axis

Before using the injector in the RCEM, a calibration needs to be performed in the constant volume cell to assess the mass flow vs. injection duration when a gaseous fuel is used. In order to characterize the selected injector, an adapter (Figure 12, left) was designed and manufactured to mount the injector in the constant volume cell (Figure 12, right).

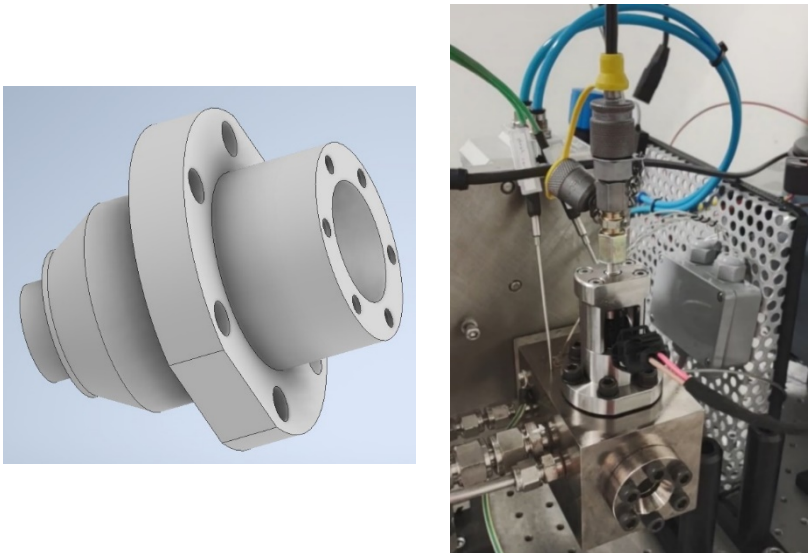

Figure 12: Adapter (left)for mounting the injector in the constant volume cell (right)

The pressure rise subsequent to an injection event was then recorded (Figure 13). The value of the pressure rise at 0.4 ms after rising peak was then used in the universal gas law to estimate the injected mass.

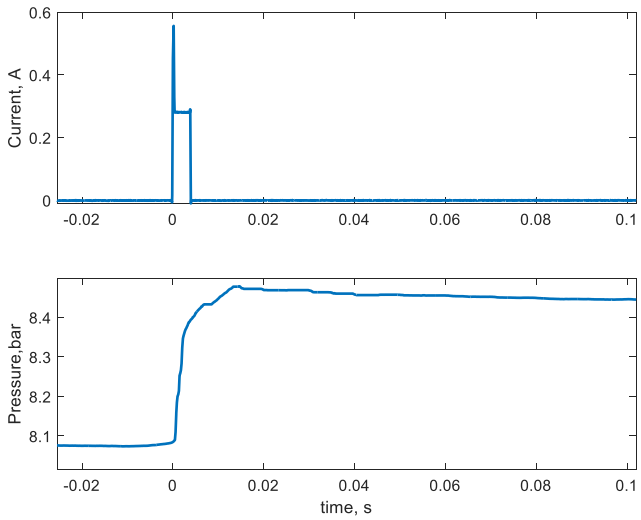

Figure 13: Example of current delivered to drive the injection (top plot) and subsequent pressure rise in the constant volume cell (bottom plot). Injection pressure 90 bar, nitrogen injection.

The HDEV1 injector was calibrated using hydrogen, at injection pressures of 50, 70 and 90 bar. Tests were performed by filling the constant volume cell with air at 2 bar, then injecting the gas 20 times (time between injections: 2 s) and recording the pressure traces.

The results of the injector calibration with hydrogen are shown in Figure 14. The injected mass linearly increases with injection duration, and the trends tends to intercept the axis at zero. Some stochastic effects appear at low injection durations (< 1 ms).

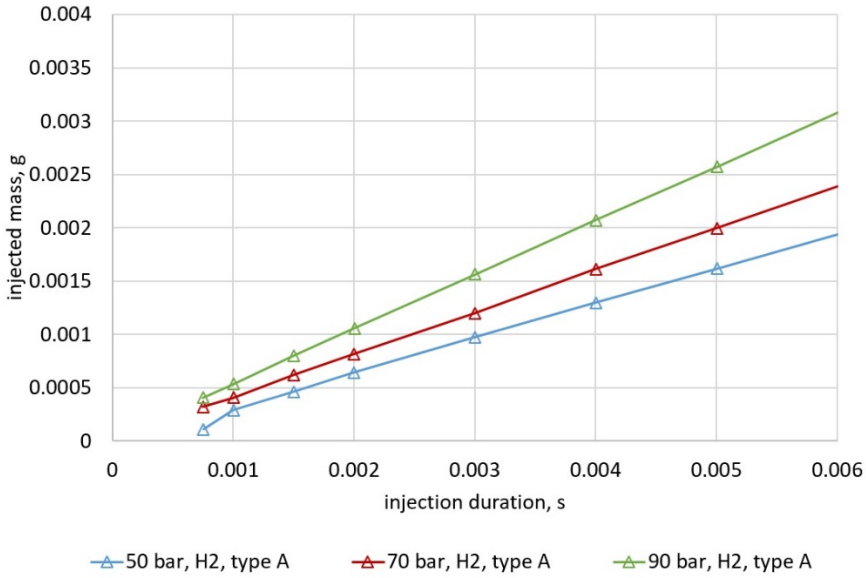

Figure 14: Injected mass vs. injection duration for HDEV type A injectors, at three different injection pressures. Injected gas: hydrogen

The overall mass flow in g/s was calculated for the tested injector, for injection durations in the range 1 ms to 6 ms, and is 0.52 ± 0.01 g/s for hydrogen at 90 bar injection pressure.

Since in the RCEM, the injection pressures is of 110 Bar, which is higher then the maximal injection pressure that can be tested in the CVC due to hardware limitations the calibration results are used to assess the most meaningful conditions for the RCEM test campaign.

The injected mass in the RCEM is measured based on the pressure rise in the RCEM when the piston is at BDC (premixed case). Since for equal energizing time of the injector's coil, the injected mass shows negligible scatter for the jet-guided experiments, the mass of fuel injected is assumed to be the same as for the premixed cases (for the same injection duration). This assumption is valid if always choked injections are present, i.e., if the pressure ratio between the pressure at the injector's nozzle and the cylinder pressure is lower than the critical pressure ratio for the entire injection duration.

4.1.3 SIBS method development

With the general aim of understanding the injection, ignition, and combustion in jet-guided mode, the measurement of the mixture concentration (λ) at the ignition location is of significant importance. For this purpose, the light emitted during the electrical discharge is captured, and a spectral emission is performed to estimate the local AFR[53]. The SIBS method allows determining the local mixture concentration at the ignition location by examining the gas spectral emission during the electrical discharge, focusing in particular on the H-alpha (656 nm) line and the atomic oxygen emission at 777 nm. Such method was successfully implemented in the constant volume cell using a lens optical path

[53] Kammermann, Thomas, et al. "Spark-induced breakdown spectroscopy of methane/air and hydrogen-enriched methane/air mixtures at engine relevant conditions." *Spectrochimica Acta Part B: Atomic Spectroscopy* 148 (2018): 152-164.

(Figure 15, left) and a spark plug equipped with fibre optics to directly transfer the emitted light to a spectrograph (Figure 15, right).

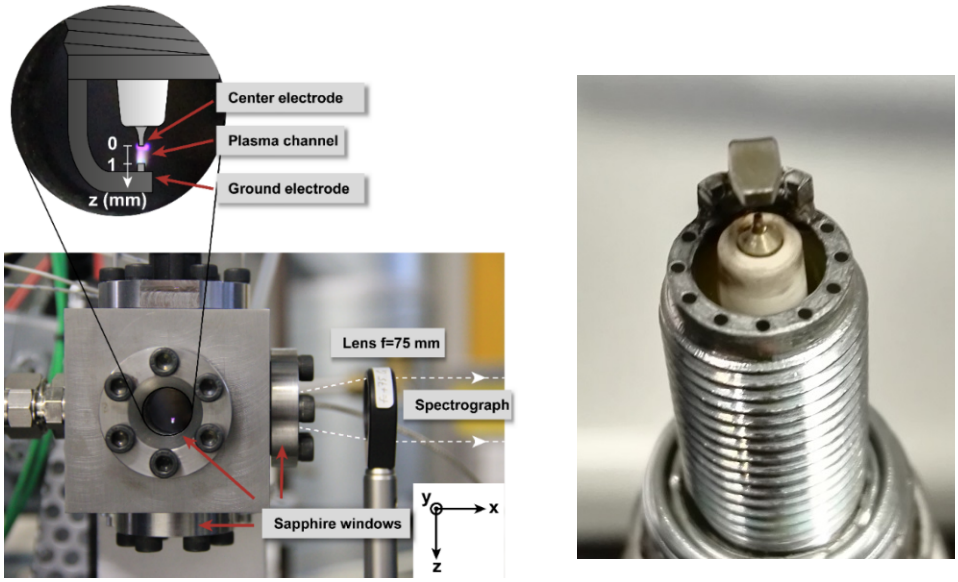

Figure 15: Schematics of the constant volume cell with optical lens setup for spectroscopy measurements (left) and detail of fibre-optics equipped spark plug (right)

The general idea behind the SIBS calibration method is illustrated in Figure 16. The electrical discharge results in a plasma forming between the spark plug electrodes. During the plasma formation, the gas molecules dissociate and ionize. After the discharge, ions and electrons recombine, emitting photons at specific wavelengths. The photons emitted during this relaxation process are then collected at the spectrometer collector and can be analyzed to correlate the spectral features to the parameters of interest, in our case λ.

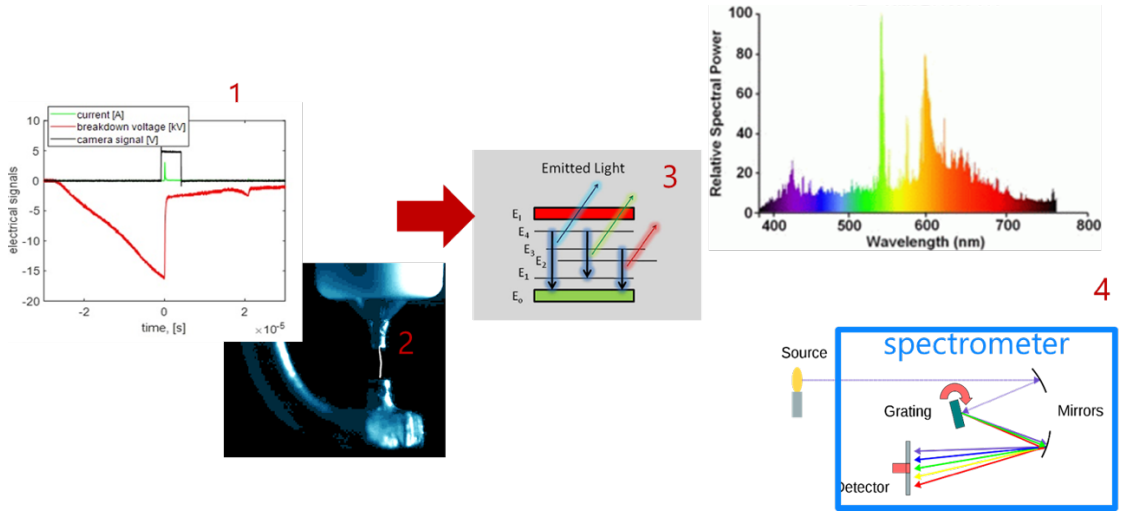

Figure 16: Schematics of the SIBS calibration method

The SIBS technique is calibrated in the CVC at different AFRs using H_2 as a fuel at a pressure of 10 bar and at atmospheric temperatures.

From tests performed with standard coil ignition, the spectra (not reported here) obtained in the RCEM experimental conditions were very weak, making it difficult to resolve the atomic peaks. To allow for better spectral analysis at the ignition location NRPD ignition has been applied, giving the additional benefit to test the difference resulting when higher energy during ignition is provided.

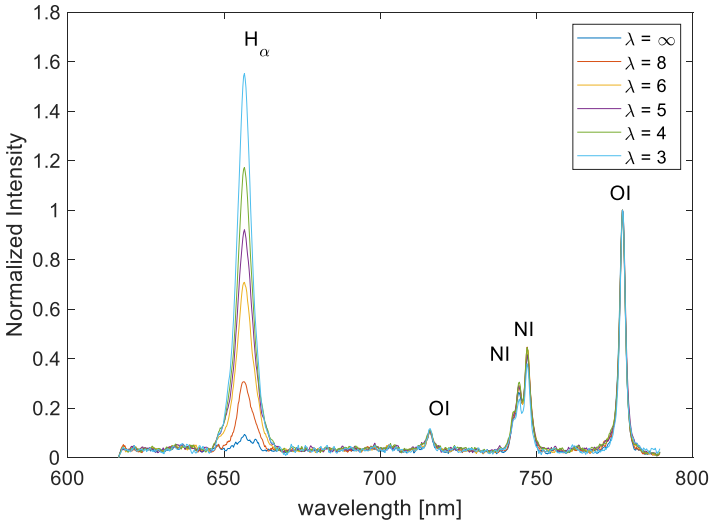

Figure 17: Post-processed SIBS spectra for different λ values

Eleven AFRs are tested in the CVC, starting from air up to a λ of two. For each AFR, the experiments are repeated 20 times for the reactive and 40 times for the non-reactive experiments. The spectra are acquired 400 ns after the breakdown with a 500 ns exposure time. Before calculating the peak ratios, the spectroscopy images are filtered and averaged over the special component; afterward, a baseline is subtracted to eliminate the continuum emission, which exhibits a stochastic variation and would result in wrong AFR estimation if not accounted for.

Figure 17 shows the sum of all the post-processed spectra having the same AFR starting from air up to λ = 3. The spectra are normalized by dividing the spectra by the O (777) intensity. The different atomic emissions are reported on top of the relative peak.

Clear emissions from atomic hydrogen, oxygen, and nitrogen are visible in the analyzed spectral range. The ratio between oxygen and nitrogen remains constant by varying the AFR while their intensity to hydrogen changes. The ratio of emission between hydrogen and oxygen or hydrogen and nitrogen can be used to estimate the AFR.

Results of the SIBS calibration for hydrogen-air mixtures in terms of atomic emission ratios vs. λ are shown in Figure 18 and Figure 19 for H/O and H/N emission ratios, respectively.

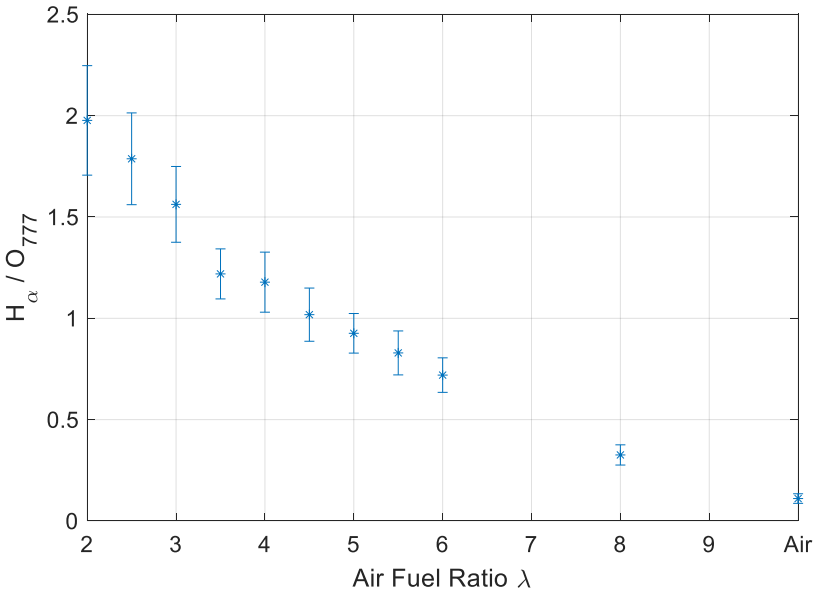

Figure 18: H/O atomic emission ratio vs. λ for the different mixtures investigated

The H/O ratio (Figure 18) decreases with increasing λ. A similar behavior is observed for the H/N ratio (Figure 19).

The standard deviation around the H/O emissions ratio for the tested AFR is 13%. A quadratic regression is fitted to the H/O atomic emission ratio. In the RCEM, a peak ratio of 1 is often measured, which would result in a λ estimation of 4.6 with an uncertainty of ca.± 0.5.

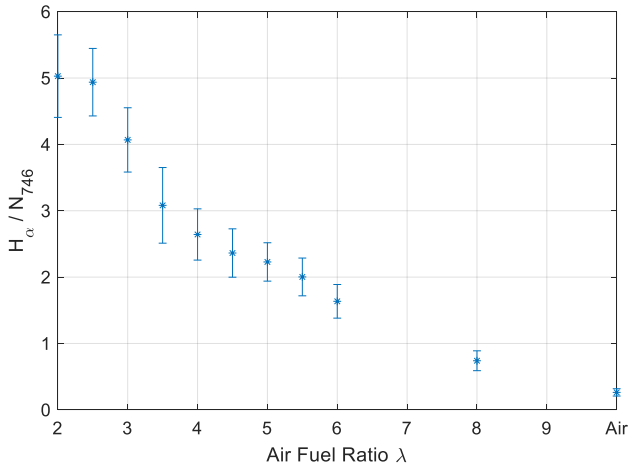

Figure 19: H/N atomic emission ratio vs. λ for the different mixtures investigated

Since the SIBS technique reports an instant composition between the electrodes at ignition timing in the RCEM experiments for jet-guided combustion, due to the turbulence induced by the injection and since the ignition happens at the periphery of the jet, high variability in the AFR for the repetition of the same experiment is expected.

4.1.4 RCEM setup

The DI injection system was integrated in the RCEM and the gas supply of the selected mixtures was set-up. A new cylinder head had to be re-designed and manufactured for the selected injectors to allow simultaneous OH and schlieren imaging while ensuring the possibility of injecting and igniting near TDC. The cylinder head design was discussed in close cooperation with IFS to allow results comparison in the two setups (WP1 and WP3). The sparkplug has been allocated in the middle of the cylinder head axial to the piston, while the injector has been placed tangentially 5 mm below the upper part of the combustion chamber. Figure 20 shows a rendering of the setup during reactive experiments.

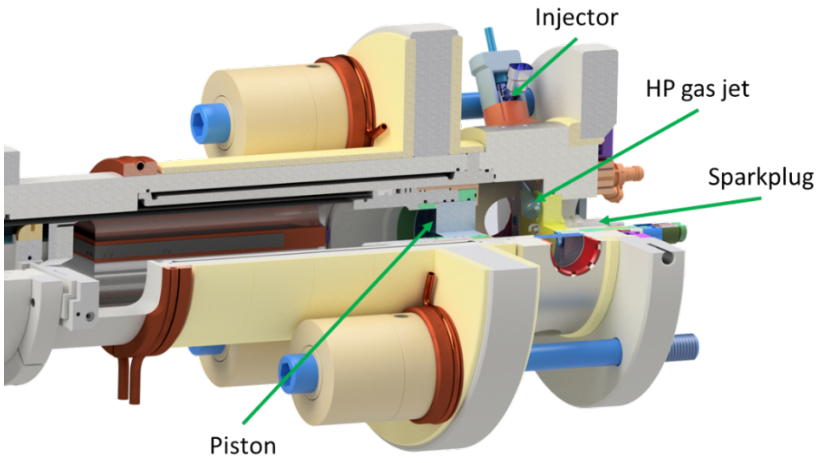

Figure 20: New cylinder head configuration for allocation of HDEV1 injectors. Overall view (left) and detail of the injector cone position (right)

Figure 21 shows the expected jet visualization during the reactive experiments for the OH chemiluminescence and Schlieren imaging, left and right, respectively.

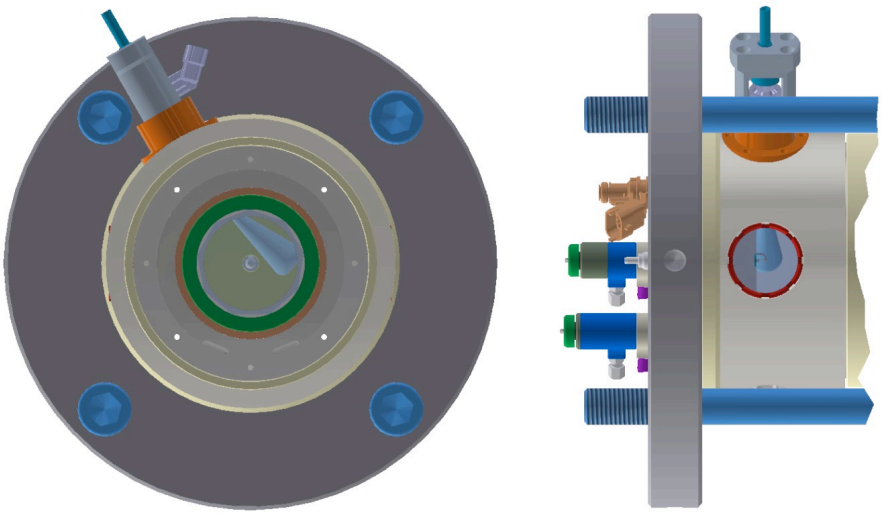

Figure 21: Visualisation trough the piston (left) and side wiew (right)

Additionally, non-reactive optical experiments are performed to characterize the hydrogen jet, where Schlieren high-speed videos are recorded through the piston view, which offers a larger visualization area. In fact the visualization diameter through the piston is 52 mm while through the side is only 36 with the additional disadvantage that the upper part of the head occupies 13 mm of the side window. The sparkplug and holder have been removed and substituted with a glass window to perform the non reactive experiments.

4.1.5 Optical setups

The cylinder head allows for an effective Schlieren visualization. The new Schlieren setup is performed through the two optical windows on the opposite sides of the cylinder head, thus leaving the piston optical access available for OH chemiluminescence visualization only, as shown in Figure 22. This solution optimizes both the area for jet visualization in the Schlieren setup and the angle for OH visualization. As shown in Figure 22, the Schlieren visualization of the combustion chamber allows for a profile view of the spark plug, while the OH chemiluminescence provides a frontal view.

Ad hoc optical equipment and supporting structures were designed and acquired based on the needed configuration for the Schlieren setup. A Xenon Nova lamp for Schlieren visualization was used. For the OH chemiluminescence visualization, an UV lens and a 310 nm bandpass filter were used.

The designed optical setup also includes the possibility of simultaneously acquiring spectroscopy measurements in the ignition location. SIBS will be performed using a fibre-optics spark plug and a dedicated spectrometer, as described in Section 2 and depicted in Figure 22.

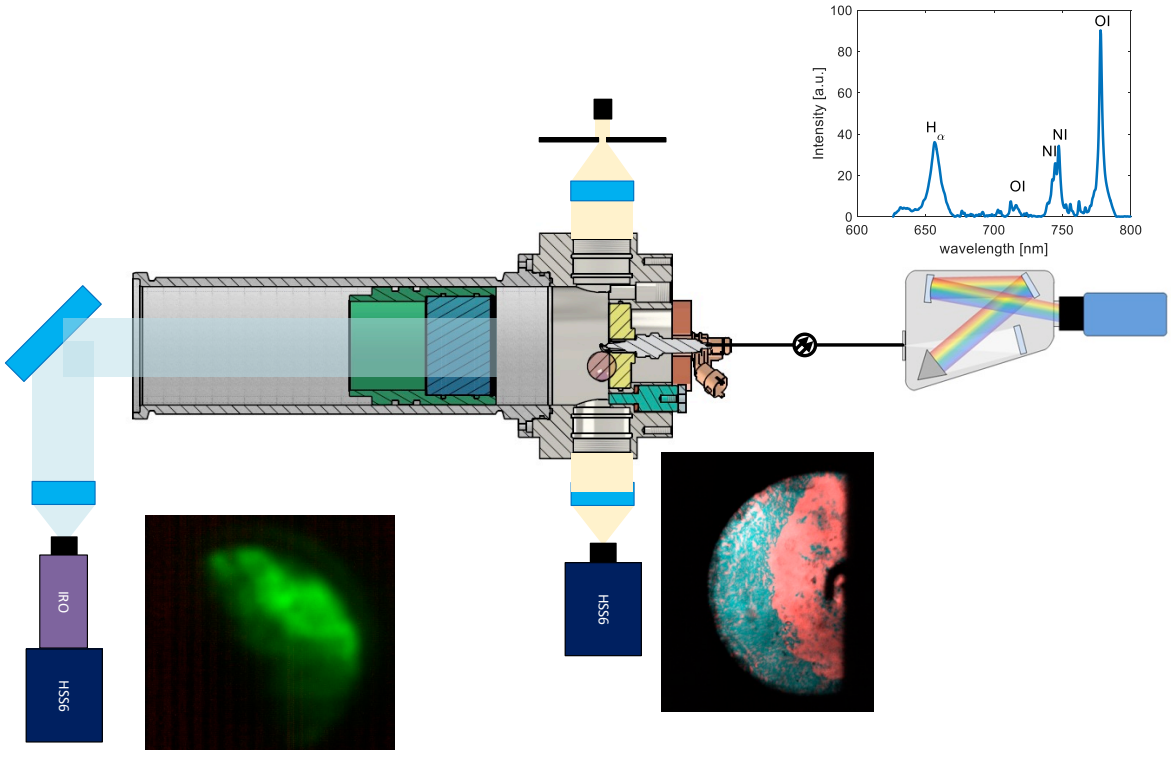

Figure 22: Optical setup schematics based on the newly designed RCEM's cylinder head

4.1.6 Heat Release Rate analysis

The combustion Heat Release Rate (HRR) inside the RCEM is calculated using a thermodynamic 2-zone analysis approach which accounts for compression and expansion heating, wall heat losses, and blowby. The calculation uses multiple constants, the working piston position and the measured cylinder pressure value as variables. The wall heat losses are modeled according to the equation proposed by Woschni[54]. The heat losses are well captured before ignition and, after the combustion, and also during the premixed combustion. It is not a priori clear if they are well captured for the jet-guided combustion.

4.1.7 Ignition systems

The ignition of under-expanded hydrogen jets is investigated using two different ignition systems, a commercially available ignition coil (BERU) providing up to 60 mJ of energy with a maximum duration of 2.2 ms, and a solid-state pulse generator capable of delivering multiple nanosecond pulses at pulse repetition frequency up to 10 kHz. The ns-pulse has a duration of 50 ns, 80 mJ of energy, and a maximum amplitude over the spark gap of 30 kV[55].

4.1.8 RCEM results: H_2 combustion

The test in the RCEM are performed using the aforementioned HDEV1 injector with a 110 Bar pressure in the hydrogen line feeding the injector.

Tests were performed with pure hydrogen injection in air (initial pressure in combustion chamber 1.2 bar), simultaneously acquiring Schlieren and OH chemiluminescence visualizations, in different experimental conditions. Namely, the injection timing is varied with respect to the ignition timing, resulting in different combustion regimes, as described in the following.

When the injection phase ends well before the spark onset, the hydrogen has time to fully mix with the air in the combustion chamber before the spark onset (**premixed condition**). A typical result of premixed condition test is shown in terms of pressure and piston position plots in Figure 23 (end of hydrogen injection 3.6 s before ignition, overall λ=2.4). The sequence of Schlieren and OH chemiluminescence visualization for this test is shown in Figure 24. In all the frame sequences shown in this Section, the time zero corresponds to ignition trigger.

Examining the presented results, it can be observed that the spark onset triggers a regular combustion, that tends to result in a spherical flame front developing from the ignition location, as shown in the frame sequence (Figure 24).

[54] Woschni, Gerhard. *A universally applicable equation for the instantaneous heat transfer coefficient in the internal combustion engine*. No. 670931. SAE Technical paper, 1967.

[55] Merotto, L., et al. "Comparison of ignition and early flame propagation in methane/air mixtures using nanosecond repetitively pulsed discharge and inductive ignition in a pre-chamber setup under engine relevant conditions." *Combustion and Flame* 237 (2022): 111851.

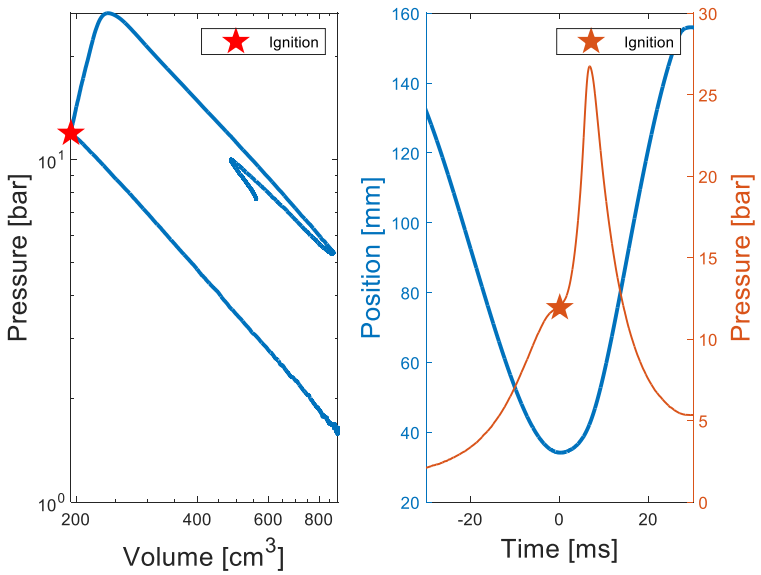

Figure 23: Pressure vs. piston position (left) and piston position and pressure vs. time (right) for a premixed case (pure hydrogen injected in air)

The first flame kernel appears approximately 0.6 ms after spark triggering (top left frame in Figure 24). At 1.2 ms (top right frame) a spherical flame kernel is developing around the spark plug in the Schlieren image, while the first faint OH chemiluminescence is visible. The OH flame front becomes clearly visible in the following frames (2 ms, 3 ms and 4 ms), developing into a regular expanding sphere. The last frame shows that the entire mixture has burnt in about 5.4 ms.

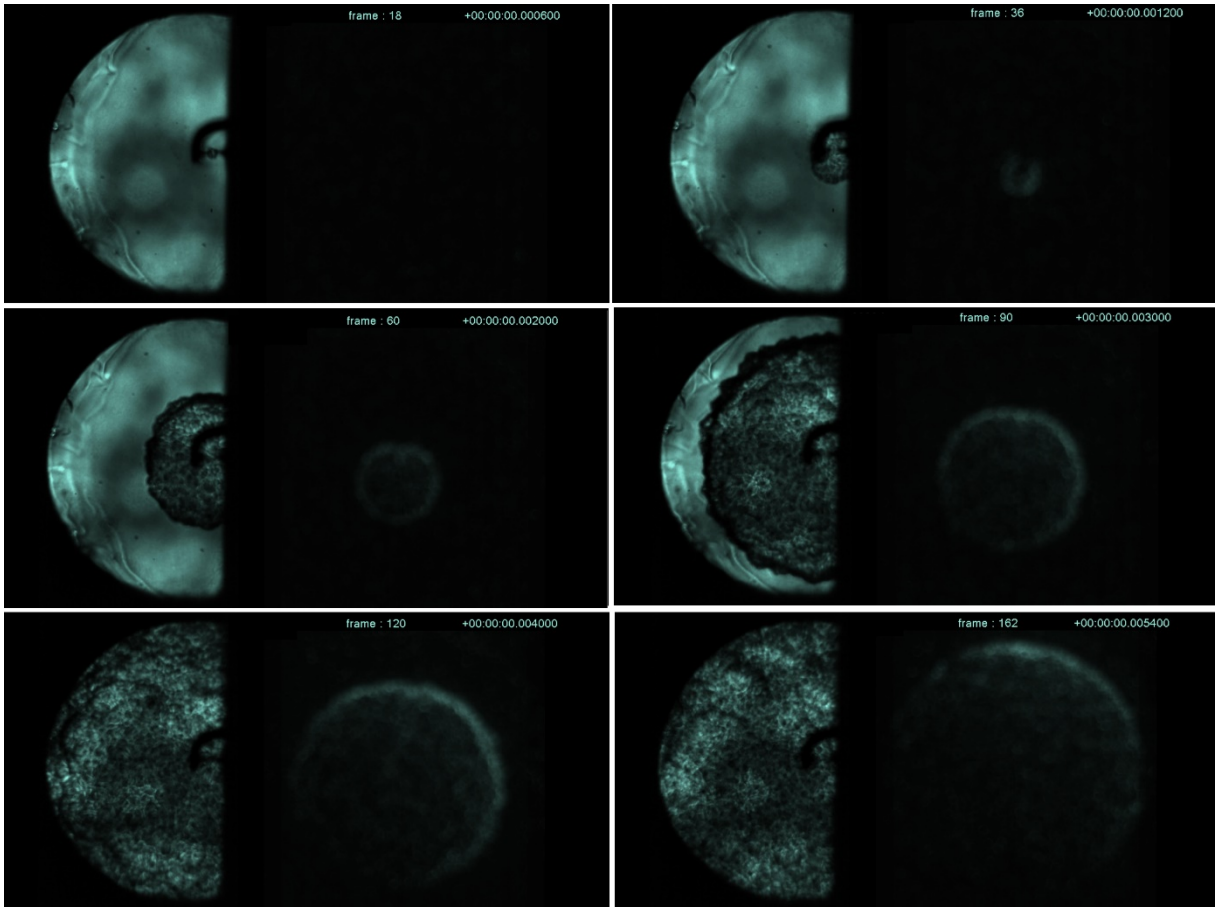

Figure 24: Schlieren (left) and OH chemiluminescence (right) visualization of a premixed combustion test (hydrogen injection in air). P-V diagram of this test is shown in Figure 23

In spite of laminar (quasi quiescent) conditions being present before ignition, it is interesting to notice that already at 2 ms after ignition, the flame front presents a rather wrinqled surface.

A different behavior is seen when a **partially premixed case** is examined (Figure 25 and Figure 26). In this regime, the time delay between injection end and start of ignition (spark onset) is notably shorter (10 - 20 ms), but still sufficient for a partial premixing of hydrogen and air to take place. The pressure vs. piston position diagram for typical partially premixed combustion case is shown in Figure 25 together with the pressure and piston position vs. time. In the pressure-position diagram, the injection phase is highlighted in red and is in the compression phase. For this case the overall λ is 3.28, and the time delay between end of injection and spark onset is 6.38 ms.

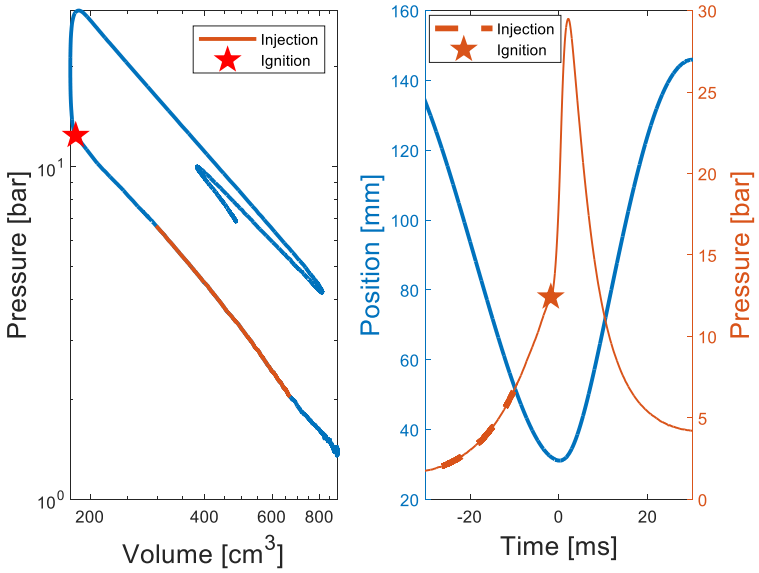

Figure 25: Pressure vs. piston position (left) and piston position and pressure vs. time (right) for a partially premixed case (pure hydrogen injected in air)

The corresponding Schlieren and OH chemiluminescence visualization (Figure 26) shows that at spark onset the mixture is still mixing and turbulence from injection is still present (Schlieren visualization, top left frame, corresponding to approximately 0.6 ms. The first OH chemiluminescence is visible after 1.2 ms from spark onset (top right frame). The following frames (taken at 1.5 ms, 2 ms, 3 ms and 4 ms) show how the flame front develop less regularly than in the premixed case, but lead to complete combustion in approximately 4 ms.

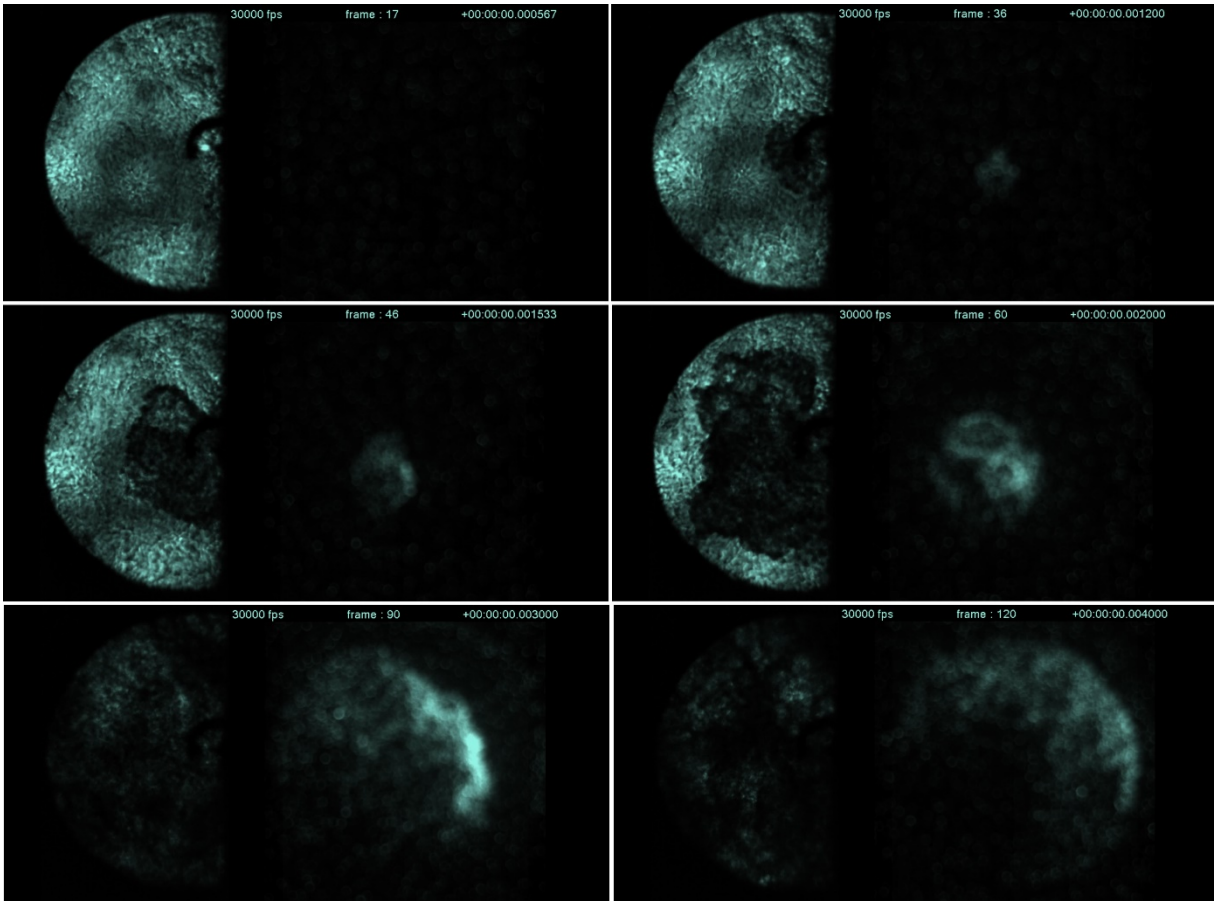

Figure 26: Schlieren (left) and OH chemiluminescence (right) visualization of a partially premixed combustion test (hydrogen injection in air). P-V diagram of this test is shown in Figure 25

When the hydrogen jet is injected in the combustion chamber roughly at the same time as the spark onset (injection ending after spark onset, and time delay between end of injection and start of ignition smaller than 5 ms), ignition is started when the jet arrives at the location of the spark plug (**diffusion combustion**).

Figure 27 shows pressure and piston position diagrams for a typical case of ignition at the jet periphery in diffusion conditions. In this case, the hydrogen injection duration is 8 ms, starting at the ignition timing. The λ at the end of injection over the entire volume is 6.55, it is clear that due to the stratified combustion typical of jet-guided combustion, the AFR where combustion takes place is much richer than this value.

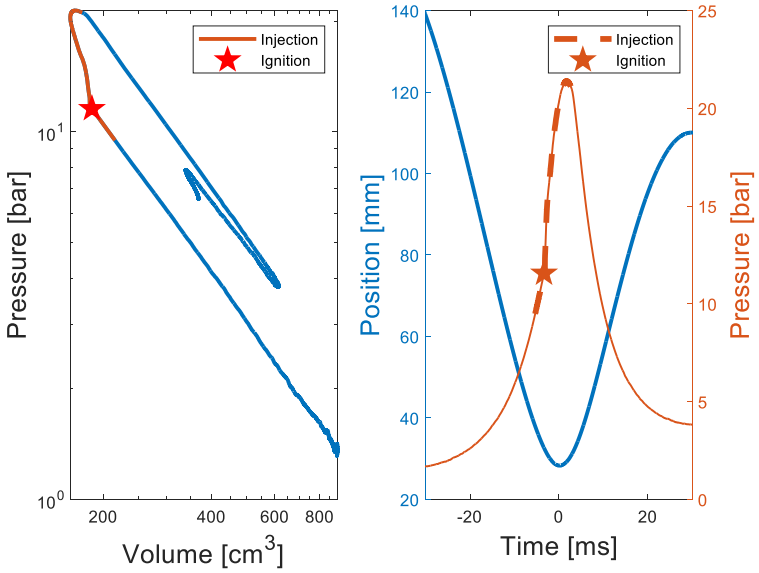

Figure 27: Pressure vs. piston position (left) and piston position and pressure vs. time (right) for a diffusion case (pure hydrogen injected in air)

The Schlieren and OH chemiluminescence sequence for this case is shown in Figure 28. At 1 ms (top left frame) a small ignition kernel starts forming between the spark plug's electrodes, while the hydrogen jet is approaching (slightly visible on top of the Schlieren image). The first OH chemiluminescence appears at 2 ms (top right frame), when the initial kernel is surrounding the spark plug. It is interesting to note how in the following frames (central left and central right frame, corresponding to 2.1 and 2.5 ms) the flame quickly develops to encompass the entire visible region, while the OH chemiluminescence clearly corresponds to the injected hydrogen coming from the left top corner of the OH images. Examining the sbusequent instants (bottom frames, 6 and 8 ms), the Schlieren image is completely dark (burnt mixture) from 2.5 ms on, while the OH visualization shows that the incoming jet continues burning for all the duration of injection.

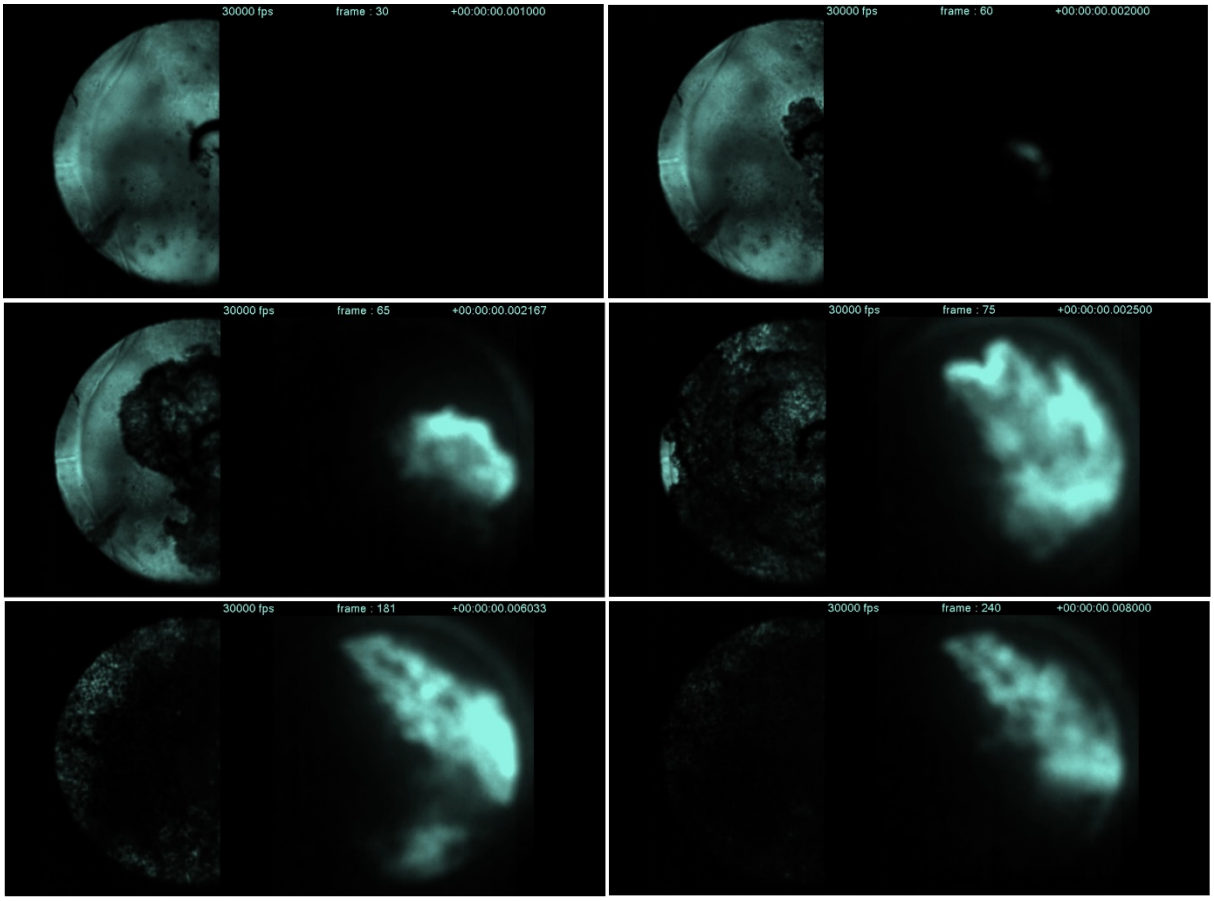

Figure 28: Schlieren (left) and OH chemiluminescence (right) visualization of a partially premixed combustion test (hydrogen injection in air). P-V diagram of this test is shown in Figure 27

While the premixed condition is easier to ignite and results in robust ignition for all the compositions within the ignition limits, the ignition attempt at the incoming jet periphery is far more aleatory and strongly depends on the jet orientation and velocity.

Injection orientation is defined in this work as the angle at which the injector hole is pointing when the injector is mounted on the cylinder head. A scheme of the injector orientation is shown in Figure 29, where the piston view (OH* chemiluminescence) and the Schlieren view through the cylinder head windows are also depicted. The jet cone shown in the figure is reduced for clarity reasons.

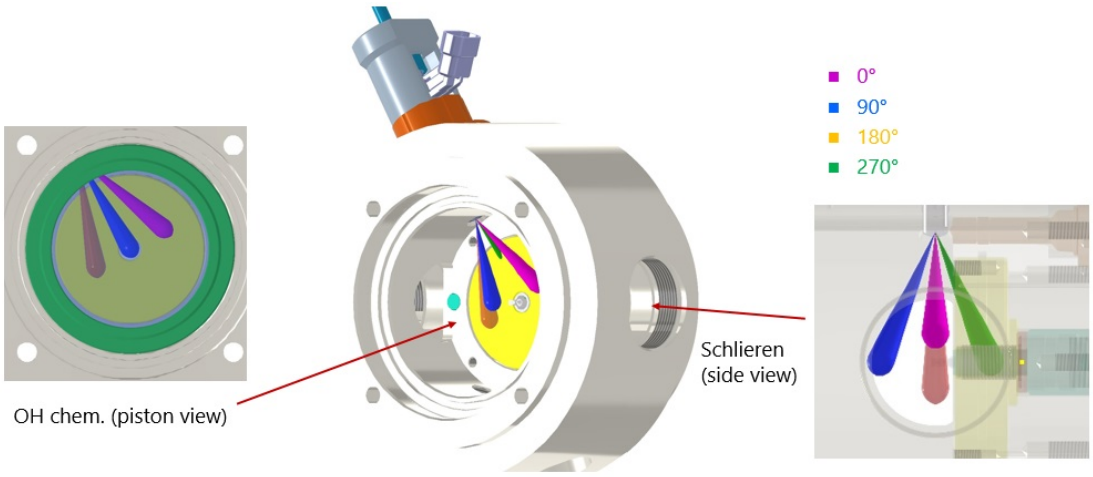

Figure 29: Injection orientation scheme and jet cone visualization (the cone angle is reduced to 10° in the illustration for clarity reasons)

In order to clarify the behaviors observed with both Schlieren and OH chemilumiscence visualization, the heat release rate for the investigated combustion processes was calculated. The calculation is based on a detailed 2-zone model and uses a wall heat-loss model by Woschni, as well as the measured pressure vs. position. The simulation for the diffusion-controlled case was performed as a modified Diesel combustion in which only H atoms are present and the LHV of H_2 is used.

The heat release rate (HRR) and its integrated value over time are shown in Figure 30 and in Figure 31 for typical premixed and diffusion cases, respectively. It can be seen from the HRR trends that the combustion behavior already observed when examining the reacing surface is found. Namely, a peak (around 110 J/ms) is obtained for premixed combustion, while in diffusion cases a much higher peak (approximately 300 J/ms) appears at the beginning (premixed combustion phase), followed by a lower HRR phase (90-100 J/ms) corresponding to the diffusion combustion phase.

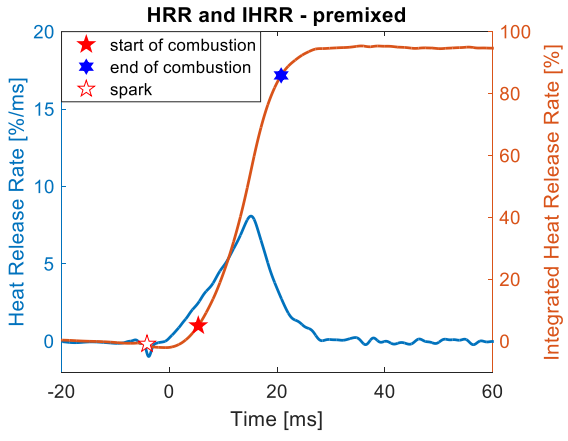

Figure 30: Heat release rate and integrated heat release rate calculation for a premixed case

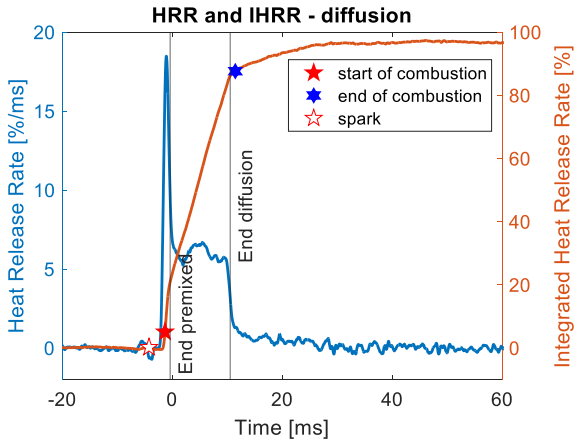

Figure 31: Heat release rate and integrated heat release rate calculation for a diffusion case

It is worth noticing that the slope of the integrated HRR does not change for the premixed case, while in diffusion conditions a slope change is detected corresponding to the beginning of the diffusion combustion phase, as described when examining the visualization results.

Based on the analysis of the pressure-position traces, and on the heat release rate calculations, important insights on the combustion processes of hydrogen jets were obtained, and are summarized in Table 2. The presented results are an average of 20 repetitions for each test condition, and the corresponding standard deviation is given in brackets.

Table 2: Ignition success, ignition delay and integrated heat release rate for different combustion cases.

	premixed (baseline)	**injector orientation 0°**	**injector orientation 90°**	**injector orientation 180°**	**injector orientation 270°**
ignition success, %	100	95	0	25	100
ignition delay, ms	11.20 (1.24)	2.78 (0.81)	nAv	4.59 (1.01)	0.78 (0.10)
integrated HRR, J	1297.58 (16.84)	1337.41 (27.26)	nAv	1289.63 (16.82)	1114.56 (30.48)

The ignition and the combustion development in diffusion conditions dependence on the injector orientation is apparent in the results summarized in Table 2. The best result for ignition success (100%) is obtained for injector orientation of 270°, followed by the orientation 0° (95%). Only 25% ignition success rate is obtained for 180° orientation, while 90° never ignites. It has to be pointed out here that the ignition success is only valid for the given RCEM setup and it can be completely different (better) in a real engine because of turbulence effects.

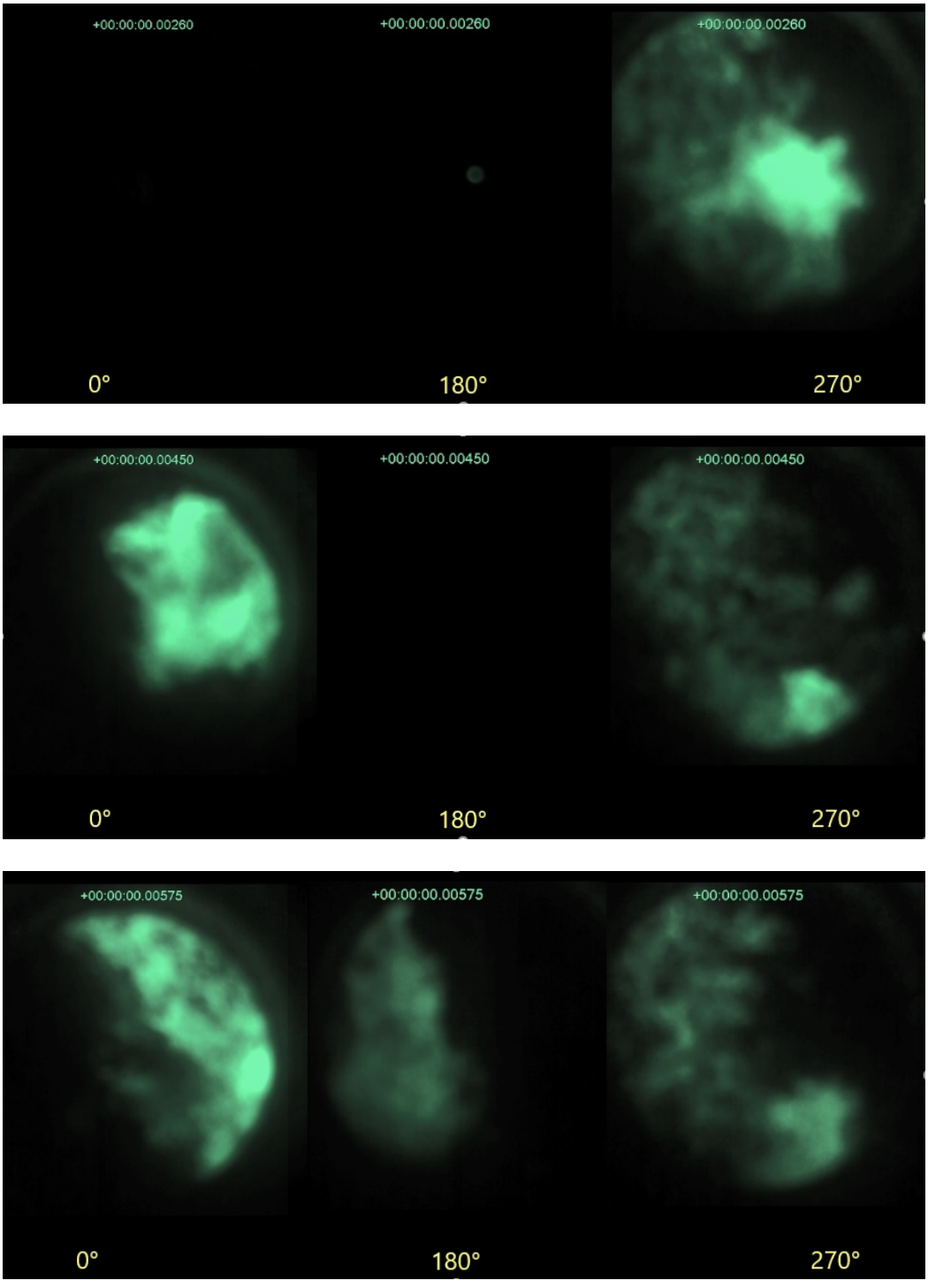

Figure 32: OH* chemiluminescence for three different injection orientation and for different times after ignition: 2.6 ms (top), 4.5 ms (centre) and 5.75 ms (bottom)

The ignition delay, defined as the time when 5% of maximum heat release rate is reached, is notably shorter in diffusion conditions (ranging from 0.78 ms to 4.59 ms) when compared to premixed conditions (11.20 ms). The shortest ignition delay is obtained again for 270° orientation (0.78 ms), followed by 0°

(2.78 ms). The orientation 180° shows the longest ignition delay in the diffusion cases (4.59 ms). The integrated HRR is close to 100% of the injected mass in premixed cases (approximately 1300 J) and in most of the diffusion cases (injection orientation 0°, and 180°, with 1337 and 1290 J respectively). Only the 270° orientation shows a lower integrated HRR (1115 J), thus suggesting that the combustion is less complete in this case (approximately 80% of the injected mass).

The observed behavior can be explained by examining the OH* chemiluminescence visualization for three representative cases of each injector orientation. In particular, examining the OH* emissions at different times (Figure 32) it can be seen that 2.6 ms after ignition start, only in the 270° case the combustion has started, and it is visible as a pseudo-spherical luminosity distribution approximately located at the spark plug position. At 4.5 ms, the jet injected at 270° has already impinged the chamber wall on the opposite side, and the combustion is distributed irregularly in the chamber, with no clear indication of the incoming jet position. At the same time, the jet injected at 0° has ignited, and the OH* visualization clearly follows the jet shape for all the injection duration. The jet injected at 180° has not yet shown any OH* chemiluminescence at 4.5 ms, while its combustion can be followed later on, for example at 5.75 ms. At this time, the different orientation of the three jets can be appreciated, together with a different emission intensity (higher for the 0° case).

In conclusion, the obtained results suggest that an optimum orientation of the hydrogen jet exists for ignition in the investigated conditions. Injecting the hydrogen at 0° ensures a 95% ignition success rate and shows that the combustion occurs mainly in diffusion conditions. Therefore, the subsequent tests are performed with 0° jet orientation.

Two further variables substantially affect the combustion in the jet-guided mode in the current configuration: the location of injection and ignition. Since the spark timing is the input that most affects the combustion start, its location has been held constant slightly before TDC, while the Start Of Injection (SOI) is varied by keeping its duration and, therefore, the injected mass, constant. Figure 33 shows the results of 60 experiments where three different start of injections are used, resulting in a delay between SOI and spark of 1, 4, and 7 ms, respectively. The figure shows for each delay a representative experiment with combustion, where the location of the heat release rate peak was the closest to the mean of all the experiments having the same injection and ignition location. Figure 33, on the left, depicts in double logarithmic scale the pressure-volume trace in blue, the ignition locations with red stars, and the locations where hydrogen is injected are in green. On the right, the pressure against time is plotted in blue, and the HRR in red. The different line styles (full, dashed, pointed) are used in both plots for the same delays between injection and ignition. The time scale of the plot on the right has been shifted so that time zero is always the start of the injection.

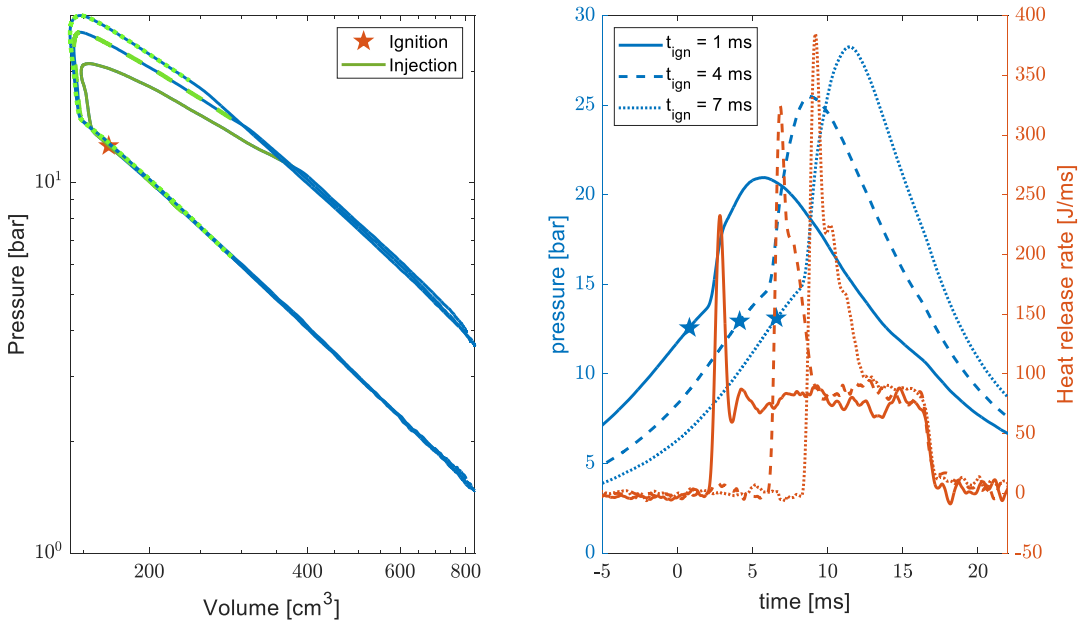

Figure 33: Delay between SOI and ignition: effect on pressure-volume trace (left) and heat release rate (right). Inductive ignition, low CR

A straight line in the double logarithmic plot shows a process that is close to polytropic because for a polytropic change of state pV^n is constant (where p is the pressure, V is the volume, and n is the polytropic exponent). For n equal to 0, the process is isobaric. When n is equal to 1, the process is isothermal, while if it tends to infinity, it is isochoric, and for air, when n is equal to ca. 1.4, the process is isentropic.

The ignition timing is held constant at the time when the piston is at 29 mm from the cylinder head. The pressure at ignition time is practically the same between the three experiments. The delay between SOI and ignition affects the HRR and the resulting pressure-volume trajectory. The longer the delay, the more time the fuel has to mix with the air, resulting in a higher and longer premixed peak. Since the ignition timing and the injection duration are held constant, advancing the SOI results in a shorter diffusion part of the HRR. For delays of 1 and 4 ms after the premixed peak, the HRR reaches a quasi-constant HRR (70-90 J/ms). The compression in the left subplots is close to isentropic. The fast (premixed) heat addition results in a quasi-isochoric process. During the expansion, two processes close to polytropic are present. After EOI, the expansion polytropic exponent is slightly higher than during compression due to the higher wall heat losses, while the polytropic exponent is lower when heat is added to the system.

The process is polytropic if the equation below is fulfilled. Since the added heat (dq) is very high during the premixed portion and constant during the second part, both processes are close to polytropic, with n tending to infinity in the beginning and n smaller than the isentropic coefficient (i.e. the wall heat losses are proportional to the added heat) in the second part (Eq.1).

$$n = (1 - \gamma)\frac{dq}{dw} + \gamma \qquad \text{(Eq. 1)}$$

Once the under-expanded jet is fully developed and ignited, the mixing rate and the heat release should be constant and proportional to the mass flow rate of hydrogen. For this reason, the fuel power input

(P_{fuel}) is defined according to Eq. 2, where Δt_{inj} is the time when the coil of the injector is energized and m_{fuel} is the total injected fuel mass.

$$P_{fuel} = \frac{m_{fuel}}{\Delta t_{inj}} LHV \qquad \text{(Eq. 2)}$$

Figure 34 shows the heat release rate and the energy released for the same experiments as in Figure 33.

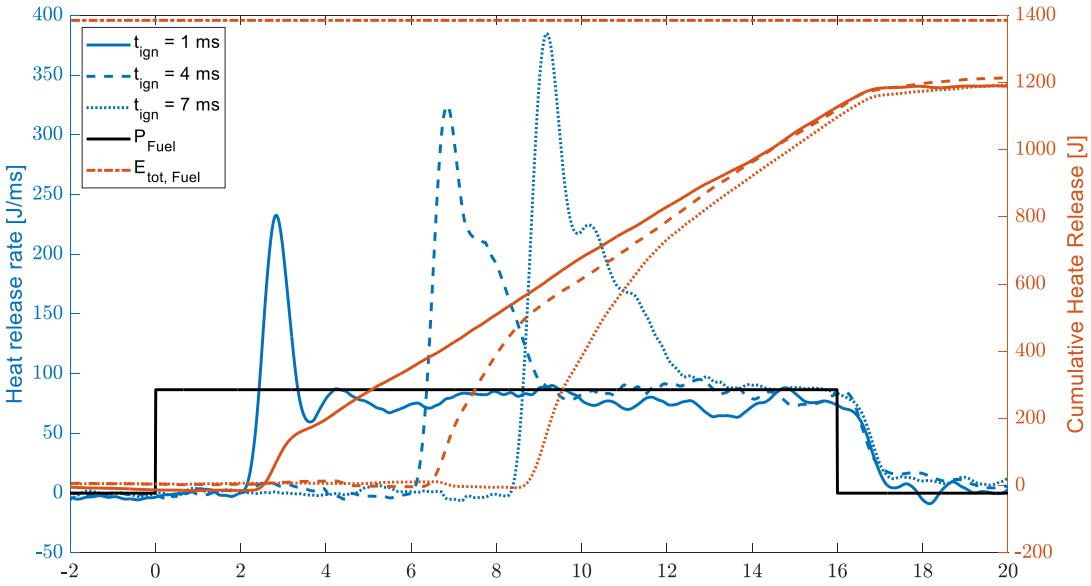

Figure 34: Delay between SOI and ignition: effect on heat release rate and energy released

The dashed horizontal line represents the fuel energy input, while the black line represents the fuel power input. After the premixed peak, the HRR closely follows the fuel power input. The total heat release rate reaches only approximately 88%. Two factors can explain the low conversion rate. First, the wall heat losses are simulated following the Woschni approximation[82], which gives good agreement before and after the combustion process, as can be seen from the flat line before 0 and after 16 ms of the cumulative HRR. Still, they could largely be underestimated during the combustion process due to the jet-wall interactions. An increase of 50% in the wall heat losses during combustion could increase the cumulative HRR to approximately 100%. Second, due to the high jet-momentum flow typical of under-expanded jets, a large portion of hydrogen could "escape" the flame front without contributing to the HRR. Since it is not a priori clear if the wall heat losses are higher than computed the calculation isn't modified, results from rCFD will be needed to estimate where these losses come from.

Table 3 reports the data of the experiments shown before (all data). The delay between SOI and ignition should be equal among all experiments, but since ignition and injection are controlled based on the piston position and the RCEM is a free-floating device, slightly different pressure in the working or the driving volume results in slightly different trajectories and therefore also delays. The premixed peak duration is defined as when the HRR is 20% above the fuel power input, while the energy is the cumulative HRR until the HRR drops below this 20% threshold. The standard deviations of the data are reported in brackets. The ignition success rates for the experiments in the table are respectively 80, 80 and 100% for increasing delay.

Table 3: Injection to ignition delay data and premixed peak data for the tests reported in Figure 33

Injection to ignition delay	Ignition to premixed peak delay	Premixed peak intensity	Premixed peak duration and energy
$\boldsymbol{t_{ign} = 0.83\ ms}$ $\boldsymbol{(0.04\ ms)}$	$\Delta t_{ign,HRR} = 1.95\ ms$ $(0.41\ ms)$	$HRR_{max} = 275.3 \frac{J}{ms}$ $\left(36.4 \frac{J}{ms}\right)$	$\Delta_{pk} = 0.7\ (0.1)\ ms$ $E_{pk} = 146\ (201)\ J$
$\boldsymbol{t_{ign} = 4.14\ ms}$ $\boldsymbol{(0.04\ ms)}$	$\Delta t_{ign,HRR} = 2.70\ ms$ $(0.53\ ms)$	$HRR_{max} = 374.8 \frac{J}{ms}$ $\left(30.5 \frac{J}{ms}\right)$	$\Delta t_{pk} = 3.5\ (1.4)\ ms$ $E_{pk} = 613\ (133)\ J$
$\boldsymbol{t_{ign} = 6.59\ ms}$ $\boldsymbol{(0.04\ ms)}$	$\Delta t_{ign,HRR} = 2.59\ ms$ $(0.51\ ms)$	$HRR_{max} = 421.9 \frac{J}{ms}$ $\left(40.5 \frac{J}{ms}\right)$	$\Delta t_{pk} = 5.2\ (0.8)\ ms$ $E_{pk} = 905\ (76)\ J$

The longer the delay between SOI and ignition, the larger the maximum heat release rate, the higher the premixed energy release, and the longer the ignition delays are. The maximum pressure rise rate increases for increasing delay: 12 bar/ms for the shortest delay, 15 for the 4 ms delay, and 17 bar/ms for the longest delay.

Two factors are required to achieve a precise and reproducible HRR in jet-guided mode: a constant injected mass flow, which can be achieved with a stable injection pressure and a constantly chocked condition through the injector's nozzle, and a constant ignition delay.

A longer delay between start of injection and ignition results in longer ignition delay and more variability between the experiments (Table 3). Ignition using the conventional inductive ignition system is compared against the NRPD ignition in Figure 35. The NRPD discharge is composed of ten pulses at 10 kHz PRF. Figure 35 shows the HRR analysis for a representative experiment with combustion, where the location of the heat release rate peak was the closest to the mean of all the experiments. The dashed line is used to show the inductive system, while the full line is used for the NRPD.

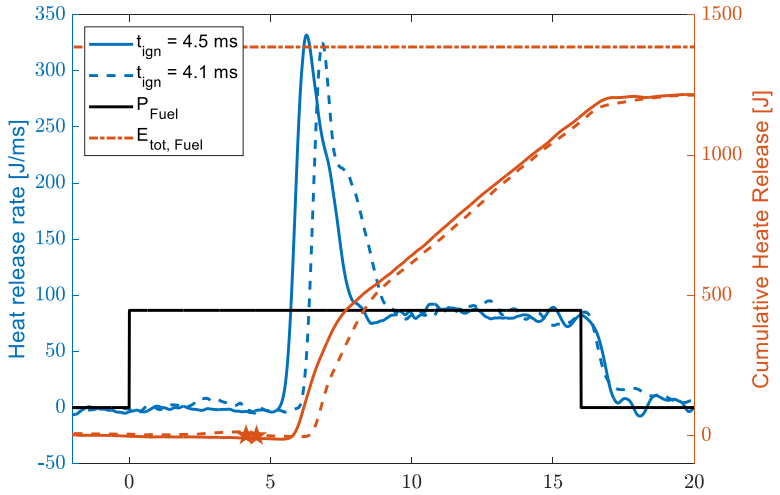

Figure 35: Inductive (dashed line) vs. NRPD (full line) comparison: heat release rate, low CR

Table 4 reports some data (mean value and standard deviation in parentheses) from the experiments' 20 repetitions.

Table 4: Injection to ignition delay and premixed peak: inductive vs. NRPD comparison

Injection to ignition delay	Ignition to premixed peak delay	Premixed peak intensity	Maximum Cumulative HRR
NRPD $\boldsymbol{t_{ign} = 4.52\ (0.06)\ ms}$	$\Delta t_{HRR} = 1.90\ (0.16) ms$	$HRR_{max} = 420(35)\ \frac{J}{ms}$	$iHRR_{max} = 89\ (0.5)\%$
Inductive $\boldsymbol{t_{ign} = 4.14\ (0.04\ )\ ms}$	$\Delta t_{HRR} = 2.70\ (0.53) ms$	$HRR_{max} = 375(30)\ \frac{J}{ms}$	$iHRR_{mx} = 88\ (0.9)\%$

The experiments using NRPD show a higher success of ignition (95 vs 90%). Even though the spark occurs slightly before for the inductive experiments, the peak of the HRR occurs earlier. For similar conditions, the later the HRR peak is (wrt SOI), the higher its intensity. The opposite occurs when inductive ignition is compared to NRPD, meaning that a higher share of the fuel injected before ignition reacts during the premixed part when NRPD ignition is used. This higher conversion is kept till the end of combustion.

The delay between start of injection and ignition is also varied using NRPD ignition. Figure 36 shows, for each delay, a representative experiment with combustion, where the location of the heat release rate peak was the closest to the mean of all the experiments having the same injection and ignition location. The spark timing is slightly later (compared to the inductive experiments) and held constant when the piston is at 26 mm from the cylinder head.

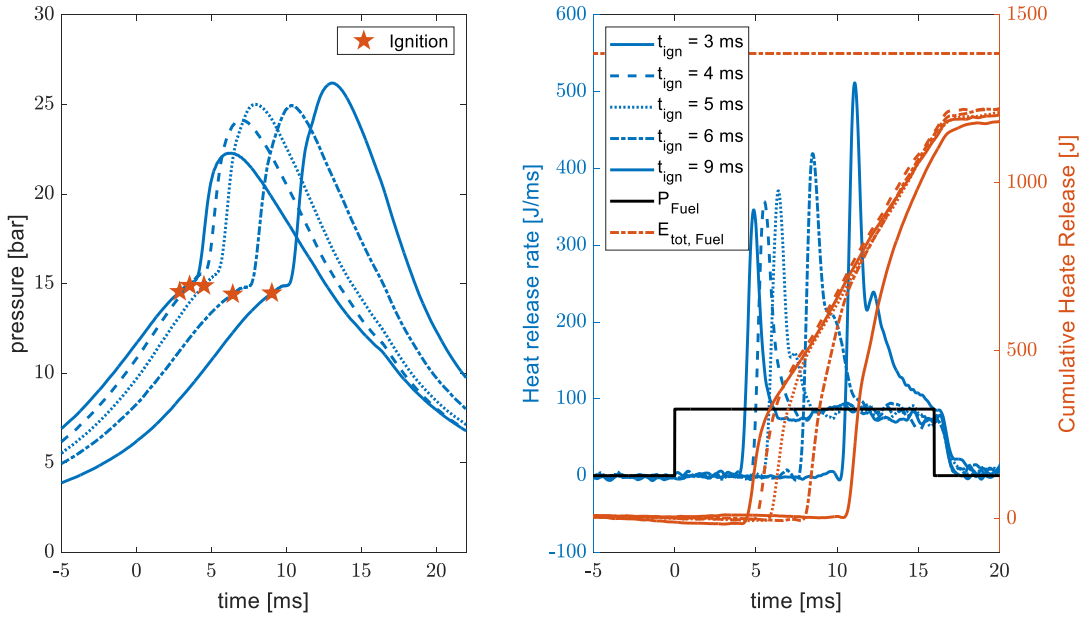

Figure 36: Delay between SOI and ignition: effect on pressure-time trace (left) and heat release rate (right). NRPD ignition, low CR

As for the inductive case, an increased delay between SOI and ignition results in a higher premixed peak, and during the diffusion portion of the combustion, the heat release rate closely follows the fuel power input. Figure 37 shows the pressure-volume trace in a double logarithmic scale for the experiment where the delay between injection and ignition is 6 ms.

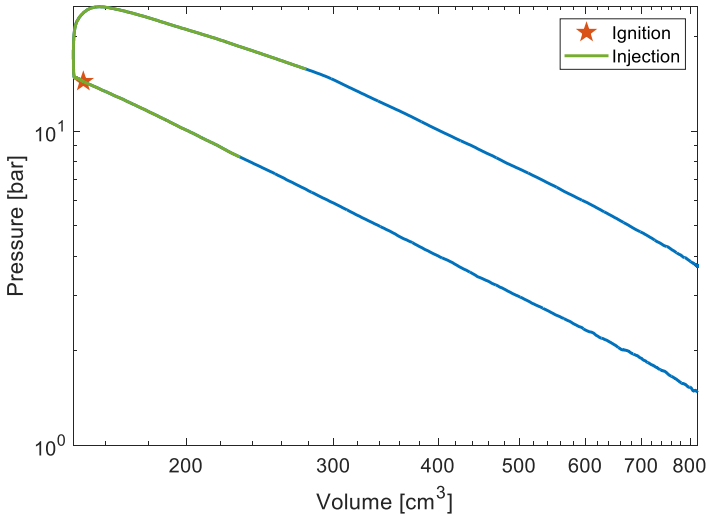

Figure 37: Pressure-volume trace for a test with a 6 ms delay between SOI and ignition. NRPD ignition at low CR

Since the ignition timing is closer to TDC and the ignition delay is short when NRPD ignition is applied, the two polytropic processes during combustion are clearly visible in Figure 36. In fact, during the premixed portion a rapid increase in pressure near TDC is present (isochoric process), while the diffusion portion results in an expansion with a constant polytropic exponent.

Figure 38 shows four frames of the recording of the OH chemiluminescence on top and the pressure and HRR trace against time on the bottom, with points signalizing the times where the frames are taken.

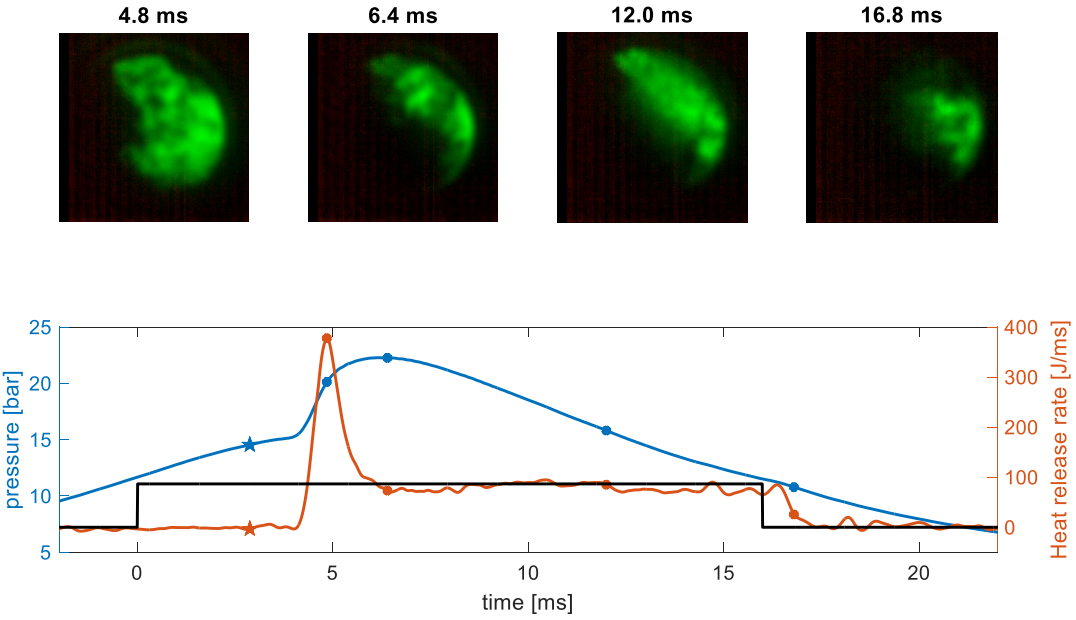

Figure 38: OH chemiluminescence (top), pressure, and HRR traces (bottom) for a 2.9 ms delay between SOI and ignition case. Low CR, NRPD

After the HRR peak visible from a large area where OH intensity is present (4.8 ms), the OH chemiluminescence intensity is pretty stable in location and is cone-shaped, exiting the injector's tip. After EOI a tail of HRR is present with the OH chemiluminescence active near the top right corner (at the wall opposite to the injector axis). Table 5 reports the relevant data (mean value and standard deviation in parentheses) from the experiments' twenty repetitions.

Table 5: SOI to ignition delay variation, NRPD ignition low CR

Injection to ignition delay	**Ignition to premixed peak delay**	**Premixed peak intensity**	**Premixed peak duration and energy**
$\boldsymbol{t_{ign} = 2.9\ ms}$	$\Delta t_{HRR} = 1.9\ (0.3) ms$	$HRR_{max} = 415(34)\ \frac{J}{ms}$	$\Delta t_{pk} = 1.4\ (0.3)\ ms$ $E_{pk} = 343\ (55)\ J$
$\boldsymbol{t_{ign} = 3.5\ ms}$	$\Delta t_{HRR} = 1.9\ (0.3) ms$	$HRR_{max} = 395(40) \frac{J}{ms}$	$\Delta t_{pk} = 2.0\ (1.0)\ ms$ $E_{pk} = 417\ (106)\ J$
$\boldsymbol{t_{ign} = 4.5\ ms}$	$\Delta t_{HRR} = 1.9\ (0.2) ms$	$HRR_{max} = 420(35)\ \frac{J}{ms}$	$\Delta t_{pk} = 3.1\ (1.4)\ ms$ $E_{pk} = 567\ (121)\ J$
$\boldsymbol{t_{ign} = 6.5\ \ ms}$	$\Delta t_{HRR} = 2.0\ (0.5) ms$	$HRR_{max} = 464(25)\ \frac{J}{ms}$	$\Delta t_{pk} = 3.5\ (0.8)\ ms$ $E_{pk} = 761\ (84)\ J$
$\boldsymbol{t_{ign} = 8.9\ \ ms}$	$\Delta t_{HRR} = 2.0\ (0.3) ms$	$HRR_{max} = 519(38)\ \frac{J}{ms}$	$\Delta t_{pk} = 4.7\ (0.7)\ ms$ $E_{pk} = 1020\ (74)\ J$

The delay and its scatter between the premixed peak and ignition is shorter when NRPD ignition is used. The lower scatter and the later ignition result in the premixed part of the combustion being closer to isochoric. Due to the lower scatter and the later spark timing, the average pressure gradient for similar delay remains lower for the NRPD experiments when compared to coil ignition tests.

The goal of jet-guided combustion is to achieve high efficiency without knock occurrence. Higher compression ratios and pressures are, therefore, investigated. The RCEM driving and filling pressure are varied to achieve higher peak cylinder pressure during combustion. The resulting operating point represents a point with a higher CR (8.7) when compared to the previous experiments (6.2). The filling pressure is also higher for these experiments (1.3 vs 1.1 bar). Figure 39 shows the results of 80 experiments where four SOI are used, resulting in a delay between ignition and spark of 1.7, 2.5, 3., and 4.2 ms. The figure shows for each delay a representative experiment with combustion, where the location of the heat release rate peak was the closest to the mean of all the experiments having the same injection and ignition location. Figure 39 shows on the left the pressure against time (blue), while on the right, the HRR and the cumulative HRR are plotted in blue and red, respectively. The different line styles are used in both subplots for the same delays.

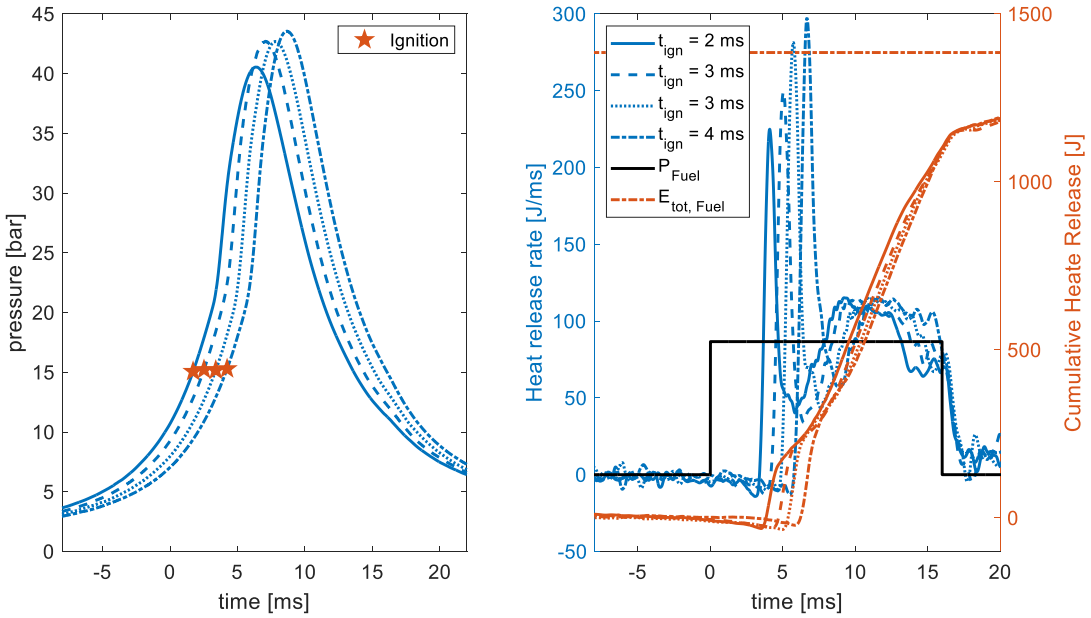

Figure 39. Delay between SOI and ignition: effect on pressure-time trace (left) and heat release rate (right). NRPD ignition, high CR

As for the previously reported experiments, the injection duration is 16 ms. The injected mass is the same if choked conditions are present in all experiments. Due to the higher driving pressure used in these experiments, higher peak pressures are reached (ca. 40 vs. ca. 25 bar). As previously, the premixed peak increases the longer the delay between SOI and ignition. Nevertheless, at these higher pressures, the diffusion part of the combustion is not as constant as for the low-pressure experiments. The HRR after the premixed peak falls lower than the fuel power input (black line in Figure 39 right) afterward, it re-increases above the black line. This pulsation is also visible from the OH chemiluminescence recording. The peak pressure for these experiments is as high as 47 bar. The minimum of the HRR values are reached when the in-cylinder pressures are close to the peak pressure.

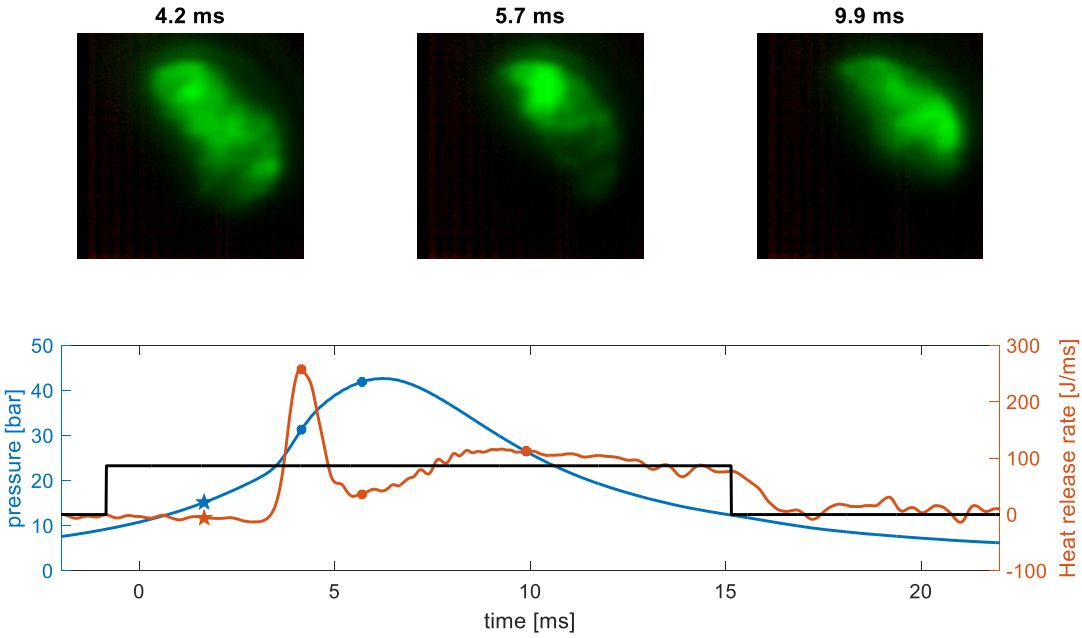

Figure 40. OH chemiluminescence (top), pressure, and HRR traces (bottom) for a 2.5 ms delay between SOI and ignition case. High CR, NRPD

Figure 40 shows three frames of the recording of the OH chemiluminescence on top and the pressure and HRR trace against time on the bottom with points signalizing the times where the frames are taken.

At the HRR peak (4.2 ms), a large area shows OH activity, indicating a large zone where the fuel is reacting. After the peak, the HRR drops, and the OH chemiluminescence moves closer to the injector tips as the pressures increase to the maximal pressure. As the pressure decreases, the OH signal moves further from the injector, and the OH active area increases as the HRR does. The brightest spot in OH chemiluminescence moves towards the injector as the pressure increases and back towards the wall as it decreases.

Table 6 reports the data (mean value and standard deviation in parentheses) from the experiments' twenty repetitions. The ignition success of all the experiments was 100%, with the exception of one experiment for the 1.7 ms delay where one misfire was present.

Table 6: SOI to ignition delay variation data (tests in Figure 39), high CR tests NRPD ignition

Injection to ignition delay	Ignition to premixed peak delay	Premixed peak intensity	Maximum Cumulative HRR
$\boldsymbol{t_{ign} = 1.7\ ms}$	$\Delta t_{HRR} = 2.5\ (1.0) ms$	$HRR_{max} = 246(25)\ \frac{J}{ms}$	$iHRR_{max} = 91.7\%$
$\boldsymbol{t_{ign} = 2.5\ ms}$	$\Delta t_{HRR} = 2.5\ (0.8) ms$	$HRR_{max} = 275(33)\ \frac{J}{ms}$	$iHRR_{max} = 92.3\%$
$\boldsymbol{t_{ign} = 3.3\ ms}$	$\Delta t_{HRR} = 2.4\ (0.4) ms$	$HRR_{max} = 288(21)\ \frac{J}{ms}$	$iHRR_{max} = 92.2\%$
$\boldsymbol{t_{ign} = 4.2\ ms}$	$\Delta t_{HRR} = 2.6\ (0.9) ms$	$HRR_{max} = 304(26)\ \frac{J}{ms}$	$iHRR_{max} = 91.6\%$

Slightly higher completeness of combustions are reached in the high compression ratio cases compared to the low ones (Table 6 and Table 5). Also, the premixed peak intensities are lower for similar delays between SOI and ignition.

For the higher CR cases, the HRR isn't as flat as for the lower ones. Three factors can lead to this effect. First, the higher CR results in the piston reaching a position closer to the cylinder head (16 and 25 mm) and, therefore, to the injector nozzle (5 mm from the head), which can result in an interaction between the piston and the incoming jet, temporarily reducing the HRR. Second, the higher pressures in the cylinder slow the jet penetration speed[56], possibly reducing the region where combustion is possible and temporarily reducing the fuel burn rate. Third, since it is not sure how high the pressure is at the injector nozzle, it is unclear if choked conditions are present when the combustion pressures are high. The pressure of the hydrogen line is at 110 bar, which should be enough to achieve choked conditions in all the experimented conditions. Nevertheless, it is possible that pressure drops inside the injector reduce the pressure enough to have sub-critical conditions at the injector's nozzle. Since the calculated HRR depends on the estimated injected mass, and the estimated mass is correct only if chocked conditions are present for the entire injection duration, the subcritical condition should not be present or only for a short time and without substantially affecting the total injected mass.

4.1.9 Evaluation of injection conditions

The present section discusses the conditions needed for a choked injection and estimates the actual injection pressure and effective diameter which is used as a base for the rCFD simulations. The pressure of the hydrogen line is at 110 bar, and the measured injector's diameter is 0.6 mm.

Since the HRR closely matches the fuel power input for the low CR cases, it can be assumed that choked conditions are present, giving a lower bound for the injection pressure. By assuming no friction in the flow, no inertial effects, and zero-dimensional flow, (Eq 3)[57] describes the mass flow rate, while real gas effects are considered in the isentropic coefficient and in the density of hydrogen, retrieved from the NIST database[58].

$$\dot{m} = c_d A \sqrt{\gamma \rho_0 p_0 \left(\frac{2}{\gamma+1}\right)^{\frac{\gamma+1}{\gamma-1}}} \qquad \text{(Eq. 3)}$$

The measured injected mass in the RCEM is 11.54 mg for the 16 ms injection duration. By assuming a constant mass flow rate, the mass flow is 0.72 mg/ms. Results from preliminary CFD tests show that a constant injection mass flow rate is usually reached in some hundreds of µs, therefore negligible in comparison to a 16 ms injection duration. Figure 41 shows combinations of discharge coefficients (cd) and injection pressures (p0) that result in the estimated mass flow (blue line). The maximal cylinder pressure to have choked conditions is reported in red.

From this estimation, for example, an actual injection pressure at the injector's nozzle of 80 bar and an effective diameter of 0.44 mm could explain the measured mass flows. Since it is unknown the internal geometry of the injector, which was developed for gasoline injection, a pressure loss of 30 bar does not seem impossible. Since the sharpness of the hole is also unknown and the diameter is approximately measured, also the 0.44 mm effective diameter (cd=0.53) seems plausible. CFD simulations should clarify this uncertainty.

[56] Sakellarakis, Vasileios David, et al. "The effect of high-pressure injection variations on the mixing state of underexpanded methane jets." *International Journal of Engine Research* 22.9 (2021): 2900-2918.
[57] Guzzella, Lino, and Christopher Onder. *Introduction to modeling and control of internal combustion engine systems*. Springer Science & Business Media, 2009.
[58] https://webbook.nist.gov/cgi/cbook.cgi?ID=1333-74-0

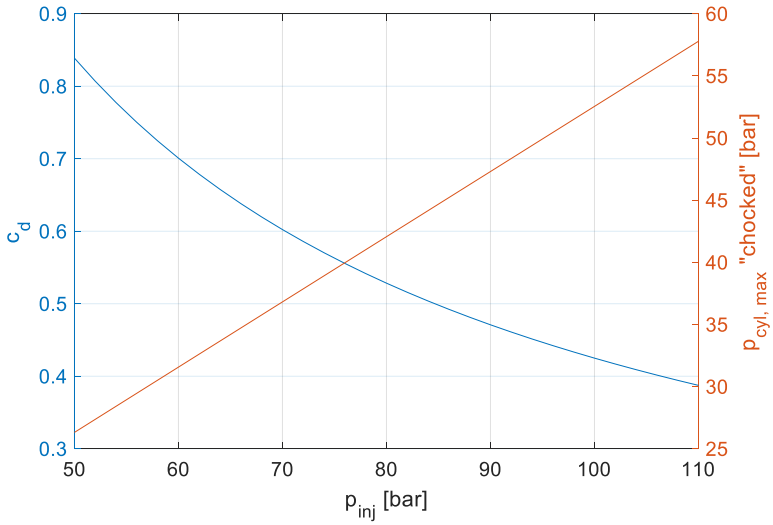

Figure 41: Discharge coefficient and injection pressure for the measured mass flow

4.1.10 RCEM results: SIBS measurements

The SIBS technique estimates the local AFR during reactive experiments at the ignition location and time. Figure 42 and Table 7 report the results from the SIBS investigation performed during the reactive experiments using NRPD ignition at low CR. Figure 42 shows the sum of all the post-processed spectra having the same delay between SOI and ignition, starting from 3 ms up to 9 ms. The spectra are normalized by dividing the spectra by the respective OI (777) intensity. The different atomic emissions are reported on top of the relative peak.

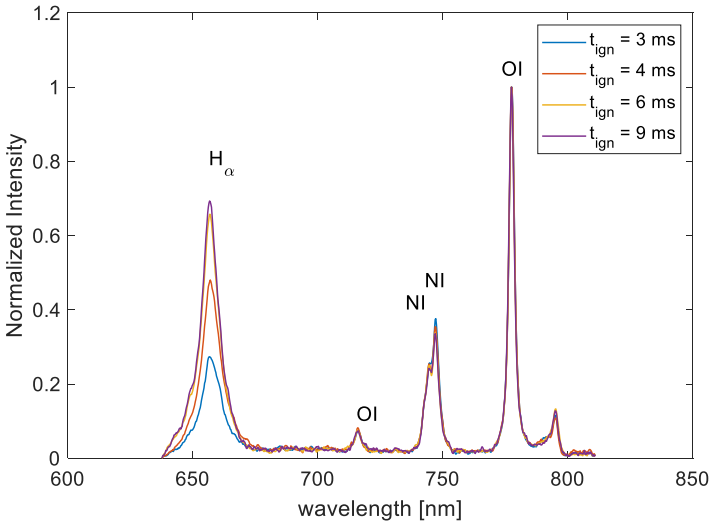

Figure 42: SOI to ignition delay effect on SIBS features: NRPD ignition low CR

The oxygen and nitrogen peaks have practically the same relative intensity between the experiments. This outlines that the spectral technique is capable of returning relative concentration since the nitrogen-

to-oxygen ratio is not expected to vary for different locations and AFRs. The normalized hydrogen intensity increases for increasing delay between SOI and Ignition, which outlines an increase in local λ.

Table 7 reports quantitative results from the SIBS technique for the different delays between SOI and ignition. The λ single experiments and λ sum spectra report the average λ measured over the 20 repetitions. To calculate the "λ single experiments" for each experiment out of 20 repetitions, the intensity of H_α over O_{777} is calculated, and the respective λ interpolating from the polynomial calibration (Section 4.1.4) is calculated. The mean value is then reported with its standard deviation. To calculate the " λ sum spectra" all 20 spectra are summed, and one λ is then calculated from the polynomial calibration. The deviation of the value is dependent on the calibration precision. From an investigation of the calibration, it is unclear which of these two values is more precise. The λ minimum and maximum values over the 20 experiments are also reported. Table 7 also reports the ignition success rate in percentage.

Table 7: SOI to ignition delay effect on SIBS measurements: NRPD ignition low CR

Injection to ignition delay	**λ** **(single experiments)**	**λ** **(sum spectra)**	**λ_{max} (single experiments)**	**λ_{min} (single experiments)**	**Ignition success rate**
$t_{ign} = 2.9\ ms$	8.8 (1.5)	$8.7^{9.7}_{7.7}$	Air	4.4	70%
$t_{ign} = 3.5\ ms$	7.9 (2.0)	$7.2^{8.2}_{6.4}$	Air	4.6	100%
$t_{ign} = 6.5\ \ ms$	6.2 (1.4)	$6.2^{7.0}_{5.5}$	8.6	2.8	100%
$t_{ign} = 8.9\ \ ms$	6.3 (1.4)	$6.0^{6.7}_{5.3}$	8.9	2.8	100%

Big variations in λ are obtained. The SIBS technique measures an instantaneous mixture composition between the electrodes at ignition timing. Due to the turbulence induced by the injection and since the ignition happens at the periphery of the jet, high variability in the AFR for the repetition of the same experiment is expected. In the CFD environment, the average λ and its variation over the cell in the ignition location and time could be compared to these results for validating the model.

Despite that very high λ are measured in single experiments (up to air), high ignition success are present. This could seem strange, but if the ignition energy is deposited in air and, before substantial cooling, is mixed with a combustible mixture, ignition is still possible. Since in the RCEM only the injection process generates turbulence, ignition if the hydrogen jets is likely to be more difficult than in engines. In fact, during the engine experiments in Stuttgart, stable operation was also present for experiments where the ignition was before SOI. If mixing is sufficient, the deposition of the ignition energy in pure air is enough to ignite the H_2 jets.

4.1.11 RCEM results: non-reacting tests

Figure 43 shows four post-processed frames at 0.4, 0.8, 1.5, and 4 ms after SOI for the non-reactive optical experiments recorded with the Schlieren technique through the piston view. The piston view offers a larger visualization area when compared to the tangential view, but since the sparkplug is removed to allocate the window, only non-reactive experiments are possible in this configuration. The sparkplug location in the reactive experiments would correspond to the middle of the circle. Due to the low density of hydrogen, postprocessing of the Schlieren images is needed to visualize the jet morphology. A routine that enhances the difference between an image before injection (background) and the actual image is developed. The background image is depicted on a blue scale while the intensity of the difference is increased and depicted with red shades of color.

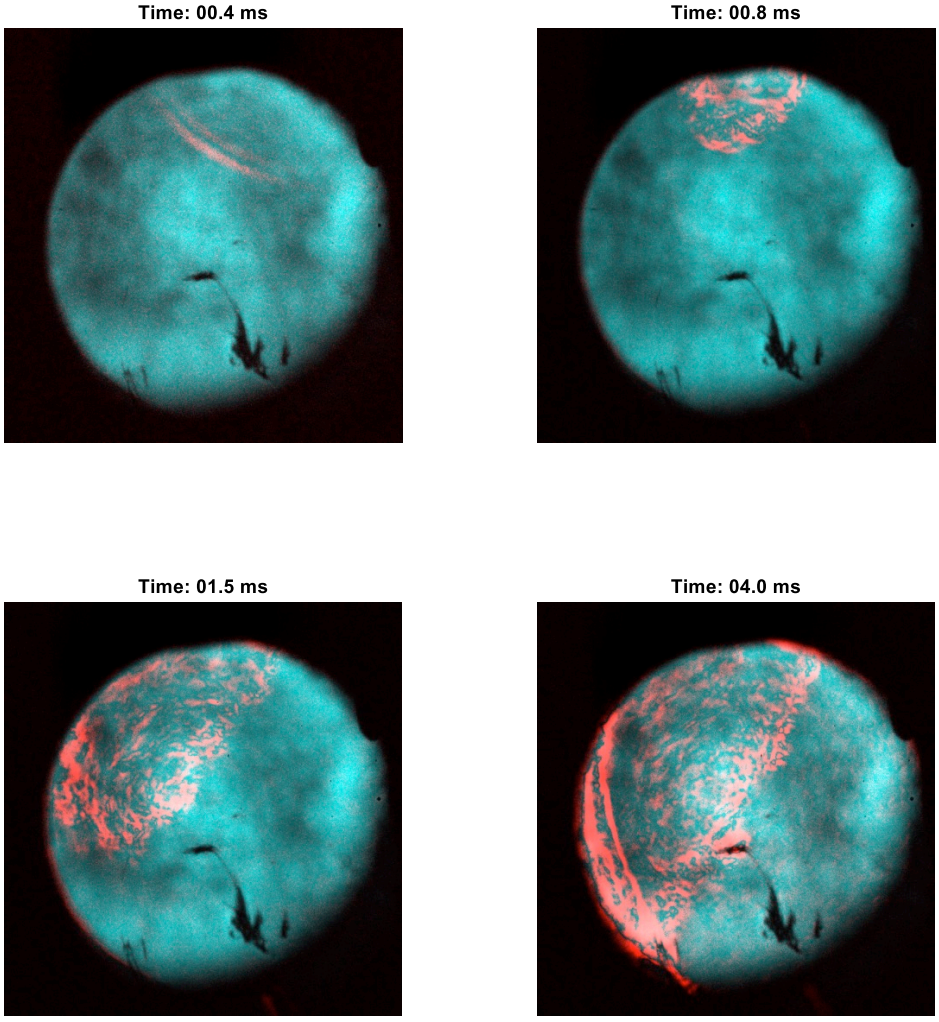

Figure 43: Schlieren visualization for non-reacting tests. Backpressure 8-13 bar

For one frame at 400 µs, two circular lines are visible. The shutter speed is 2.5 µs, and the lines are only visible for a single frame. These lines are the shockwaves characteristic of the formation of under-expanded jets. The hydrogen jet appears at around 0.6 ms in the top right corner. Since the injector hole has an inclination of about 20° with respect to the axis that passes in the middle of the window (sparkplug location), ignition happens at the periphery of the jet, as can be seen in the frame at 1.5 and 4 ms. In non-reactive experiments, the pressure varies only due to the piston's ballistic motion, therefore the pressure during injection ranges between 8 to 13 bar. The recorded jet morphology is only representative of the reacting experiments before ignition and combustion. Afterward, the increase in pressure will shrink the jet, as can be seen from the OH chemiluminescence in the reacting experiments (Figure 40).

4.1.12 Comparison with single-cylinder engine results

Jet-guided hydrogen combustion is investigated on a 0.5L single-cylinder research engine at IFS. The engine is fitted with a Bosch HDEV4 piezo injector. Figure 44 shows some results where the injection duration is held constant at 37°CA while the ignition timing is changed between 8.3, 4.2, and 0.2 °bTDC.

For all the experiments reported in Figure 44, the overall λ is 1, and the injection pressure is 190 bar. The pressure-volume diagram is depicted on the right in double logarithmic scale, while on the right, the HRR and his integration are reported respectively in blue and red. The vertical red dashed line on the right subplots reports the total injected fuel energy, while the black rectangle reports the fuel power input with the same scale as the HRR.

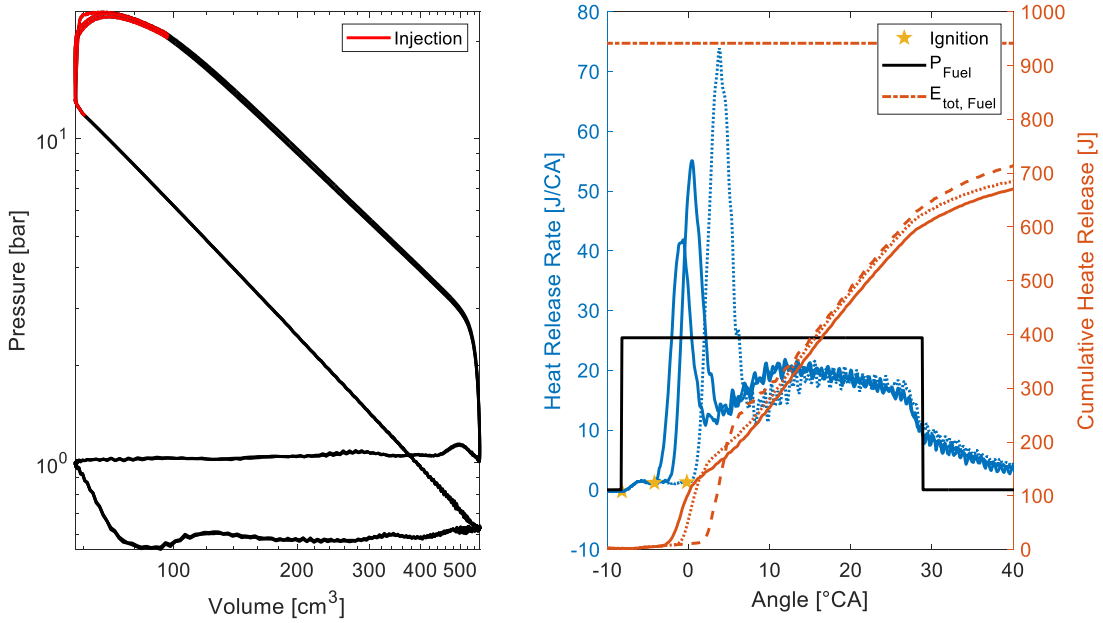

Figure 44: pressure-volume diagram (left) and HRR vs. °CA for single-cylinder engine tests

In spite of the different test rigs and injectors, similar heat release rate shapes, as recorded in the RCEM, are present in the engine. The longer the delay between injection and ignition, the higher the premixed peak. As for the high CR experiments in the RCEM, the diffusion part of the combustion exhibits an HRR that is not constant. The cumulative HRR at EOI is low when compared to the fuel energy input (63-68%, depending on the ignition timing). After EOI, a long tail of HRR is present, lasting till the middle of the stroke (90°CA), reaching conversions of up to 85%. This long heat release after the fast burning part could be present due to the stoichiometric operation. Due to the jet-diffusion combustion, it can be expected that good mixing will not be present, making it difficult to combust the fuel completely. In fact, ca. 4% of the injected hydrogen is measured in the exhaust (unburned).

The high-pressure loop cycle of an ideal engine is usually composed of an isentropic compression till TDC, afterward, an instantaneous isochoric heat addition, and again an isentropic expansion till BDC[59]. Additional constraints are often posed to the heat addition, for example, a maximal pressure for mechanical protection or a maximal pressure gradient constraint to limit the noise[60]. The fast HRR that is measured in both the RCEM and the engine setup outlines the possibility of shaping the HRR of jet-guided hydrogen combustion. The isochoric portion of the heat addition can be controlled with the delay between SOI and ignition, the mass flow rate, the geometrical distance between the injector and the sparkplug, and the jet development limits the "isochoric" portion. Due to the high hydrogen diffusivity and reactivity, a constant heat release rate dependent on the injection rate can be achieved, resulting

[59] Pischinger, Rudolf, Manfred Klell, and Theodor Sams. *Thermodynamik der Verbrennungskraftmaschine*. Springer-Verlag, 2009.

[60] Moretto, Giordano, Severin Hänggi, and Christopher Onder. "Optimal combustion calibration for direct-injection compression-ignition engines using multiple injections." *International Journal of Engine Research* 24.4 (2023): 1414-1431.

in a quasi-polytropic process dependent on the mass flow rate. In the engine experiments, the high-pressure gradients present during the premixed combustion results in pressure fluctuations similar to the ones detected in cold start of Diesel engines[61] or in HCCI combustion[62].

4.1.13 Mixtures comparison

Tests on the three different mixtures selected for this project show that hydrogen addition to methane does not result in higher ignition success rate in diffusion regime, only in (slightly) faster combustion when the ignition is successful. A typical example of different flame kernel development at the same time after ignition is shown in Figure 45 for the three different mixtures tested in this project. In engines, it was noticed that hydrogen addition results in reduced cycle-to-cycle variation and reduced knock tendency. Also in the present case the observed faster combustion is likely to indicate lower knocking.

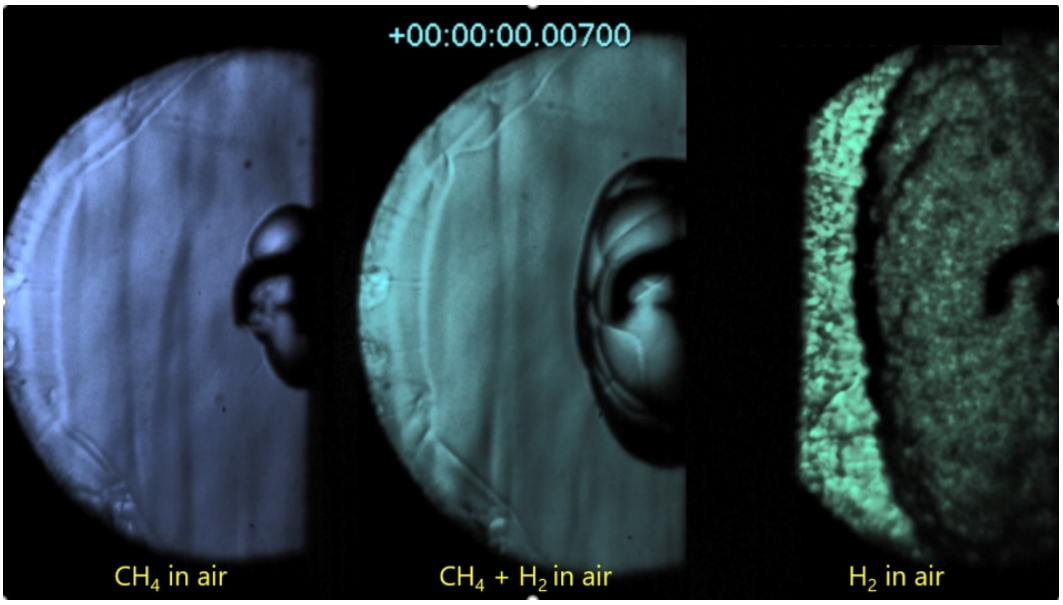

Figure 45: Different flame kernel development at the same time after ignition (7 ms) for the three different mixtures investigated

When testing methane and methane/hydrogen mixtures, the coil ignition system was unable to ignite the jet in diffusion-controlled conditions. Preliminary tests were performed with NRPD ignition, showing an ignition success rate of approximately 20-25%.

Therefore, the obtained results suggest that NRPD is a promising technique to improve ignition robustness in challenging conditions, and to improve SIBS-based local λ measurement reliability.

[61] Kyrtatos, Panagiotis, Clemens Brückner, and Konstantinos Boulouchos. "Cycle-to-cycle variations in diesel engines." *Applied Energy* 171 (2016): 120-132.

[62] Vressner, Andreas, et al. "Pressure oscillations during rapid HCCI combustion." *SAE transactions* (2003): 2469-2478.

4.2 **Work Package 2: Computational Fluid Dynamics**

4.2.1 Task 2.1 – 5.1 Non-reactive under-expanded jets in canonical configuration

Canonical geometries with the nozzle bore and a small plenum (3 mm diameter and 8 mm length) were generated, as shown in Figure 46. A trimmed hexahedral grid was employed with two prism layers at walls (80 µm on the cylinder head and 20 µm along the nozzle bore). The injector orifice is included in the geometry with considerable refinement (50 µm) to capture the jet structure. This inner refinement extends roughly five orifice diameters downstream and three orifice diameters radially. Farther downstream and around the inner refinement, a second static refinement with 100 µm is used (ten and six times the nozzle diameter, respectively).

Figure 46: Schematic of the canonical setup used to study underexpanded jets.

The internal geometry of the injector is unknown, and the injector was developed for gasoline injection; therefore, notable pressure loss inside the injector could be present as seen in [53]. Since it is unknown whether the edges of the injector hole are rounded or sharp, the hole is not axial and the pressure drop in the injector is unknown, three possible combinations of injection pressure and discharge coefficient (effective nozzle diameter) from the data reported in Figure 41 in section 4.1.9 are selected for the CFD, as reported in Table 8.

Table 8: Non-reactive CFD simulations: combination of injection pressure and discharge coefficient.

Combination 1	**Combination 2**	**Combination 3**
$c_d = 0.7$ $p_{inj} = 60\ Bar$ $d_n = 0.39\ mm$	$c_d = 0.53$ $p_{inj} = 80\ Bar$ $d_n = 0.44\ mm$	$c_d = 0.42$ $p_{inj} = 100\ Bar$ $d_n = 0.50\ mm$

These estimated injection pressures are prescribed at the nozzle inlet (stagnation inlet), constant pressure at all plenum outlet boundaries and wall boundaries at the "cylinder head" and nozzle bore.

Turbulence is modelled using the realizable variant of the k-epsilon model with a two-layer wall treatment. Standard second-order spatial discretization is used while time integration uses the Pressure Implicit with Splitting of Operators (PISO63) scheme 1.0e-8 s integration time steps between 1.0e-8 and 1.0e-7 seconds. Under-relaxation factors had to be lowered to 0.4 and 0.7 for the pressure and enthalpy equations, respectively.

Figure 47 shows the pressure distribution 6 µs after SOI for the three combinations reported in Table 8, where hydrogen is injected against technical air at a back pressure of 8 bar.

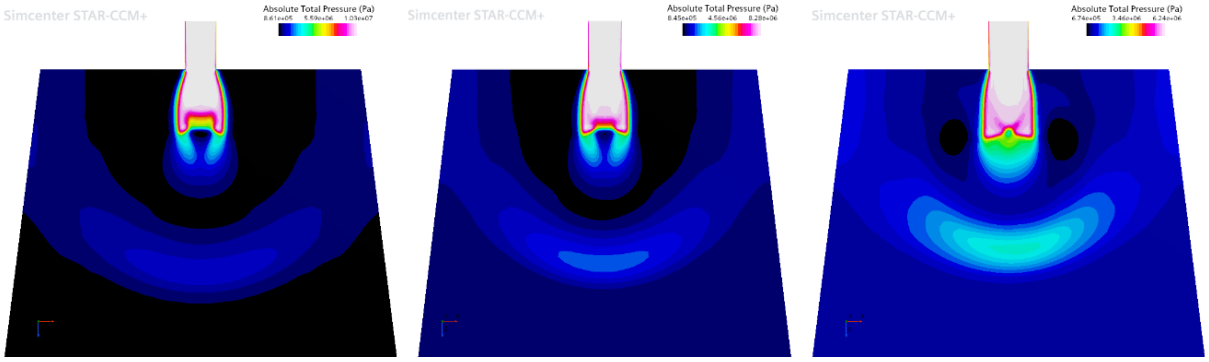

Figure 47: Comparison of jet structure 6 µs after SOI, visualized by the pressure distribution.

For all the tested conditions, the gas jet becomes highly under-expanded assuming the barrel shaped shock pattern and a Mach disk near the nozzle.

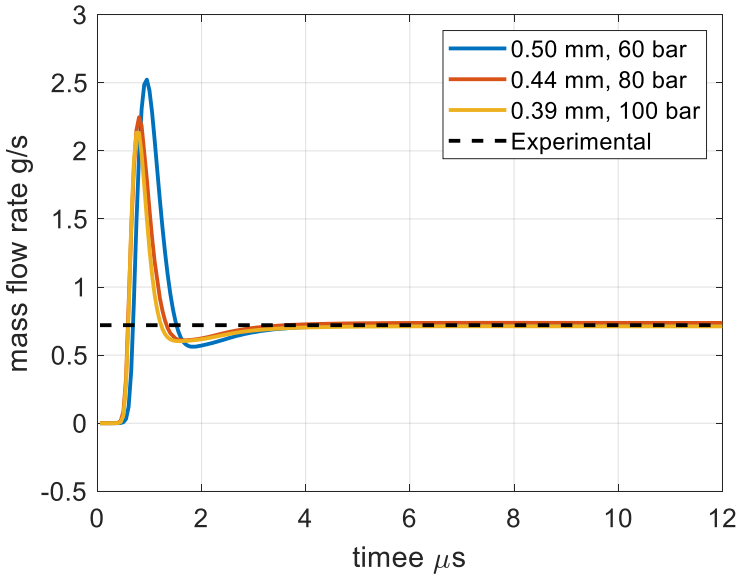

Figure 48: Mass flow rates for the three conditions.

Figure 48 shows the computed mass flow rates for the three combinations. The flow starts to become choked roughly 1 µs after the start of injection and only minor differences can be seen concerning the location and maxima between the three combinations. Around 4 µs the initial transient is over and the

[63] R.I. Issa, A.D. Gosman, A.P. Watkins, The computation of compressible and incompressible recirculating flows by a non-iterative implicit scheme, Journal of Computational Physics 62 (1986) 66–82. https://doi.org/10.1016/0021-9991(86)90100-2.

mass flow rate stabilizes and very similar mass flow rates (0.71-0.74 g/s) closely matching the experimental measurements (0.72 g/s) are established.

In non-premixed combustion, the Scalar Dissipation Rate (SDR) has a strong impact on the diffusion flame structure, as high values can potentially lead to extinction of the jet flame.

In an RANS context, the SDR is calculated as follows:

$$\tilde{\chi} = c_\chi \frac{\tilde{\varepsilon}}{\tilde{k}} \widetilde{\xi''^2}$$

Where k and epsilon denote the turbulent kinetic energy and dissipation rate, respectively. The last term on the right hand side is the Mixture Fraction Variance, which is calculated as follows:

$$\frac{\partial \overline{\rho}\widetilde{\xi''^2}}{\partial t} + \frac{\partial}{\partial x_j}\left[\overline{\rho}\tilde{u}_j\widetilde{\xi''^2} - \left(\overline{\rho}D_{\tilde{\xi''^2}} + \frac{\mu_t}{Sc_{\tilde{\xi''^2},t}}\right)\frac{\partial \widetilde{\xi''^2}}{\partial x_j}\right] = \frac{2\mu_t}{Sc_{\tilde{\xi''^2},t}}\left(\frac{\partial \tilde{\xi}}{\partial x_j}\right)^2 - \overline{\rho}\tilde{\chi}$$

The first term on the Right Hand Side is a production term due to gradients of the Mixture Fraction, while the second term is a destruction term due to SDR. Both the Mixture Fraction (MF) and its Variance (MFV) have been implemented as passive scalars with standard transport equations calculated by the flow field solver, while the necessary source terms have been manually implemented by means of field functions.

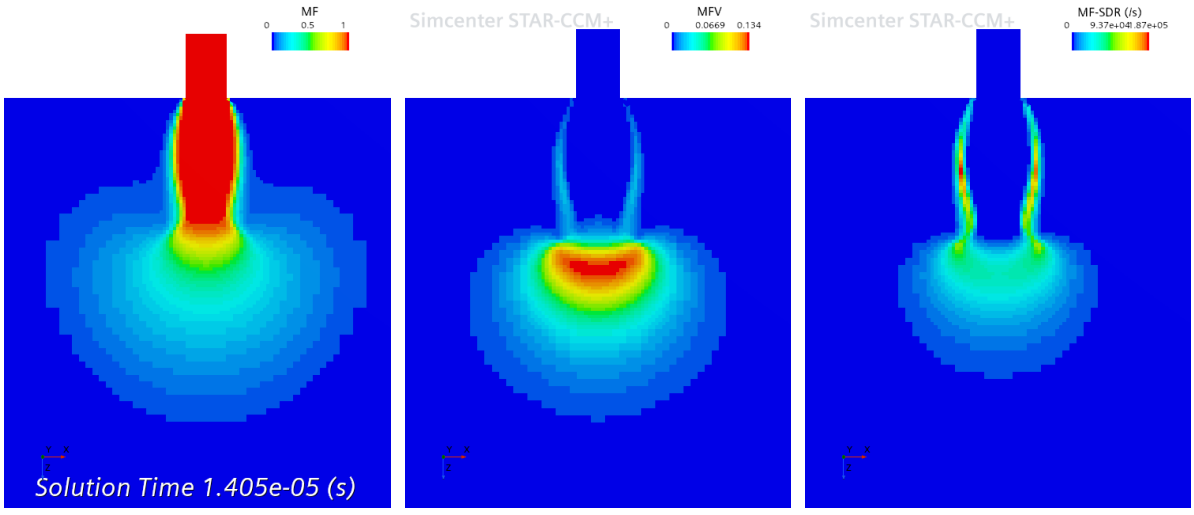

Figure 49: Distributions of Mixture Fraction (left), Mixture Fraction Variance (middle) and Scalar Dissipation Rate (right).

Figure 49 shows distributions of all three quantities roughly 14 us after start of injection in a slice through the nozzle axis. Extremely high values of the Scalar Dissipation Rate can be seen, which can be expected due to the very high velocities associated with the under expanded nature of the jet and the high turbulence levels generated in the shear layer.

For reactive stratified and fully jet-guided simulations, the SDR can conceptually be used as a proxy for the ignitability of the jet at the spark location.

4.2.2 Task 2.2 – reactive simulation in the RCEM

A model was been developed for the RCEM geometry, for which a schematic is given in Figure 50. Two prism layers are also employed here and a refinement has been introduced around the spark location.

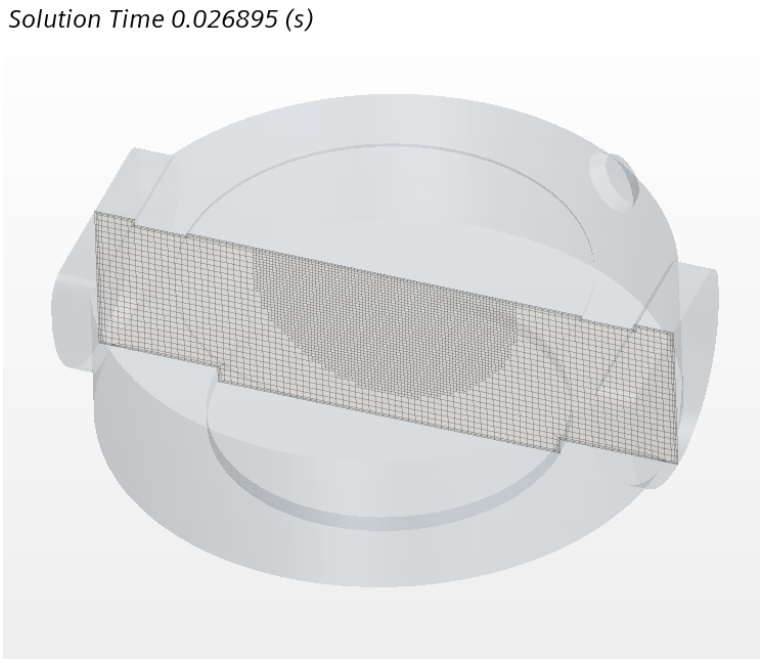

Figure 50: Schematic of the RCEM simulation geometry close to Top Dead Centre.

A macro is utilized to prescribe the motion of the free floating piston based on the measurement of one individual cycle, cf. Figure 51.

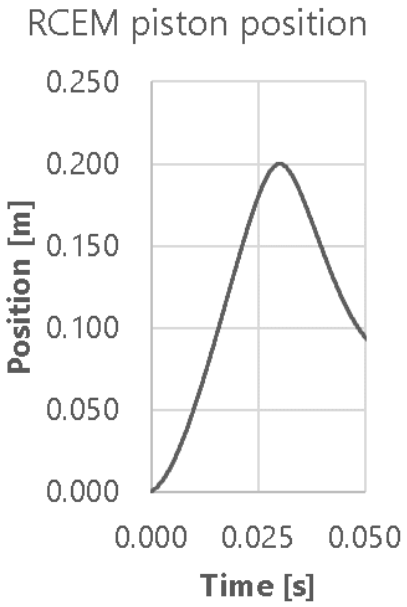

Figure 51: Example of prescribed piston position for RCEM

Mesh morphing is performed in every time step by the solver and remeshing triggered in the macro based on various mesh quality metrics: cell aspect ratio, minimum cell volume, face validity and cell quality. This ensures high quality hexahedral cells throughout the entire simulation.

Premixed cases

In addition to jet-guided combustion modes, a series of experiments were also conducted for fully premixed conditions With injection at the start of the experiment, i.e. at BDC, this allows for almost 100 ms of mixing time for spark timing around TDC. Tracer LIF experiments conducted in a previous work[64] in a glass tube corresponding roughly to the RCEM in the context of dual fuel combustion had shown, that indeed this time is sufficient for mixing. At the time, methane was used and it can be estimated, that this will hold true even more for hydrogen which has considerably higher diffusivity.

Two premixed cases with lambda 2.39 and 3.12 have been computed using the built-in Turbulent Flame Closure (TFC) model in conjunction with chemical kinetics for hydrogen from[65]. The TFC model employs the Takeno Index, i.e. examines the alignment of gradients of fuel and oxidizer to determine which combustion regime to employ (detailed kinetics or turbulent premixed flame). For the turbulent flame speed the Peters correlation[66] is employed with unaltered model constants. For spark Ignition, the ISSIM model was used with standard constants in combination with a sphere of 1 mm radius for the energy deposition.

For both air/fuel ratios, the laminar flame speed has been pre-computed at the thermodynamic conditions at spark advance. Alternatively, pre-tabulated laminar flame speeds could be used, which are generated for given ranges of the air/fuel ratio, pressure and temperature levels as well as EGR.

Grid resolutions amounted to 2 mm during compression, 1 mm during combustion, 0.5 mm in the spark region (20 mm sphere around spark plug) and two prism layers were employed at all walls with a total thickness of 0.5 mm

Figure 52 shows the simulated pressure traces for a non-reactive compression-expansion (blue) and with premixed combustion for the lambda 2.39 case. Very good agreement for the compression phase is evident, confirming accurate geometry representation of the model. The sharp pressure rise due to the very fast combustion seen in the experiment (orange) is slightly overpredicted. Images highlight the temperature at four time instants, namely shortly after ignition, flame propagation in the bulk before impingement on the liner or piston, shortly before the maximum pressure is reached and late in the expansion.

The flame shape is illustrated by means of temperature distributions in the centre-plane at four destict time instants: shortly after ignition, during the rapid flame propagation phase, shortly before the end of combustion (shortly before the pressure peaks) and during expansion, where only some regions in the boundary layers can be seen which are still "cold".

[64] Srna A, Bruneaux G, von Rotz B, Bombach R, et al. Optical investigation of sooting propensity of N-dodecane pilot/lean-premixed methane dual-fuel combustion in a rapid compression-expansion machine. SAE Technical Paper 2018-01-0258; 2018. https://doi.org/10.4271/2018-01-0258.

[65] J. Warnatz, U. Maas, R.W. Dibble, Combustion, 4th Edition, Springer Verlag, 2006

[66] Peters N. The turbulent burning velocity for large-scale and small-scale turbulence. J Fluid Mech 1999; 384: 107–132.

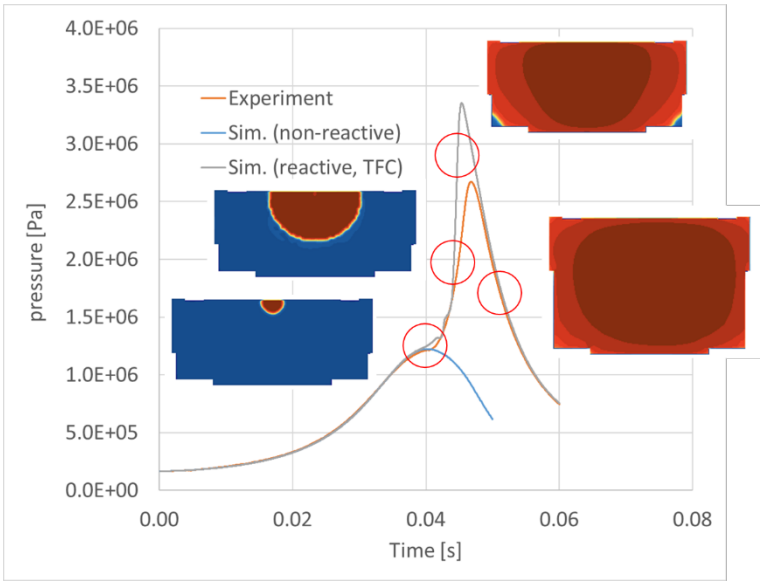

Figure 52: Comparison of reactive and non-reactive pressure traces of premixed λ =2.39 case.

For the less reactive condition at lambda 3.12, combustion progress is initially very slow but a late speed-up can be observed around 40 ms. Both phases are reproduced by the simulation, although the effect is over pronounced. From the temperature distributions it can be seen, that the flame is being elongated due to the piston expansion, increasing the flame area leading to the acceleration between 40 and 45 ms.

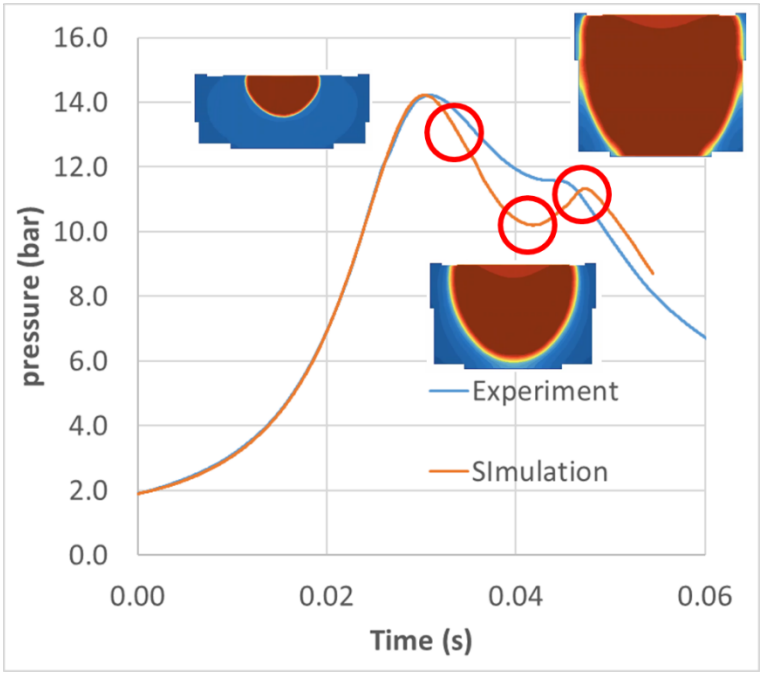

Figure 53: Comparison of reactive and non-reactive pressure traces of premixed λ =3.12 case.

It is important to note that no case specific tuning of model constants has been performed to achieve better agreement with the experiment, but the models have been used "as is". Further investigations should include the sensitivity of the predictions to the chemical kinetics and the numerical settings for the chemical kinetics solver, the choice of laminar flame speed formulation, model constants in the

turbulent flame speed correlation, the ISSIM spark model options as well as the size of the flame kernel and the turbulence model. For premixed hydrogen/air flames, the importance of accounting for thermo-diffusive instabilities, especially at lean conditions as discussed in[67] should also be studied.

Finally, it is important to note, that turn-around times for such calculations from BDC to well after the end of combustion typically amount to less than 8 hours on 48-64 CPUs, depending on the operating condition. This enables the exploration of many combinations in terms of ignition and combustion model to determine the best possible parameter set for spark and turbulent combustion models as well as choice of chemical kinetics and lamiar flame speed.

HPDI simulation in RCEM

Following the calibration of the high pressure injection in the canonical configuration, insights w.r.t. mesh resolution, time stepping and numerical settings were applied to study HPDI in the RCEM for which the geometry outline and a slice through the nozzle axis for the reference position is shown in Figure 54.

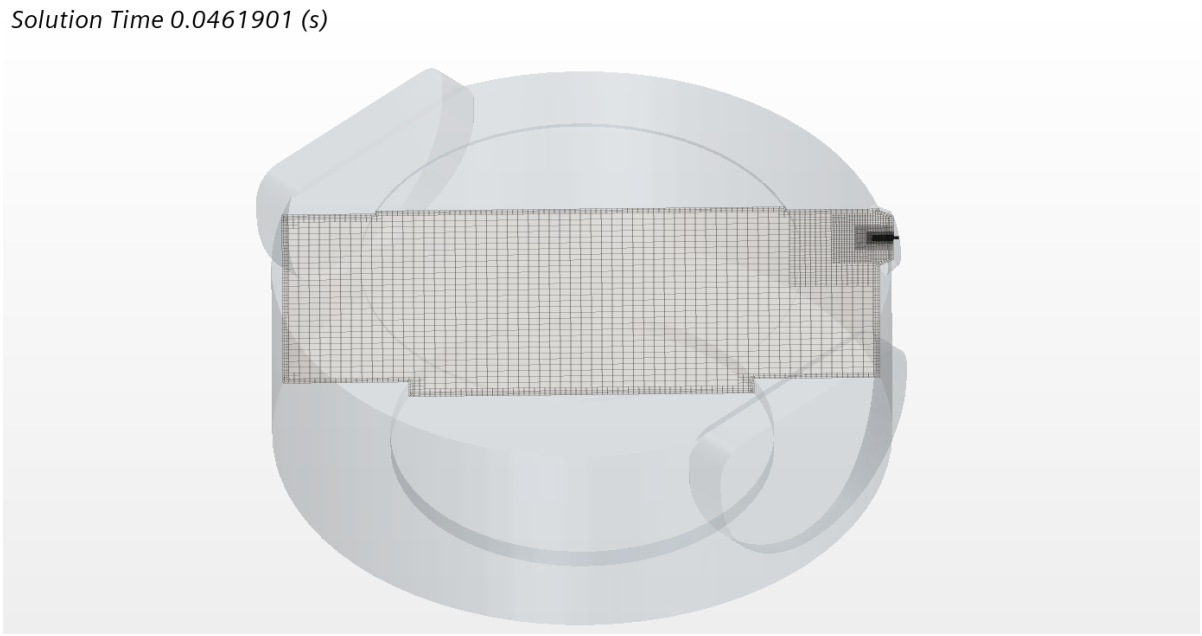

Figure 54: Schematic of RCEM with injector mounted at the reference position.

Very high velocities are present in the vicinity of the injector, rendering the calculations very costly due the small time steps required during injection and the comparatively long process duration (30 ms injection/combustion duration).

[67] C.E. Frouzakis, N. Fogla, A.G. Tomboulides, C. Altantzis, M. Matalon, Numerical study of unstable hydrogen/air flames: Shape and propagation speed, Proceedings of the Combus-tion Institute 35 (2015) 1087–1095. https://doi.org/10.1016/j.proci.2014.05.132

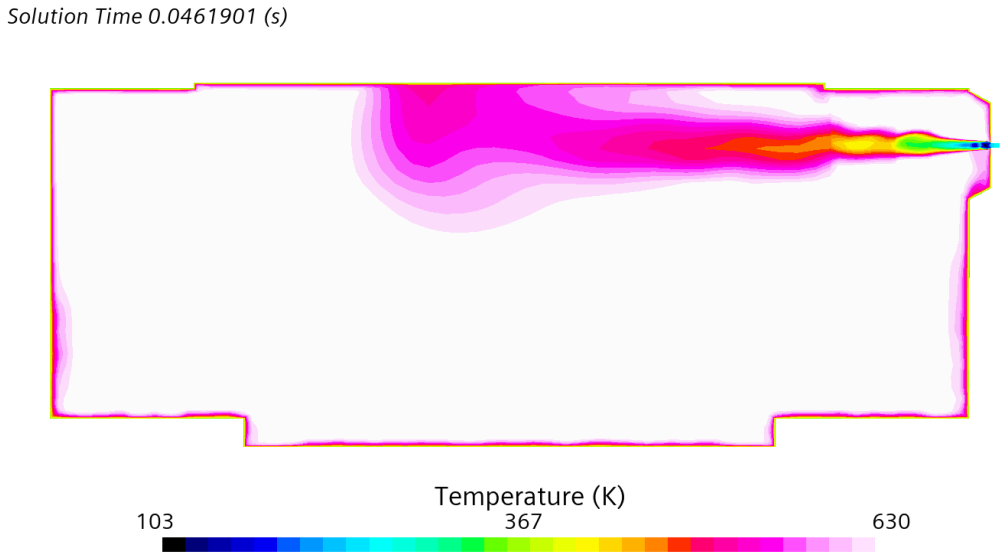

Figure 55: Temperature distribution in a slice through the nozzle axis roughly 1 ms after SOI.

Figure 55 shows an example of the temperature distribution in a slice through the nozzle axis roughly 1 ms after SOI. The under expansion leads to very low temperatures in the near-nozzle region and very high velocities are present as can be observed in Figure 56; Mach numbers in the near-nozzle region are above 3.

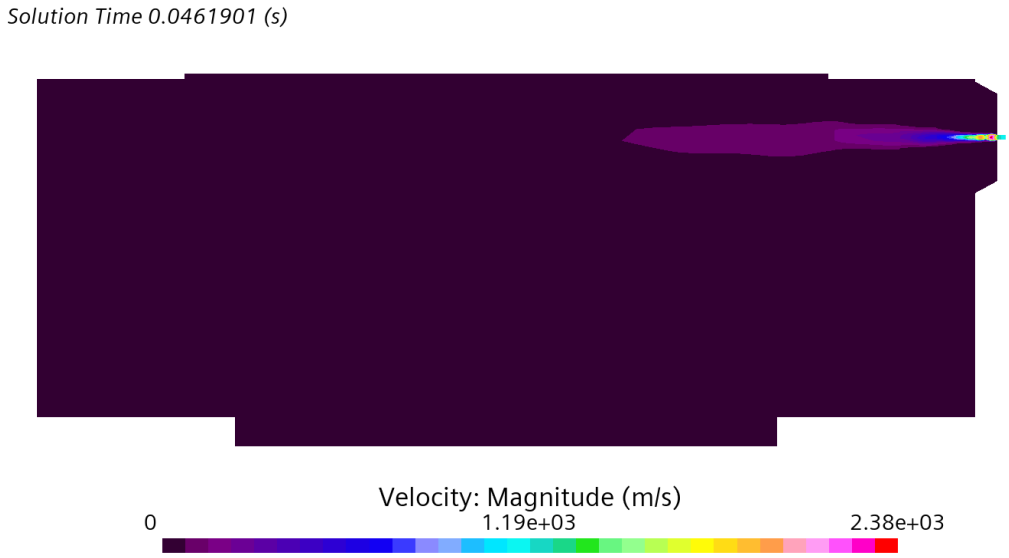

Figure 56: Velocity magnitude in a slice through the nozzle axis roughly 1 ms after SOI.

Reactive simulations have also been performed for an operating condition with start of injection 4.7 ms and a spark advance of 1.2 ms before TDC, corresponding to 45.3 ms and 48.2 ms absolute time.

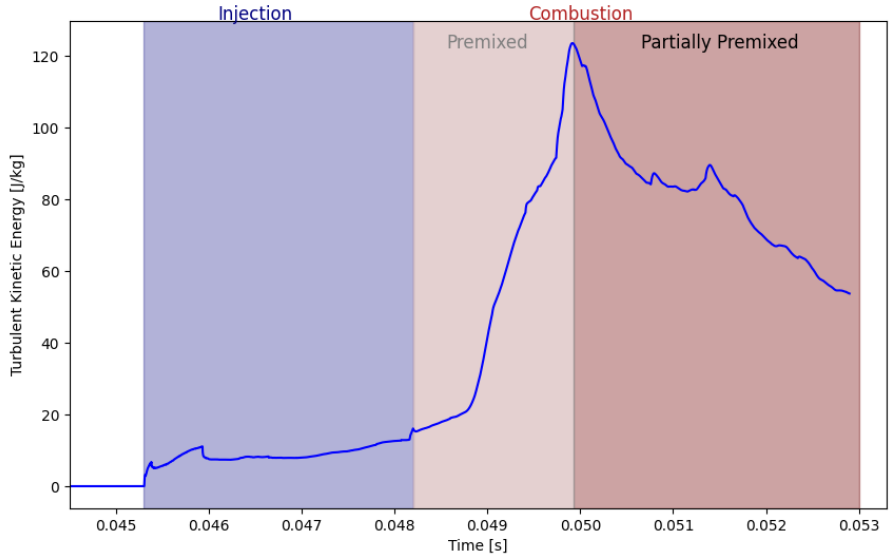

Figure 57: volume averaged turbulent kinetic energy in the domain for a jet-guided case;TDC corresponds to 50 ms..

A notable increase of the volume averaged turbulent kinetic energy is present as soon as the injection commences as is evident from Figure 57, even if only a small portion of the domain is affected by the jet. Sparking occurs at 48.2ms, following which the available fuel/air mixture in the jet is ignited and converted in a large premixed mode, leading to a considerable increase in the turbulent kinetic energy. From TDC onwards, fuel conversion is largely mixing-controlled and the turbulent kinetic energy levels start to decline.

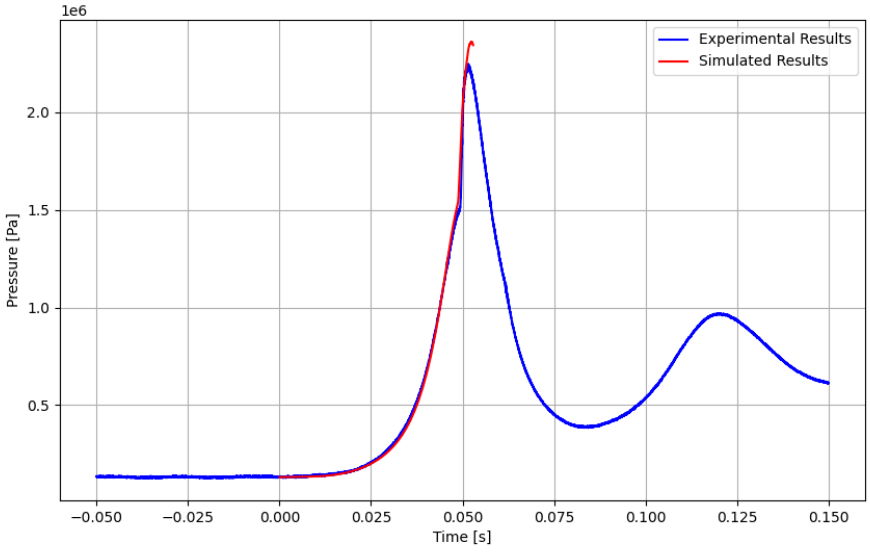

Figure 58: Predicted and simulated pressure trace for a jet-guided case.

Figure 58 shows a comparison of the predicted and measured pressure trace. Excellent agreement is evident throughout the compression, while the simulation shows a slightly earlier pressure rise and higher peak pressure.

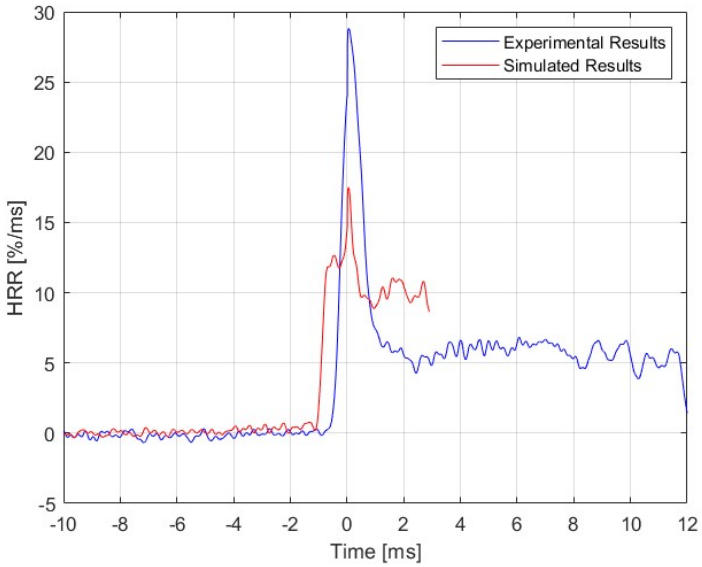

Figure 59: Predicted and simulated heat release rate for a jet-guided case.

The earlier rise is evident also in the heat release rate shown in Figure 59Figure 60. While the peak value of the premixed phase is slightly underpredicted, which can be expected due to the smaller volume of the plume available for conversion at the onset of combustion, a significant drop in the heat release rate following the transition to a mixing-controlled combustion mode is nonetheless well reproduced.

Solution Time 0.0529001 (s)

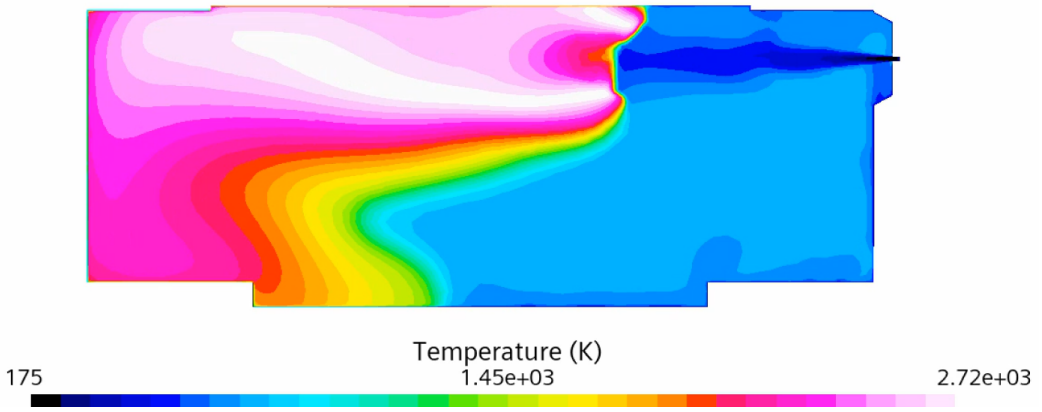

Figure 60: Temperature distribution in a section through the injection plane, showing a stabilized lifted jet flame

Figure 60 shows the temperature distribution in a slice through the injector axis. A lifte jet flame with a considerable lift-off length is well evident. Although hydrogen is a high-reactivity fuel, the lift-off length is considerably higher than would be expected of a hydrocarbon spray flame. This can be attributed to the considerable higher velocities present and also to the very low temperatures present due to the under-expanded nature of the jet.

All these results were obtained shortly before project conclusion, longer simultation times and further improvements in the predictions can therefore certainly be anticipated.

4.3 **Work Package 5: Assessment of the potential**

4.3.1 Assessment of the project results, open questions, comparison with fuel cell technology

The main goal of this project was to find out whether or not late hydrogen injection, ignition of the "hydrogen spray tip" and a mainly diffusion-controlled combustion is possible at engine-relevant conditions (Figure 61). The motivation is that classical premixed hydrogen combustion in reciprocating engines has major challenges regarding unwanted knocking or pre-ignition phenomena. The process behind these phenomena is that hydrogen/air mixtures have too much time for the chemistry which leads to knock or pre-ignition. So, drastically reducing the time for these unwanted reactions by largely omitting mixing is a very promising way

1. for engine efficiency increase (i.e. the compression ratio can be increased),
2. for power density increase (i.e. combustion at global stoichiometries towards λ=1 are possible and an engine can be build smaller), as well as for
3. lower technical complexities of engine boosting devices (i.e. the engine's boost pressure demand is reduced).

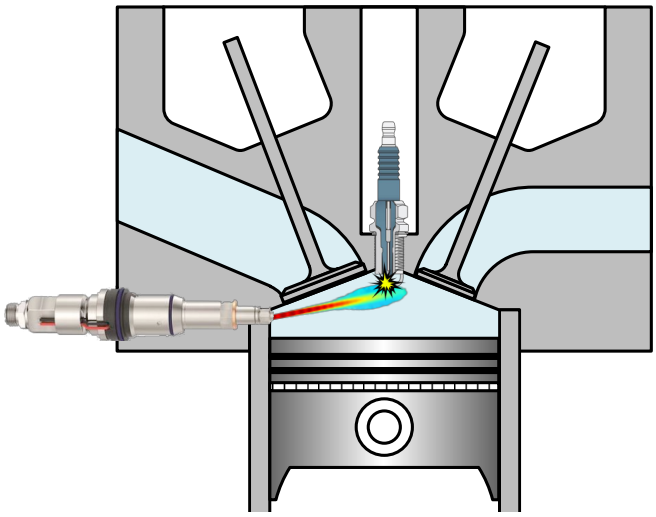

Figure 61: Sketch of the hypothesis of this project – hydrogen can be directly injected in the TDC region, the developing underexpanded jet can be ignited at its periphery and the main heat release occurs in a diffusion-controlled process

The main conclusion is: the project was a full success, the project team could prove that such a mainly diffusion-controlled (Diesel-like) combustion process of hydrogen is possible. This could not only be seen in the specialized optical test rigs at Empa (TRL 2-3), where the results led to an understanding of the involved processes and to the validation of numerical tools, but also at a single-cylinder engine at the University of Stuttgart (TRL 3-4).

For Diesel and gasoline injection and combustion processes, it took nearly one century to optimize not only the injection components but also to develop high-fidelity numerical tools which are needed to understand all involved processes. For hydrogen, this project opened up a new, uncharted, field for future research to transfer the combustion principle to higher TRLs. However, before going in this direction the following questions have to be addressed:

- Which injection principle is optimal for this combustion process to guarantee good diffusion/mixing and to minimize flame/wall intereactions and wall heat transfer (inwards-opening multio-hole injectors, outwards-opening hollow-cone injectors)?
- Which parameters are available and how to choose them to control the amount of the premixed combustion which precedes the diffusion-controlled mode?
- Which parameters are available and how to choose them to control NO_x formation?
- Do the advantages of this combustion concept overcompensate the challenges of injecting gas at high pressure levels?

However, it is likely that, with the combustion concept demonstrated in this project, diesel-like efficiencies of H_2 engine are within reach. The authors estimate, for typical heavy-duty applications with a peak power demand of around 300 kW, the efficiency potential of current and future H_2 ICE technologies versus current PEM fuel cell technologies as shown in Figure 62. Of course, fuel cells have an efficiency increase potential as well but the authors believe that it is rather limited as large advances in Nafion membrane polarization curves are rather unlikely which leaves the optimization potential mainly on the balance-of-plant components on the cathode side (efficient air supply and humidification) as well as on the cooling concepts.

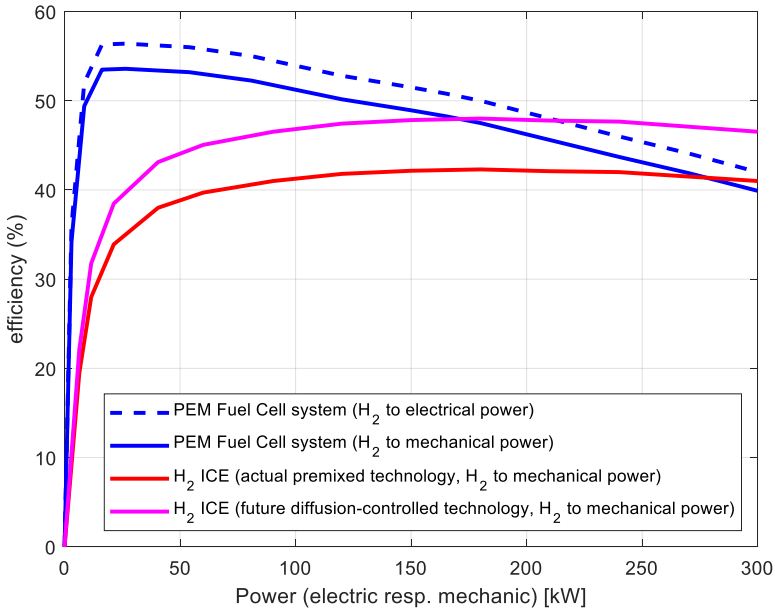

Figure 62: Efficiency potential of current (premixed, λ around 2) and future (diffusion-controlled) H_2 ICE technologies versus current PEM fuel cell technologies (based on Empa data/estimations)

As the estimations in Figure 62 show, the efficiency level of ICEs and PEM fuel cell systems is very similar for medium-to high-load applications. Therfore, it is very likely that fuel cells and hydrogen ICE solutions are close competitors in the heavy-duty segment as they offer very similar efficiencies but have strengts and weaknesses with regard to differerent parameters. Table 9 compiles an assessment of several such parameters. The authors believe, that both technologies will find their places in the heavy-duty vehicle, mobile machinery and medium-range maritime segment. One main desisive question may be if it will be possible to produce and distribute hydrogen in extremely clean quality to fulfil the very demaning life expextancy requirements, if PEM fuel cell technologies are used. Combustion systems are much more fuel-quality tolerant.

Table 9: Qualitative assessment of relevant PEM fuel cell and H_2 ICE engine parameters

Parameter	PEM Fuel Cell System	H_2 ICE
Efficiency at low load	excellent	okay
Efficiency at medium load	good	good
Efficiency at high load	good	good
Pollutant emissions	none	Possible NO_x emissions, no issue if developed carefully
H_2 emissions (short-term greenhouse gas)	Quantities unknown, but likely problematic during start-up and shut-down phases	Quantities unknown, likely unproblematic with an oxidation catalyst
H_2 purity demand	extremely high	very tolerant
Durability	medium	high
Robustness	weak on vibrations	high
Cold start	needs conditioning	good
Cost	expensive, economy of scale not yet proven, critical / expensive materials	affordable, no critical/expensive materials
Vehicle / machine integration	usually unproblematic as FC system / battreries / e-drive components can be placed quite freely	more challenging due to a direct mechanical power take-off
Cooling demand	challenging, as the temperature level of the heat is low	unproblematic
Noise for on-road heavy-duty vehicle use	unproblematic	challenging at speeds below around 30 km/h
Maturity	Low-medium (some systems on the market, competition starts to build-up)	Medium (basic engines on the market, better technologies in R&D)

4.3.2 Hydrogen in the future mobility system

Figure 63 shows the distribution of road freigt transport distances for Switzerland and for the EU. Switzerland is in a special situation: Swiss vehicles operate mainly within Switzerland, long-range transport is rather unusal for Swiss-registered vehicles. So, the majority of Swiss-registered heavy duty vehicles drive less than 300 km per trip. In contrast, EU heavy duty vehicles have frequent missions of (well) above 500 km. The majority of the EU transport capacity is performed by vehicles registed in Poland, Germany, France ans Spain. A significant part of Alp-crossing heav-duty traffic between EU countries goes through Switzerland.

Figure 63: Distance distribution of road freight transport for Switzerland and the EU

As a consequence, Swiss-registered heavy duty road vehicles have a much larger potential for direct electrification, which is an interesting option for decarbonization from a tank-to-wheel perspective. On an EU level, a direct electrification of a relevant part of the heavy duty fleet is much harder to achieve. Approaches to electrify medium and long-distance freigt transportation on the road do exist, 0.7-3 MW fast charger technologies are being developed and medium-haul vehicles with battery capacities above 600 kWh are under consideration.

According to a recent study of the European Automoile Manufacturers Association[68], heavy duty BEV vehciles cannot rely on passenger car charging infrastructures. For the estimated phase-in of around 200'000 BEV vehicles with more than 3.5t gross vehicle weight until 2030, 200'000 depot infrastructure slow charging points (<100 kW) will be needed, plus 40'000 charging points above 350 kW, distributed along majour routes.

However, even such ambitious direct electrification goals for commercial vehicles and buses cover only around 200'000 commercial vehicles out of a total EU commercial vehicle fleet of around 37 million until 2030. It is therefore likely that renewable fuel will become important in this segment over a long period of time. But the need for renewable fuels will likely also become much more important because of the build-up of renewable fluctuating energy production sites in Europe, which will lead to exces electricity situations at the ame time over large redions (e.g. central Europe), where electrical energy has to be either stored in a chemical way, or it will be “lost” (curtailment). Since hydrogen is the simplest chemical energy carrier which can be produced from electricity, it is likely that electrolysis will play a certain role in the future energy system of Switzerland, and Europe, e.g. to use electricity when supply is high and demand is low.

Business cases are challenging for production and storage technologies with low yearly load factors. It is therefore very likely that the majority of the energy needed for medium-long-distance transports will continue to be imported from resource-rich regions. Regading PV production, Switzerland (and most of the EU) suffer from high seasonal variations. Figure 64 shows the yearly-averaged PV production (kWh/kWp per day) versus the seasonality index (ratio between the highest and lowest average monthly photovoltaic power potential). Switzerland is in the rather difficult situation, that the PV seasonality is

[68] ACEA Position Paper Charging and re-fuelling infrastructure required for heavy-duty vehicles (ACEA, 2020)

relatively high (above 3) and the winter electricity demand is large and increasing. Sun-belt countries such as Namibia, Jordan, Egypt, Yemen, Oman, Saudi Arabia have a much higher yearly-averaged PV production and the seasonality index in these regions is close to one. This makes such sun-belt regions much more appropriate for an economically meaningful production of chemical energy carriers.

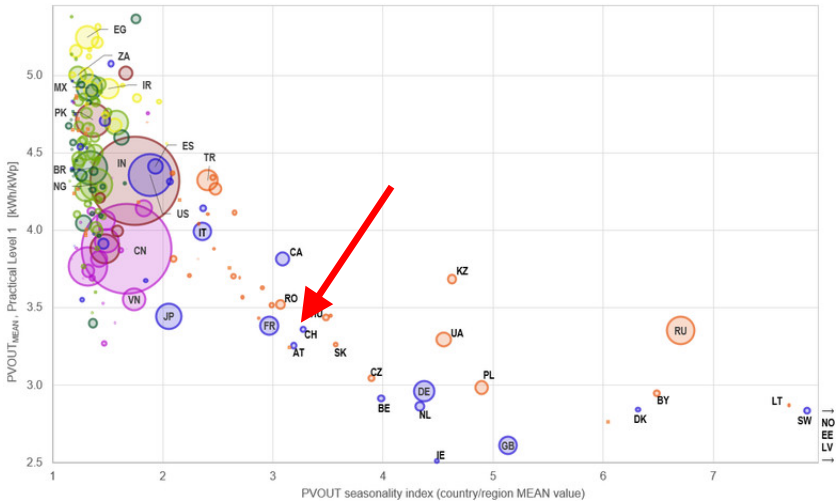

Figure 64: Absolute values of practical PV power potential (PVOUT) of indicidual countries / regions compared to PV seasonality index[69]

Figure 65 shows the World Bank's estimation of realistic PV production potential across the Globe (i.e. excluding complex terrain, large water bodies, forests, protected areas, cropland, areas without infrastructure). Europe is in the stuation, that the PV potential is rather low, with the exception of the Spanish peninsula. However, the largest potentials are rather far away from Europe which makes it likely, that Europe will have to import energy from these regions.

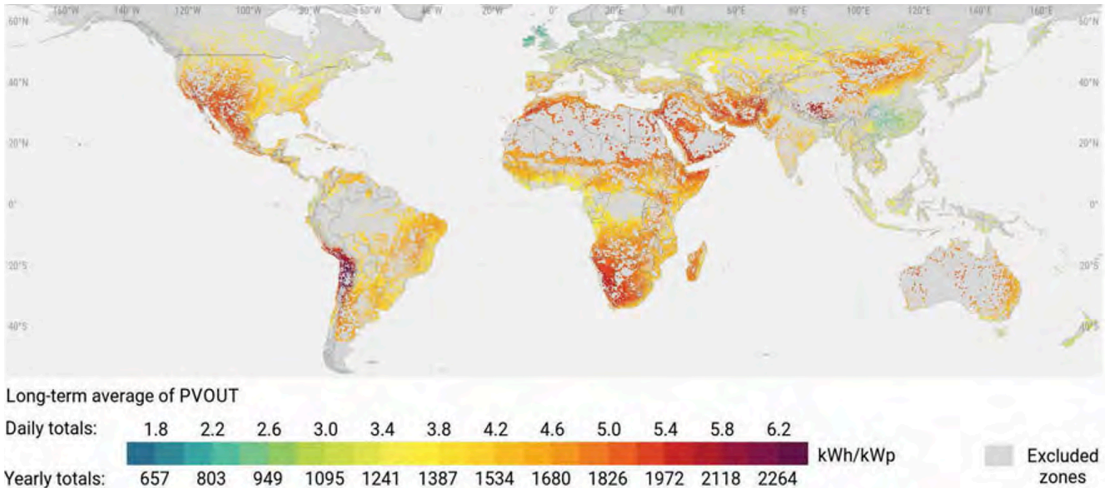

Figure 65: Absolute values of practical long-term average PV power potential (PVOUT)[70]

[69] Solargis study fort he World Bank, 2020, https://solargis.com/blog/best-practices/seasonality-and-socioeconomics-assessing-global-pv-potential-for-the-world-bank

[70] Global Photovoltaic Power by Country, The World Bank, 2020, https://documents1.worldbank.org/curated/en/466331592817725242/pdf/Global-Photovoltaic-Power-Potential-by-Country.pdf

Looking at the Swiss situation, a PV production potential of around 35 TWh/a PV is estimated on rooftops with very good or good suitability[71], but with the aforementioned problem of a high seasonality. If the same amount PV installation is placed in the sun-belt, as for example in Oman, about double the amount of electricity is produced (or even around the 2.5-fold amount for solar tracking technologies), and this with low seasonality. It is therefore understandeable, that countries like Chile, Brasil, Morocco or Oman are active in establishing production of large amount of renewable energies as they have the potential for producing renewable chemical energy carriers at competitive costs, despite energy conversion losses from electrolysis. Oman, as an example for such a potentially important export country for renewable chemical energy carriers, has identified around 50'000 km^2 for the production of such energy carriers from PV and wind[72].

In addition to PV, mainly onshore wind is a sector which still has a comparably large potential in some regions of the world. Figure 66 shows the estimated onshore wind potential across the globe. Regions like Patagona are very well suited for wind power production.

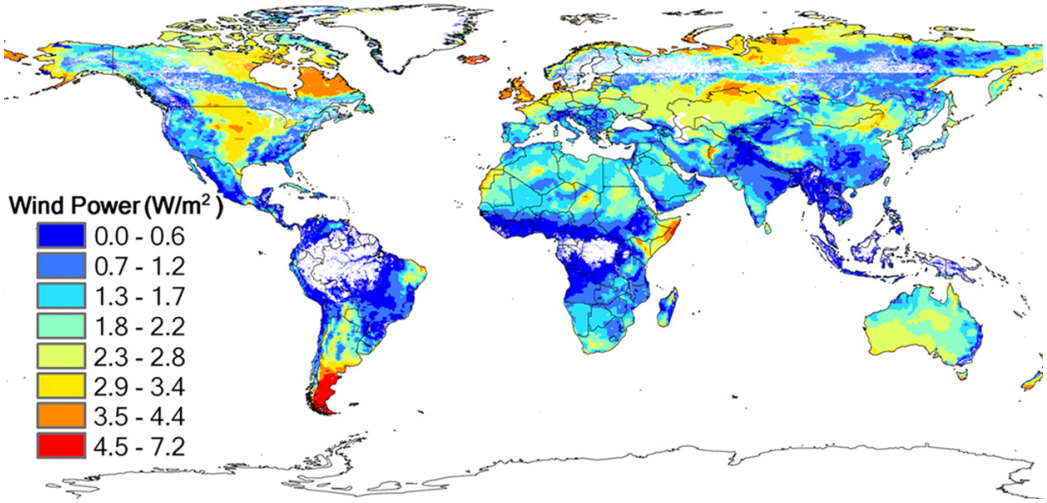

Figure 66: Global distribution of annual average onshore wind power potential accounting for spatial limitations on placement (without tlimitations on potential realizable capacity factors)[73]

As hydrogen production from electrolysis is estimated to ramp-up, the actual capital costs for electrolysis are estimated to considerably drop from actually above 1400 US$/kW to around 500 US$/kW according to IEA's Global Hydrogen Review 2022. In regions with a large potential for PV or wind and with low seasonality, hydrogen production is expected to become very competitive. Figure 67 shows IEA's estimation for 2030 for some selected countries / regions. Good regions are expected to be able to produce rather soon renewable hydrogen at costs around 1.5 US$/kg (this corresponds to around 0.045 US$ per kWh lower heating value of hydrogen).

[71] Walch A, Rüdisühlli M, Strategic PV expansion and its impact on regionalel ectricity self-sufficiency: Case study of Switzerland, Applied Energy, 2023, https://doi.org/10.1016/j.apenergy.2023.121262

[72] Renewable Hydrogen from Oman, International Energy Agency, 2023, https://www.iea.org/reports/renewable-hydrogen-from-oman

[73] Lu et al., Global Potential of Wind Generated Electricity, Proceedings of the National Academy of Sciences, 2008, http://dx.doi.org/10.1073/pnas.0904101106

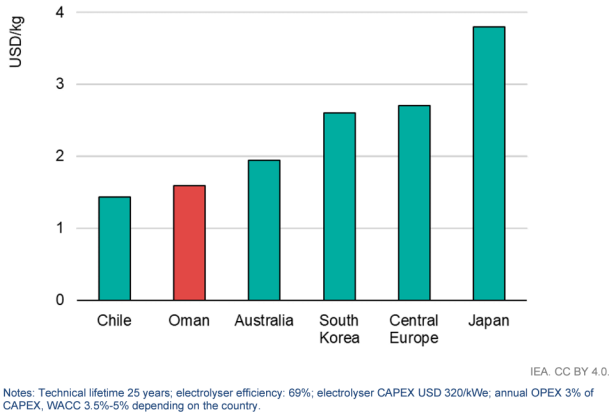

Figure 67: Renewable hydrogen production costs (estimations for 2030)[72]

4.3.3 Hydrogen distribution

As the potential to store hydrogen is very limited, the distribution is rather complex. Pipeline transport is feasible, but expensive and very inflexible, as such an infrastureucture has to be built first. Pipeline hydrogen distribution across Europe is possible to some extend and such initiatives do exists. One example is the European Hydrogen Backbone which plans to use 60% repurposed natural gas pipelines and build 40% new H_2 pipeline stretches until 2040. Cost estimation for Europen pipeline transport is estimated to become 0.11-0.21 Euro/kg (0.0033-0.0064 Euro/kWh) for an average transport distance of 1'000 km.

As it is unlikely that Europe will be able to produce enough hydrogen (or other renewable fuels) at competitive costs, hydrogen transport over long distances is likely to become an important pillar in the future. Unfortunately, hydrogen has a very low boiling point of 20K which makes liquified hydrogen approaches very difficult from a practical perspective (in contrast to liquified methane, which is liquid at 112K and is rather straightforward to handle). Moreover, the hydrogen density of liquid hydrogen is low, compared to alternatives.Table 10 shows a comparion of some relevant properties of liquid hydrogen and hydrogen transport molecules (TM). The basic principle with hydrogen transport molecules is that they are synthesized at production regions from hydrogen and CO_2 or N_2. The resulting products are then transported with ships to the destination region, where the molecules are split (reformed) to recover hydrogen. For hydrocarbons, this reforming process is usually done via steam reforming, which is an endothermic process. Steam reforming adds hydrogen to the products, in addition to the hydrogen released from the transport molecule.

As Table 10 shows, transport molecules like methane, methanol, dimethyl ether (DME) or ammonia are able to increase the volumetric hydrogen content compared to liquid hydrogen (so, for example, one liter of liquid ammonia contains 72% more hydrogen then liquid hydrogen). Since at the destination region, additional hydrogen is produced from the reforming process, hydrocarbon molecules turn out to be a very promising way for hydrogen transport. So, for example, one liter of DME leads to 2.5 times as much hydrogen at the destination region as the transport of 1 liter liquid hydrogen. For real systems, the energy demand for the endothermic reform processes has to be considered as well.

Table 10: Comparison of liquid H2 transport and transport of H2 in molecules

Transport molecule (TM)	Density	Molar mass	Molar hydrogen content	Hydrogen mass content	Hydrogen content of transport molecule (TM)	Hydrogen content per volume of transport molecule	Molar hydrogen amount after reforming	Hydrogen content of transport molecule (TM) after refroming	Hydrogen content per volume of transport molecule (TM) after reforming
	[kg/m3]	[kg/kmol]	[kmol H/kmol]		[kg H/m3 TM]	(relative to H2)	[kmol H/kmol]	[kg H/m3 TM]	(relative to H2)
LH2 @ 20K	70	2	2	100%	70	100%	2	70	100%
LCH4 @ 112K	424	16	4	25%	106	151%	6	159	227%
CH3OH Methanol	792	32	4	13%	99	141%	6	149	212%
CH3OCH3 DME (liquid)	670	46	6	13%	87	125%	12	175	250%
NH3 Ammonia (liquid)	683	17	3	18%	121	172%	3	121	172%

Therefore, it is likely that transporting hydrogen in carrier molecules will likely be more economic than transporting hydrogen in its molecular form. Figure 68 shows an example oestimations of ship transport costs for liquid hydrogen and ammonia.

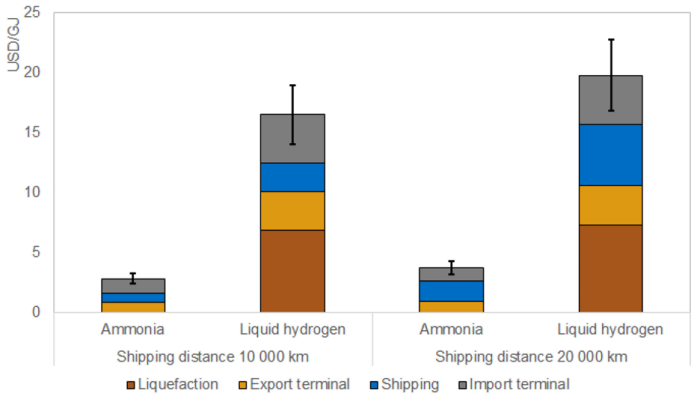

Figure 68: IEA estimates of marine transport cost estimations for liquid hydrogen and ammonia[74]

It is therefore understandable, that for the long-range transport of hydrogen, several hydrogen carriers are under considerations at the moment. Besides the carriers listed above, liquid organic hydrogen carriers (LOHC) are also in discussion. The idea behind LOHC approaches is that the carriers are loaded with hydrogen at producer regions, hydrogen is released at consumers regions and the unloaded LOHC is transported back to the producers. However, it is usually disregarded that for the simple hydrocarbons such as methane, methanol, DME, the CO_2 which is separated after the reforming process anyway could also be captured and transported back to the producer region, which would drastically reduce the demand for direct air capture of CO_2. A good quantitative description of such a DME/CO_2 strorage cycle can for example be found in[75].

[74] The Role of Low-Carbon Fuels in the Clean Energy Transitions of the Power Sector, International Energy Agency, 2021, https://iea.blob.core.windows.net/assets/01ca16c8-e493-475c-81c4-04ac5d3b9882/Theroleoflow-carbonfuelsinthecleanenergytransitionsofthepowersector.pdf

[75] Schühle P et al., Dimethyl ether/CO2 – a hitherto underestimated H2 storage cycle, Energy & Environmental Science, 2023, https://doi.org/10.1039/D3EE00228D

Figure 69 shows some possible ways to supply Switzerland with hydrogen. The solutions can be clustered as follows:

1. **Local electrolysis**

   National hydrogen electrolysis is an obvious approach and it will likely become meaningful during the summer period with a future excess of cheap renawable electricity. However, there is no forseable solution for excess (or cheap) renewable winter electricity. Decentralized solutions may be too expensive as investment costs for electrolyzers as well as for the connection to the grid are very likely to be much favourable for larger installations. Local hydrogen electrolysis and distribution projects exist in Switzerland, e.g. the activities of Hydrospider AG.

2. **Local methane conversion**

   National hydrogen production from renewable methane may become attractive. The technical solutions and trade mechanisms for liquified methane are already established and a distribution infrastructure (natural gas pipelines) exists. This makes the solution of transporting renewable energy via methane a promising option, especially if the urgent need of decarbonization over less then three decades is kept in mind.

   Methane reforming

   Local methane direct steam reforming is the classical approach to de-compose methane:

   $CH_4 + 2\ H_2O \longleftrightarrow CO_2 + 4\ H_2$

   This gives the possibility for sequestration of the separated CO_2 thus theoretically enabling negative GHG emissions.

   Methane pyrolysis

   Another, yet less mature, process is methane pyrolysis:

   $CH_4 \rightarrow 2\ H_2 + C(solid)$

   This approach has the big advantage that carbon accumulates in solid form which makes it much easier for sequestration than CO_2. Moreover, it is possible that solid carbon (carbon black) will become a raw material of value, e.g. for the building industry or for agriculture. Such approaches have become internationally in the research focus over the last years. In Switzerland, the ETH Domain Center of Excellence SCENE[76] or technology transfer projects from the “Verein zur Dekarbonisierung der Industrie” are active in this field.

3. **Ammonia, methanol or DME conversion**

   Methanol and ammonia are very often (besides of the established LNG technology) in focus for future ocean shipping[77]. Current ships on order have already powertrains for non-conventional fuels of more than 50%, Methanol engines in shpping show fast growth. Ammonia technologies are not yet ready but expected to gain on importance in the next years. DME technologies are not yet broadly discussed, despite of clear advantages (DME is a high-ractivity fuel which can be used in very efficient compression ignition engines and does not produce soot[78]). It is likely, that ships will be economically attractive, when the transport tanker’s powertrain technology matches the renewable energy transport molecule. Attractive solutions should give

[76] https://www.scene-project.ch/
[77] DNV Maritime Forecast to 2050, 2023, https://www.dnv.com/maritime/publications/maritime-forecast-2023/index.html
[78] Soltic et al., The potential of dimethyl ether (DME) to meet current and future emissions standards in heavy-duty compression-ignition engines, Fuel, 2024, https://doi.org/10.1016/j.fuel.2023.129357

the possibility, to use the transport molecule for further logistical operation (e.g. supplying the fuel close to customers, when pipeline solutions are not available). This makes methanol and DME attractive, as ammonia has most probably too high hazards when used in land logistics.

Ammonia reforming

Ammonia is a safety-critical substance. Therefore, it is likely that reforming will be concentrated in destination ports to avoid safety-critical transport on land. Thermal reforming of ammonia is the classical approach:

$NH_3 + O_2 \longleftrightarrow 2\ N_2 + 2\ H_2O + 4\ H_2$

Since no carbon is involved, GHG emissions from reforming are unproblematic. However, this also does not give ammonia the potential for negative GHG emissions. One pont of concern of the ammonia route is the N_2O formation in the involved processes (including ammonia combustion in ship powertrains).

Methanol reforming

Methanol can be reformed close to the destination port or transported close to end users and reformed there as land transport is not critical. Moreover, methanol is a suited fuel for long-haul heavy-duty (truck) engines, which give methanol an attrative perspective for land logistics. Local methanol direct steam reforming is the classical approach:

$CH_3OH + H_2O \longleftrightarrow CO_2 + 3\ H_2$

As for methane reforming, CO_2 from the methanol reforming process can theroretically be sequestrated which enables negative GHG emissions from the methanol route as well.

DME reforming

DME can be reformed close to the destination port or transported close to end users and reformed there as land transport is not critical. Moreover, DME is a ver well suited fuel for highly efficient long-haul heavy-duty (truck) engines, which give DME an attrative perspective for land logistics.

Local DME direct steam reforming is the classical approach: $C_2H_6O + 3\ H_2O \longleftrightarrow 2\ CO_2 + 6\ H_2$

As for methane or methanol reforming, CO_2 from the methanol reforming process can be sequestrated which enables negative GHG emissions from the DME route as well. One important aspect is that liquid DME and liquid CO_2 have very similar physical properties: both are liquid at comparably low pressure levels. This gives the possibility to transport CO_2 back to the DME production region in the same ship as DME was delivered, which could make such a directly closed CO_2 cycle economically attractive, as is reduces (or avoids) the need of DAC at the source region.

4. **LOHC approaches**

Liquid organic hydrogen carriers have been considered for H_2 transportation for a while. Typical loaded $\longleftrightarrow$ unloaded LOHCs looked at are molecules with aromatic structures such as methylcyclohexane $\longleftrightarrow$ toluene, decalin $\longleftrightarrow$ naphthalene, perhydro-dibenzyltoluene $\longleftrightarrow$ dibenzyl toluene or even nitrogen-containing structures[79]. One critical point seems to be the recyclability of the LOHC molecules over multiple cycles. All in all, LOHC seems to be the least mature technology, both from a technical and from an economical point of view.

[79] Rao P et al., Potential Liquid-Organic Hydrogen Carrier (LOHC) Systems: A Review on Recent Progress, Energies, 2020, https://doi.org/10.3390/en13226040

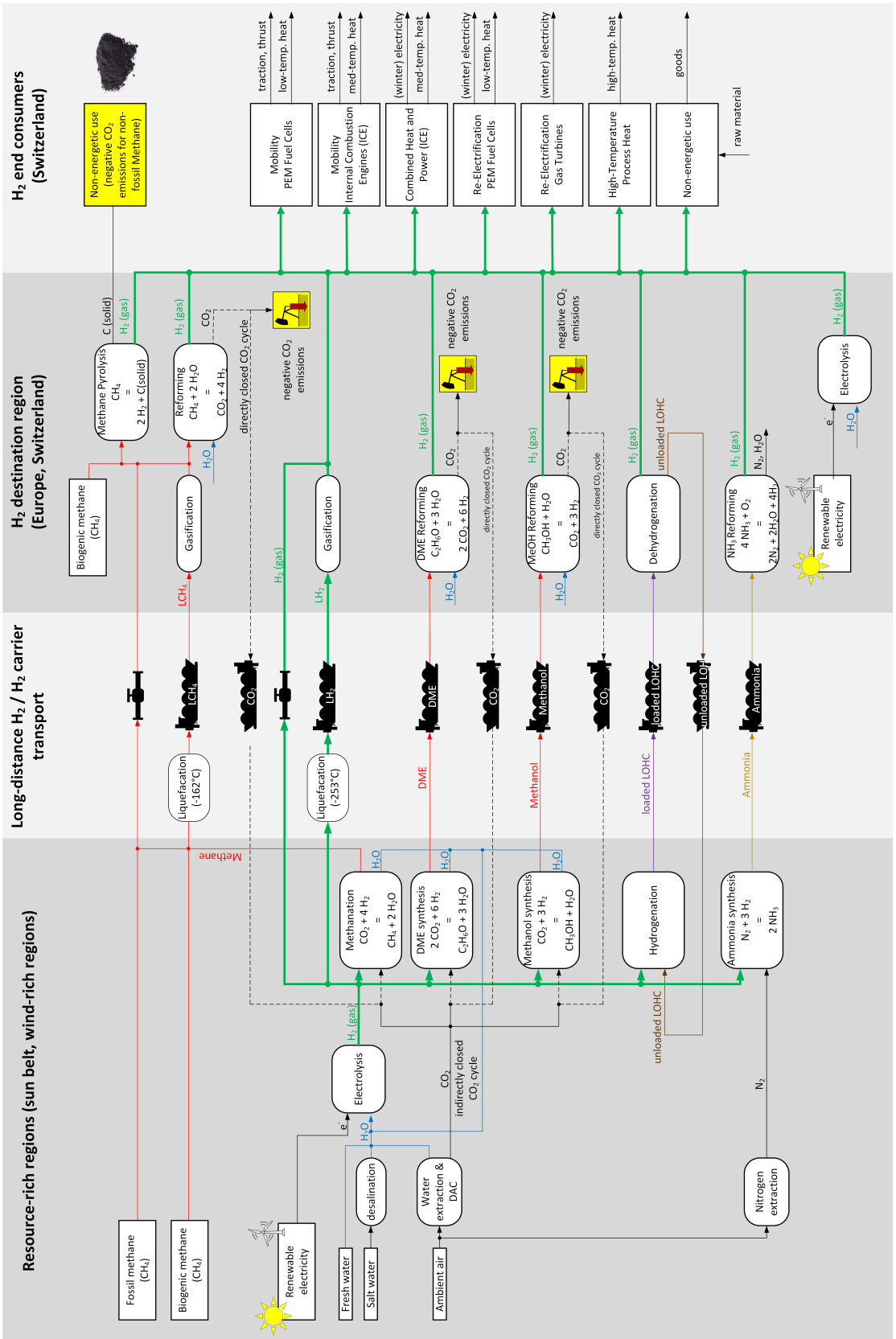

Figure 69: Possible paths to supply Switzerland with hydrogen

4.3.4 Technical and non-technical aspects

Technolgy readiness is one important aspect to assess the feasibility of solutions. Other important aspects are market- or political readiness levels.Table 11 shows a heat-map assessemt of the technology readiness for the different hydrogen supply routes discussed in the previous section. High rechnology readiness levels are found for local electrolysis (direct hydrogen route) as well as for the hydrogen via methane route, while the methanol, DME and ammonia routes show some open development needs. The LOHC route is most likely the least mature approach where not only the large-scale energy carrier technology is not ready, but also a lot of open questions do exist regarding the supply infrastructure.

Table 11: Assessment of technology readiness for the different hydrogen supply and use options

	Direct hydrogen route	Hydrogen via Methane route	Hydrogen via Methanol route	Hydrogen via DME route	Hydrogen via Ammonia route	Hydrogen via LOHC route
Fuel production technolgies	Electrolysis technology mature, efficiency increase potential, cost reduction potential	Sabatier and DAC technologies exist, still large technical and economical potential Reforming technology mature, pyrolysis technology in R&D phase	Methanol synthesis technologies mature, reforming technologies close to mature, DAC technologies exist, still large technical and economical potential	DME synthesis technologies mature, reforming technologies not yet in focus, DAC technologies exist, still large technical and economical potential	Ammonia synthesis technologies ready, (catalytic) ammonia reforming technologies in R&D	Not yet mature technology
Fuel transport (long range: pipelines and ships)	Not ready	Ready (pipeline and LNG)	In principle ready	No technologal issues but not yet rady	Ammonia transport in ships is common technolohy	Not yet mature technology
Fuel distribution to end customers	Not ready (for larger quantities)	Ready (natural gas grid with local reforming)	In principle ready (trucking, rail)	In principle ready (trucking, rail)	In principle ready (mainly rail), safety concerns	Not yet mature technology
Powertrain technologies	H_2 Fuel cells reach maturity, economy of scale not yet proven H_2 ICE technology under development, simple concepts mature, more efficient concepts in the R&D phase					
Negative GHG technologies	Not possible	Via methane reforming / pressure swing separation matue Via pyrolysis (solid C) not yet mature	Technology available but not yet fully mature for methanol (membrane/ cryogenic or amine washing)	Technology available but not yet fully mature for DME (membrane/ cryogenic or amine washing)	Not possible	Not possible

While the Technology Readiness Level (TRL) for conventional hydrogen technologies such as alkaline or PEM electrolysis, compressors, storage vessels, valves, piping, fueling stations, etc. often are assessed as high, this is less the case for Policy and Market Readiness, especially in Switzerland. The lack of clear regulations covering at least the lifetime of investment projects is assessed by investors as a risk. On the other side, also market readiness is low. Since hydrogen projects actually still are planned in small scales (<100 MW), the production costs are rather high. All in all, there is a conflict of high sustainability requirements and getting the market started with small, but expensive hydrogen projects.

This situation is not only true for Switzerland but can be seen world-wide. From actually 1'400 announced hydrogen production projects (whereof 1'000 projects with a total hydrogen production of 45 Mt/a, that shall be realized by 2030) only 5% have achieved a Final Investment Decision (FID) yet[80]. The main reason for the low funding decision rate are missing offtaker due to high production costs and bad bankability due to high risks.

On the policy side, the European Union is going forward with hydrogen strategies and regulations on how hydrogen and its derivates shall be assessed and certified. While it is more or less undisputed, that hydrogen has to be produced on a sustainable way, it is much less clear on how such sustainable ways look like. One possible answer is given by recently published acts of the European Union:

- The Directive (EU) 2023/2413 of 18 October 2023 regarding the promotion of energy from renewable sources
- The Delegated Regulation (EU) 2023/1184 of 10 February 2023 establishing a Union methodology setting out detailed rules for the production of renewable liquid and gaseous transport fuels of non-biological origin
- The Delegated Regulation (EU) 2023/1185 of 10 February 2023 establishing a minimum threshold for greenhouse gas emissions savings of recycled carbon fuels and by specifying a methodology for assessing greenhouse gas emissions savings from renewable liquid and gaseous transport fuels of non-biological origin and from recycled carbon fuels

As a threshold of the European Union (EU), the use of hydrogen has to result in a CO_2 reduction of at least 70% compared with the use of conventional energy[81]. This value has to be achieved by considering the so-called "additionality" of the renewable electricity required for hydrogen production and its temporal generation profile[82]. This means, that plants for the production of hydrogen (and derivates, such as synthetic fuels) must be "directly connected" to "new" (understood as less than 3 years old) e.g. PV and/or wind power plants for the production of renewable electricity. This is intended to prevent existing renewable electricity simply being used in a different way, what would not meet the additionality requirement. If a direct connection is not possible, the local temporal production profile of the renewable electricity used must be considered for the operation of the hydrogen production plant, which gives rise to the load flexibility requirement. This requirement is in a clear contradiction to low production costs, because such a regime would reduce the number of fulload-hours by a factor 3 – 5, what is increasing the production costs of hydrogen.

There are a number of other requirements, such as that the renewable electrical energy must be linked to a direct contract between the producer of the electrical energy and the operator of the plant for the production of synthetic energy sources or that the plant for the production of electrical energy must not be subsidized.

Proof of compliance with the requirements is provided by means of certification. Actually, only voluntary certification schemes are being recognized by the EU[83]:

- ISCC-EU according the Commission implementing Decision (EU) 2022/602 of 8 April 2022 on the recognition of the 'International Sustainability & Carbon Certification – ISCC EU' voluntary scheme for demonstrating compliance with the requirements set in Directive (EU) 2018/2001
- CertifHy™ has been initiated at the request of the European Commission and is financed by the Clean Hydrogen Partnership. It aims for hydrogen certification across Europe by providing an EU-

[80] Hydrogen Insights 2023, Hydrogen Council and McKinsey & Company, available at https://hydrogencouncil.com/en/hydrogen-insights-2023-december-update/
[81] Directive (EU) 2023/2413 of 18 October 2023 amending Directive (EU) 2018/2001, Regulation (EU) 2018/1999 and Directive 98/70/EC as regards the promotion of energy from renewable sources, and repealing Council Directive (EU) 2015/652
[82] Art. 3 of the Delegated Regulation (EU) 2023/1184 of 10 February 2023 establishing a Union methodology setting out detailed rules for the production of renewable liquid and gaseous transport fuels of non-biological origin
[83] https://energy.ec.europa.eu/topics/renewable-energy/bioenergy/voluntary-schemes_en

wide system of Guarantees of Origin. CertifHy™ is a consortium led by HINICIO and composed of GREXEL, Ludwig-Bölkow-Systemtechnik (LBST), AIB (Association of Issuing Bodies), CEA (Commissariat à l'énergie atomique et aux énergies alternatives) and TÜV SÜD[84]

Conclusion on the non-technical aspects:

The balancing act between high sustainability requirements and scaling-up a hydrogen market could be solved by taking the Technology Readiness Levels for hydrogen technologies on a more specific level into account. TRL may be high for small and constantly operated systems but they are less high for large scale and load flexible operation. For such systems, a "mixed regime" could be an enabler by allowing a share of steady state operation covered with renewable electricity certificates for first-of-its-kind plants.

[84] https://www.certifhy.eu/

5 Conclusions

This project started with the idea that it should be possible to bypass a lot of restriction from hydrogen use in internal combustion engines by finding a work-around of hydrogen's main problem, it's low knock resistance. Instead of applying classical "inertialization" measures to lower the reactiviy (e.g. high air excess, EGR, water injection), the hypothesis of this project was that it is possible to drastically reduce time for the unwanted reactions to happen. This can be achieved by reducing the time between injection and ignition as much as possible. Conseqently, direct injection has to be applied and phased as late as possible in the process. For classical fuels, "late" means that the injection has to be finished befor ignition is applied because a certain time for mixing has to be given in order to avoid excessive sooting. When using hydrogen, a fuel without any sooting problems and with extremely wide igniteability limits, late can also mean "as late as possible": give no time for the hydrogen jet(s) to mix with air.

This leads to the combustion process condisered in this project: hydrogen injection and ignition of the developing Hydrogen jet tip. Since the conditions are rather extreme (high shear, high turbulence, numerical models not validated for such conditions) it was not a prori clear if such a combustion concept would work. Luckily, it could be experimentally proven in the framework of this project that it works. A hydrogen jet can be ignited at its tip which leads to a first, fast, phase of premixed combustion, followed by a second phase of diffusion-controlled combustion, determined by the injection rate of hydrogen. Since the process parameters (heat release rate, no flame "hitting the walls") is closer to a Diesel than to a Otto process, a hypothesis could now be that it is possible to develop future combustion engines for hydrogen with similar efficiency levels as Diesel engines.

6 Outlook and next steps

This project opened up a new field of research and development for hydrogen engines. Open questions are for example how an ideal injector should look like for such a combustion process, how the share of premixed versus diffusion-controlled combustion can be influenced, how the cyclic variation can be minimized, which are adequate turbulence levels, how does exhaust gas recirculation influence this combustion mode, how should an appropriate ignition system look like and what are the hydrogen emissions formed in such a combustion mode. It is planned that most of these question will be addressed in a follow-up collaborative project with Empa working on injection, ignition and numerics fundamentals, TU Stuttgart working on sigle-cylinder experiments for larger (heavy-duty) engines and TU Berlin characterizing different H_2 injectors.

7 National and international cooperation

This project was organized as a cooperation between Empa and IFS Stuttgart and embedded in a FVV/CORNET umbrella project. The specific expertise of the two research institutes was combined to address the challenges in this research.

The embedding in a FVV umbrella means that many industrial and academic partners were closely following this project. This was done in the regular FVV project meetings (in Zürich and Stuttgart as well as online). The project results have been presented to a large audience at the FVV Spring Converence 2024 in Würzburg.

Results from this project are also disseminated through the Gas Engines Collaborative Task, within the Technical Collaboration Programme on "Sustainable Combustion" of the International Energy Agency.

8 Publications

- A Beyer "A Non-premixed Hydrogen Combustion Process Using a Spark-Ignited Hydrogen Jet" 2023 Conference on Powertrains with Renewable Energy Carriers, Stuttgart, November 28.-29., 2023
- M. Balmelli, L. Merotto, P. Soltic, J. Biela, "Ignition detection with the breakdown voltage measurement during nanosecond repetitively pulsed discharges", Energy Ccoversion and Management, 292, 2023, https://doi.org/10.1016/j.enconman.2023.117382
- L.Merotto, M. Balmelli and P. Soltic, " Hydrogen direct injection: Optical investigation of premixed and jet-guided combustion modes", International Journal of Hydrogen Energy, 61, 2024, https://doi.org/10.1016/j.ijhydene.2024.02.278
- L. Merotto, Y. Wright, P. Soltic, M. Balmelli, A. Beyer "Wirkungsgradoptimales Brennverfahren für wasserstoffbasierte Kraftstoffe", FVV Transfer + Netzwerktreffen, Informationstagung, Würzburg, March 14, 2024
- A. Beyer, M. Balmelli, L. Merotto, Y. Wright, P. Soltic, A. Kulzer "DIH2jet (DI Hydrogen Combustion Process", *in Kulzer, A.C., Reuss, HC., Wagner, A. (eds) Proceedings of the 2024 Stuttgart International Symposium on Automotive and Engine Technology. Springer Vieweg, Wiesbaden.*
- M. Balmelli, L. Merotto,Y. Wright and P. Soltic " Optical and Thermodynamic Investigation of Jet-guided Spark Ignited Hydrogen Combustion", *International Journal of Hydrogen Energy **78**: 1316-1331 (2024)*